COMPARISON BETWEEN SATELLITE-BASED AND COSMIC RAY PROBE SOIL MOISTURE ESTIMATES: A CASE STUDY IN THE CATHEDRAL PEAK CATCHMENT

THIGESH VATHER

Submitted in partial fulfilment of the requirements for the degree of MSc in Hydrology

School of Agriculture, Earth and Environmental Sciences

University of KwaZulu-Natal

Pietermaritzburg

Supervisor: Ms K T Chetty

Co-supervisors: Dr M G Mengistu

Prof C S Everson

November 2015

ABSTRACT

Soil moisture is an important hydrological parameter, which is essential for a variety of applications, extending to numerous disciplines. Currently, there are three methods of estimating soil moisture. These include: (a) ground-based (*in-situ*) measurements, which are carried out using field instruments; (b) remote sensing based methods, which use specialized sensors on satellites and aircrafts and (c) land surface models, which use meteorological data as inputs, at a predefined spatial resolution (Albergel *et al.* (2012); Mecklenburg *et al.*, 2013). In recent years the cosmic ray probe (CRP), which is an *in-situ* technique, has been implemented in several countries across the globe. The CRP provides area-averaged soil moisture at an intermediate scale and thus bridges the gap between *in-situ* point measurements and satellite-based soil moisture estimates (Zreda *et al.*, 2012). The aim of this study was to first evaluate the current techniques for soil moisture estimation, in order to identify the research gaps and limitations. The key objectives of this study were to test the suitability of the CRP to provide spatial estimates of soil moisture and use these estimates to validate satellite-based (remote sensing and modelled) soil moisture estimates in the Cathedral Peak Catchment VI. The CRP was set-up and calibrated in Cathedral Peak Catchment VI. An *in-situ* soil moisture network was created in Catchment VI, which was used to validate the calibrated CRP soil moisture estimates. Once calibrated, the CRP was found to provide spatial estimates of soil moisture, which correlated well with the *in-situ* soil moisture network dataset and yielded a R^2 value of 0.8445. The calibrated CRP was used to validate satellite-based soil moisture products. The remote sensing products used were the Level Three AMSR2 and SMOS products. The AMSR2 and SMOS products generally under-estimated soil moisture throughout, but followed the general trend of the CRP, with AMSR obtaining a R^2 of 0.505 and SMOS obtaining a R^2 of 0.4853, when compared against the CRP estimates. The CRP was used to validate modelled soil moisture products, which consisted of the SAHG product and the back-calculation of soil moisture, using equations by Su *et al.* (2003) and Scott *et al.* (2003), and products derived from the SEBS Model. The SAHG Model performed well, as it provided estimates that correlated well with the CRP dataset and yielded a R^2 value of 0.624 compared to the CRP estimates. The SEBS back-calculation technique performed very poorly, as it over-estimated in the wet periods and under-estimated in the dry periods.

DECLARATION

I, Thigesh Vather, declare that:

(i) the research reported in this dissertation, except where otherwise indicated, is my original work.

(ii) this dissertation has not been submitted for any degree or examination at any other university.

(iii) this dissertation does not contain other persons' data, pictures, graphs or other information, unless specifically acknowledged as being sourced from other persons.

(iv) this dissertation does not contain other persons' writing, unless specifically acknowledged as being sourced from other researchers. Where other written sources have been quoted, then:

(a) their words have been re-written, but the general information attributed to them has been referenced;

(b) where their exact words have been used, their writing has been placed inside quotation marks, and referenced.

(v) Where I have reproduced a publication of which I am an author, co-author or editor, I have indicated, in detail, which part of the publication was actually written by myself alone and have fully referenced such publications.

(vi) This dissertation does not contain text, graphics or tables copied and pasted from the Internet, unless specifically acknowledged, and the source being detailed in the Dissertation and in the References sections.

Signed: ……..

Thigesh Vather

Supervisor: ……..

Miss Kershani Tinisha Chetty

Co-supervisor: ……

Dr Michael Mengistu

PREFACE

The work undertaken and described in this dissertation was carried out in the Centre for Water Resources Research (CWRR), in the School of Agriculture, Earth and Environmental Science. This school is within the University of KwaZulu-Natal, Pietermaritzburg. The following dissertation was supervised by Ms KT Chetty, Dr MG Mengistu and Prof CS Everson.

This dissertation is original, unpublished, independent work by the author Thigesh Vather. The work of other authors, when used, has been given the appropriate credit.

ACKNOWLEDGEMENTS

The following Masters Research titled "Comparison Between Satellite-Based and Cosmic Ray Probe Soil Moisture Estimates: A Case Study in the Cathedral Peak Catchment'' has been funded by the Centre for Water Resources Research (CWRR) and the National Research Foundation (NRF). I am grateful for the aforementioned institutions for the funding they have contributed towards this research. I would also like to acknowledge the following people and institutions for their fundamental role in the completion of this research project:

First and foremost, I would like to thank my parents and sisters for their continuous love and support. I appreciate all that you have done for me, not only during the past two years, but throughout my life Thank you to my extended family and friends for all the love and support you have given me. Thank you to Vadinie Moodley, for all the love and support, as well as keeping me focused throughout my Masters.

- Miss KT Chetty (supervisor). Thank you for your guidance and support throughout the duration of the research project. Your mentorship has been of much value to the completion of the dissertation.

- Dr MG Mengistu (co-supervisor). Thank you for all the support and mentorship. Your contribution towards the completion of this research study has been invaluable. Thank you for all the field trips to Cathedral Peak and assisting me will all the aspects of my project, such as the setting up of the cosmic ray probe, setting up of the soil moisture network, calibrating the cosmic ray probe, teaching me how to set-up and run the SEBS model and for assisting with any problems that arose.

- Prof CS Everson (co-supervisor). Thank you for all the support and mentorship throughout the project. Thank you for making this research project possible by obtaining the cosmic ray probe. Thank you for all the well organized and productive field visits. Thank you for assisting me with the various fieldwork activities that were carried out. Thank you for organizing the various instrumentation and support throughout the project.

- Mrs S Rees. Thank you for assisting me with the editing of the dissertation. I really appreciate the time and effort that you have put into improving the dissertation.

- Mr S Mfeka and Mr C Pretorius. Thank you for all the assistance in the field and the laboratory. Thank you for always being willing to help and always approachable.

- The winter school. Thank you for assisting me with the first calibration, which was the most labour intensive and time consuming calibration. I appreciate all the work and effort that was made.

- Prof TE Franz. Thank you for assisting me with the third calibration, as well as teaching me the cosmic ray probe calibration procedure.

- Dr S Sinclair. Thank you for the assistance in providing the PyTOPKAPI soil moisture product.

- Mr S Gokool. Thank you for your assistance and advice throughout the duration of the project. Your suggestions towards improving the project were greatly beneficial and appreciated.

- Mr B Scott-Shaw. Thank you for assisting with the fire breaks.

- Mrs S van Rensburg. Thank you for organizing the accommodation and other aspects of the field trip. The work and effort that you have contributed is greatly appreciated.

- Thank you to the Staff and Students of the Hydrology Department for all the help and continuous support.

TABLE OF CONTENTS

LIST OF TABLES

Page

LIST OF FIGURES

LIST OF SYMBOLS

q_p = Pore water content (g/g)

r_{bd} = Dry soil bulk density (g/cm^3)

q_{LW} = Lattice water content (g/g)

$q_{SOC_{eq}}$ = Soil organic carbon water content (g/g)

r_v = Absolute humidity of air (g/m^3)

AL = Band specific additive rescaling factor

Ap = Band specific additive rescaling factor

BWE = Biomass water equivalent (mm)

CI = High-energy intensity correction factor

CP = Pressure correction factor

CS = Geomagnetic latitude scaling factor

CWV = Water vapour correction factor

d = Earth sun distance

E = Evaporation (mm)

e_o = Actual vapor pressure at surface (Pa)

es_o = Saturated vapor pressure at surface (Pa)

G_o = Soil heat flux energy (Wm^{-2})

H = Sensible heat flux energy (Wm^{-2})

H_{dry} = Sensible heat flux at the dry limit (Wm-^{2})

H_{wet} = Sensible heat flux at the wet limit (Wm^{-2})

I_o = Irrigation (mm)

$L\lambda$ = TOA spectral radiance (Watts/ (m2*srad*μm))

ML = Band specific multiplicative rescaling factor

Mp = Band specific multiplicative reflectance factor

Ms = Mass of soil (g)

Mt = Mass of total (g)

M_{vap} = Molar mass of water vapor (= 18.01528 g/mol = 0.01801528 kg/mol)

N = Corrected neutron counts (counts/hour)

N' = Raw moderated neutron counts (counts/hour)

Θ = Volumetric soil moisture ($m3.m^{-3}$)

Θ_r = Residual volumetric soil moisture ($m3.m^{-3}$)

Θ_{sat} = Saturated volumetric soil moisture ($m3.m^{-3}$)

P = Pressure (mb)

P_o = Precipitation (mm)

Ps = Particle density (g/cm3)

$p\lambda$ = TOA planetary reflectance

$p\lambda'$ = TOA planetary reflectance (without solar angle correction)

Qcal = Quantized and calibrated standard product pixel value (DN)

R = Universal gas constant (= 8.31432 J/mol/K)

RH = Relative humidity (%)

R_n = Net radiation (Wm^{-2})

R_{vap} = Gas constant for water vapor (J/K/kg)

T = Air temperature (^oC)

t = Time (s)

TC = Soil total carbon (g/g)

Ts = Land surface temperature (K)

Z = Vertical distance (m)

α = Land surface albedo (dimensionless)

ε_o = Surface emissivity (dimensionless)

Θ_{SE} = Local sun elevation (degrees)

λE = Latent heat flux energy (Wm^{-2})

λE_{dry} = The latent heat at the dry limit (Wm^{-2})

λE_{wet} = The latent heat at the wet limit (Wm^{-2})

Λr = Relative evaporation (dimensionless)

LIST OF ABBREVIATIONS

AMSR2	:	Advanced Microwave Scanning Radiometer
CRP	:	Cosmic Ray Probe
ESA	:	European Space Agency
ILWIS	:	Integrated Land and Water Information System
LST	:	Land Surface Temperature
NDVI	:	Normalized Difference Vegetation Index
PyTOPKAPI	:	Python Topographic Kinematic Approximation and Integration
SAHG	:	Satellite Applications and Hydrology Group
SEBAL	:	Surface Energy Balance Algorithm for Land
SEBS	:	Surface Energy Balance System
SMOS	:	Soil Moisture and Ocean Salinity
TDR	:	Time Domain Reflectometry
TOPKAPI	:	Topographic Kinematic Approximation and Integration
VWC	:	Volumetric Water Content

1. INTRODUCTION

There has been an incessant need to monitor and measure the various parameters in land surface hydrology, in order to deepen the understanding of hydrological processes, their importance in the hydrological cycle and their interactions between each other (Jackson *et al.*, 2010; Fang and Lakshmi, 2014). Soil moisture is an important parameter in the hydrological cycle and greatly impacts a variety of applications, including agricultural management, climate and weather applications, flood and drought prediction and groundwater recharge.

Although soil moisture does not directly contribute to the land surface energy balance, the properties associated with soil moisture have a strong influence on net radiation, and the partitioning between latent and sensible heat fluxes (Wang and Li, 2011). Soil moisture is a significant variable in the earth's water cycle, even though it holds a small percentage of the total global water budget (Guillem, 2010). Weather and climate applications rely greatly on soil moisture, consequently the predication accuracy of global weather forecast models and climate applications may increase, with improved estimates of soil moisture data (Guillem, 2010). Soil moisture is a key component in crop growth and is the prime regulator of a catchment's response to rainfall, as it partitions rainfall into infiltration and surface runoff (Vischel *et al.*, 2008; Zhao and Li, 2013). Due to the impacts of global change, numerous cycles, such as the hydrological cycle, have been pushed past their thresholds. Therefore, monitoring the soil moisture status of an area, such as a catchment, can assist in mitigating the negative effects of extreme environmental processes or phenomena, such as droughts and floods (Guillem, 2010).

Soil moisture is a difficult parameter to continuously monitor and measure at a catchment scale due to its heterogeneous characteristics. It varies both spatially and temporally and is thus a dynamic resource, which never remains constant. Currently, there are three methods of estimating soil moisture. These include: (a) ground-based (*in-situ*) measurements, which are carried out using field instruments; (b) remote sensing based methods, which use specialised sensors on satellites and aircrafts and (c) land surface models, which use meteorological data as inputs, at a predefined spatial resolution (Albergel *et al.*, 2012; Mecklenburg *et al.*, 2013). Inherently each of these methods possess their respective advantages and limitations, constraining their effectiveness for hydrological applications (Ni-Meister, 2005).

In-situ measurements of soil moisture are the conventional methods used by several disciplines. The point measurements obtained cannot adequately represent the spatial characteristics of soil moisture. However, these point measurements play a key role in a variety of large-scale applications and are invaluable as both calibration and validation data (Gruber *et al.*, 2013). In the past few years, the Cosmic Ray Probe (CRP) method, which is an *in-situ* instrument, has been developed and implemented in numerous countries across the globe (Kohli *et al.*, 2015). The CRP technique obtains the area-averaged soil moisture, at an intermediate scale, by observing and measuring the cosmic ray neutrons above the soil surface (Zreda *et al.*, 2012; Franz *et al.*, 2013).

Remote sensing can be described as the technique of obtaining information about an object or phenomena, with the use of special instrumentation from a distance, without making physical contact (Engman, 1991; Wagner, 2008; Mekonnen, 2009; Lakshmi, 2013). Remote sensing is extensively used today by several disciplines to observe and measure various environmental parameters. Hydrology is one such discipline, which uses remote sensing to measure parameters, such as rainfall, evaporation and surface temperature (Fang and Lakshmi, 2014). There are several remote sensing soil moisture estimating techniques, which use gamma, near infrared, microwave and thermal radiation. The passive microwave radiation technique is the most commonly used technique, as it has several advantages over other techniques. The passive microwave technique observes and measures the difference in dielectric constants of dry soil and water to estimate soil moisture (Jackson *et al.*, 2010; Lakshmi, 2013). Currently, the microwave remote sensing soil moisture products are available on a global scale; however, these products are limited by their coarse spatial resolution, which is inadequate for hydrological applications (Shin and Mohanty, 2013; Song *et al.*, 2013). Therefore, downscaling techniques have been researched and developed, to obtain soil moisture at a finer spatial resolution. (Lakshmi, 2013).

Models have been used to obtain estimates of soil moisture at an intermediate scale. A model implies a simplification of reality and aims to promote understanding, whilst simplifying and mimicking the real system. Soil moisture is an important variable in both the land surface energy and water balance and can be estimated from surface energy balance models, such as the Surface Energy Balance System (SEBS) and land surface water models, such as the Topographic Kinematic Approximation and Integration Model in Python (PyTOPKAPI).

The objective of this study is to review literature pertaining to the current methods of soil moisture estimation, which include *in-situ*, remote sensing and modelling. This is required to broaden the understanding of this field of study. This will aid in identifying the commonalities and gaps in the literature, as well as the key methods used and their limitations in the estimation of soil moisture. The key focal aspects of the literature review are to evaluate the CRP for use as a validation method. In addition, the current methods of remote sensing soil moisture products will be reviewed and the modeled soil moisture estimates will be analysed. The aim of the study is to test and evaluate the suitability of the CRP to provide spatial estimates of soil moisture in Cathedral Peak Catchment VI and use these estimates to validate satellite-based soil moisture estimates. Satellite-based soil moisture products comprise of remote sensing soil moisture products and models, which use remote sensing data as inputs.

The Research questions include:

i. How suitable is the CRP method in providing spatial estimates of soil moisture in Cathedral Peak Catchment VI?
ii. How well do remote sensing soil moisture products compare to the CRP estimates?
iii. How well do modelled soil moisture products compare to the CRP estimates?

The dissertation is divided into eight chapters, starting with the introduction in chapter one. The literature review is not a single chapter but is encompassed in chapters two, three, four and five. Chapter two outlines the *in-situ* methods of soil moisture measurement, which consists of conventional *in-situ* methods, as well as the CRP. Chapter three outlines the remote sensing of soil moisture and focuses on the current global soil moisture products. Chapter four outlines the use of modelling to obtain soil moisture estimates. Chapter five is the literature evaluation, which looks at the general themes in soil moisture measurements and evaluates the gaps in the literature reviewed. Chapter five is an important chapter, as it summarizes the evaluated literature and sets the foundation for the methodology, which is presented in chapter six. The methodology is presented in chapter six, which outlines the study area, as well as details the various procedures and techniques that were used in this research study. Chapter seven contains the results and discussion of the research study. The conclusions, limitations and recommendations of the study are discussed in chapter eight.

2. *IN-SITU* METHODS OF SOIL MOISTURE MEASUREMENT

The following section is the first component of the literature review. The remaining components of the literature review will be covered in the third and fourth chapters. A literature evaluation will be presented in chapter five.

In-situ soil moisture techniques are the conventional methods of soil moisture estimation. There are numerous *in-situ* techniques, both direct and indirect, which have been used to determine soil moisture. In recent years, the use of the CRP to measure soil moisture has gradually attracted attention and has been implemented in a number of countries across the world (Villarreyes *et al.*, 2013). The ensuing section will provide an analysis of the conventional methods of soil moisture estimation, which will be followed by a detailed review of the CRP.

2.1 Conventional Methods of Soil Moisture Estimation

In-situ soil moisture measurements have played a key role for a variety of large-scale applications and have been invaluable as calibration and validation data for satellite-based products, sensors and models (Gruber *et al.*, 2013). There are several conventional *in-situ* techniques used to estimate soil moisture, including the gravimetric method, neutron scattering and Time Domain Reflectance (TDR) (Walker *et al.*, 2004). Brief descriptions of the aforementioned techniques are discussed below:

i. The gravimetric method is a direct method of estimating the soil moisture content. This method consists of collecting soil samples at points at desired depths. The collected soil samples are then weighed, before being oven-dried for 24-72 hours at 105 ^{o}C, until all the moisture has been driven out of the sample. The dry samples are then re-weighed. The gravimetric soil moisture is then calculated by dividing the mass of water by the mass of dry soil.

   This method is commonly used as it has the advantage of being accurate, is independent of soil type and is easily calculated (Hillel, 2008). However, it is a destructive technique that is time and labour-consuming (Zazueta and Xin, 1994).

Due to its destructive nature, it does not allow for repetitive sampling at the same point. The method also requires a laboratory equipped with an oven and the time of the sample collection to the time that the samples are weighed has to be minimal, to avoid the loss of moisture from the soil (Hillel, 2008).

ii. The neutron scattering method is an indirect *in-situ* measurement, which has been used since the 1950's (Jones *et al.*, 2002). The neutron probe uses an active source of fast neutrons, which pass through the soil and collide with the soil media. These fast neutrons thus slow down with each collision and become slow neutrons. The majority of these fast neutrons collide with hydrogen in the form of water in the soil media. Thus, the more water present in the soil media, the more hydrogen and the more collisions occur. The measured slow neutrons are therefore proportional to the soil water.

iii. According to Zazueta and Xin (1994), this method has the advantage of being accurate (once calibrated) and able to measure soil profiles, with the measurement being directly related to soil moisture. However, the method is limited because of its cost, radiation hazard, the skills required and the difficulty to obtain accurate measurements near the surface, because it is time-consuming and its invasive nature, as access tubes have to be placed vertically into the soil profile.

iv. The TDR method is a common indirect *in-situ* method. According to Jones *et al.* (2002), there are different variations of TDR probes, but in general, the probe consists of two to three steel rods, which can be placed vertically or horizontally into the soil. The probe or logger sends out high frequency pulses in the Giga Hertz (GHz) range, which have a varying travel time along the wave guides(stainless steel rods), due to the dielectric constant of the medium in which the probe is placed. The dielectric constant is mostly dependent on the water content of the soil. The TDR probe is insensitive to soil composition and texture, due to the large disparity of dielectric constants, but needs calibration with soils with a high electrical conductivity (Jones *et al.*, 2002).

The TDR method is a commonly used and accurate method, due to its minimal calibration requirements, easily obtainable measurements, low cost compared to other

methods, and its ability to provide non-destructive continuous measurements (Jones *et al.*, 2002; Walker *et al.*, 2004). The TDR method is limited, as a calibration procedure is required, the depth measured is dependent on the length of the steel rod used and errors may occur from soil voids around the probes measurement area (Zazueta and Xin, 1994; Walker *et al.*, 2004) .

The major limitation of all conventional *in-situ* methods is that they provide point measurements, which do not account for the spatial characteristics of soil moisture (Qin *et al.*, 2013). Therefore, no single point measurement can be entirely representative of larger areas, because of the heterogeneity that exists in soil properties, topography and weather (Gruber *et al.*, 2013). In order to overcome this limitation, dense soil moisture networks can be set up. However, the high costs of operation and maintenance make the setup of the network financially unfeasible (Gruber *et al.*, 2013).

2.2 Cosmic Ray Probe

Understanding the variability of soil moisture, is of great interest for various disciplines (Villarreyes *et al.*, 2013). The CRP is a relatively new technique, which has the capability of providing soil moisture data for large-scale studies. It is the only *in-situ* technique that can obtain the average soil moisture content over hundreds of meters, something that would require a dense *in-situ* point measurement network (Zreda *et al.*, 2012; Ochsner *et al.*, 2013). The CRP method can play a vital role in the calibration and validation of satellite-based soil moisture retrievals and land surface models (Villarreyes *et al.*, 2013).

As shown in Figure 2.1, the CRP system comprises of neutron counters (moderated and bare tubes), a data logger which includes barometric pressure, humidity and temperature sensors, and a telemetry system with antenna to connect to an iridium satellite, and a battery and solar panel for powering the system.

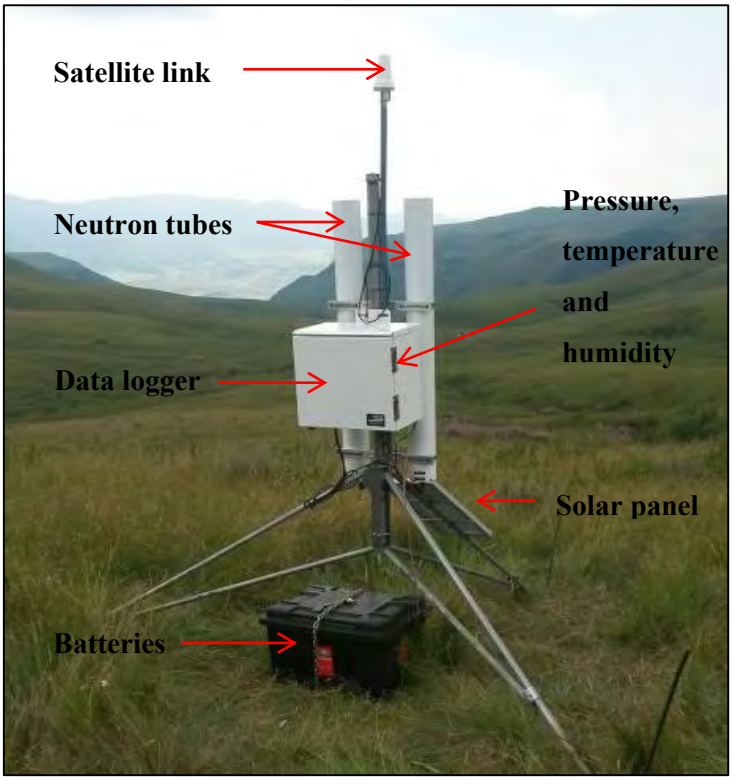

Figure 2.1 CRP system in Cathedral Peak Catchment VI

2.2.1 Production of cosmic ray neutrons

Cosmic ray neutrons originate in space, where they are produced by the blast waves of exploding stars. Shards of atoms are accelerated and energized, until they eventually reach a high enough speed to break away and escape to the galaxy. Some of these high energy particle flows in space reach the earth's atmosphere, where they are affected by the earth's magnetic field (Jiao *et al.*, 2014). The high energy particles are captured into the earth's atmosphere and collide with atmospheric nuclei to initiate a cascade of secondary cosmic rays (Ochsner *et al.*, 2013). Fast neutrons are created, as these secondary cosmic rays pass through the atmosphere and then through the top few meters of the biosphere, hydrosphere and lithosphere, (Desilets *et al.*, 2010).

These fast neutrons undergo elastic collisions with nuclei present in the soil, thereby losing energy (Desilets *et al.*, 2010). Some of the fast neutrons are adsorbed by the soil during the collision, whilst others will be scattered above the surface of the soil (Jiao *et al.*, 2014). The cosmic ray neutrons lose energy with each collision, therefore high energy neutrons become fast neutrons (in the atmosphere), which further lose energy and become thermal neutrons (in

the soil). Due to fast neutrons being strongly moderated by hydrogen present in the environment, their measured intensities relate to changes in soil moisture, as well as other hydrogen sources at the earth's surface (Zreda *et al.*, 2008; Zreda *et al.*, 2012; Franz *et al.*, 2013).

2.2.2 Moderation of neutrons

According to Ochsner *et al.* (2013) and Jiao *et al.* (2014) the moderation process of cosmic ray neutrons depends on three factors:

i. The scattering probability or the elemental scattering cross-section;
ii. The logarithmic decrement of energy per collision; and
iii. The number of atoms of an element per unit mass of material, which is proportional to the concentration of the element and to the inverse of its mass number.

The combination of the abovementioned factors, defines the neutron stopping power of a material (Ochsner *et al.*, 2013). Hydrogen, which is found mainly as water in the soil, plays the most significant role in moderating cosmic ray neutrons in the soil. Hydrogen has an extraordinary high stopping power, as the hydrogen atom has a high probability of scattering a neutron, due to its fairly large elastic scattering cross-section (Jiao *et al.*, 2014). Hydrogen is the most efficient element, with regards to the decrement of energy per collision and has a low atomic mass and makes up a substantial portion of all the atoms in many soils, due to the presence of water in the soil (Jiao *et al.*, 2014). The presence of water within the soil pores plays an important and central role in moderating the concentration of cosmic ray neutrons above the soil surface (Desilets and Zreda, 2013).

2.2.3 Cosmic ray probe measurements

The fast neutrons that are produced in the air and soil travel in all directions between the air and soil, thus creating an equilibrium concentration of neutrons. This equilibrium concentration is shifted due to changes (addition or subtraction) in the hydrogen content of the media. The soil moisture content is estimated by the concentration of low energy cosmic ray neutrons, which are generated within the soil and moderated predominantly by hydrogen,

before being diffused back into the atmosphere (Zreda *et al.*, 2008). The soil moisture content can therefore be inferred directly from these neutron fluxes (Desilets *et al.*, 2010).

Dry soils are highly emissive, so that neutrons are more efficiently removed from the soil (Zreda *et al.*, 2008). This results in more neutrons escaping to the surface of a dry soil, which will result in a higher concentration of neutrons above the soil surface, see Figure 2.2 (Franz *et al.*, 2012b).

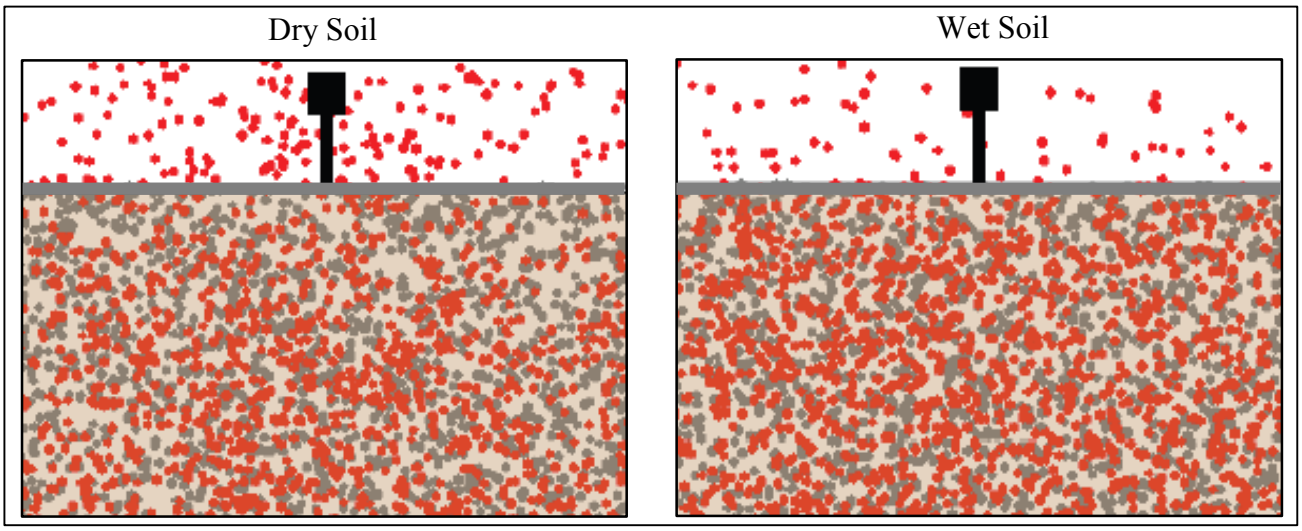

Figure 2.2 Difference in neutron concentration according to soil moisture content (Franz *et al.*, 2012b).

The CRP system consists of two sensors. The moderated sensor (encased in perspex) measures the fast neutrons, which are attributed to the soil moisture, whilst the bare tube measures the slow neutrons, which are attributed to the water above the soil surface (biomass and snow). The fast neutron intensity above the soil surface is inversely proportional to the amount of soil moisture in the soil surface (Kohli *et al.*, 2015).

2.2.4 Measurement footprint and depth of the cosmic ray probe

The CRP senses all hydrogen present within the distance that fast neutrons can travel in air, water, soil and other materials near the earth's surface. Thus, the measurement distance varies according to the density and chemical composition of the material (Ochsner *et al.*, 2013). The footprint (measurement area) of the CRP, is defined as the area around the probe from which 86% of the counted neutrons arise (Jiao *et al.*, 2014). The footprint is primarily associated

with the chemical and physical properties of the air and is inversely proportional to the air density (Jiao *et al.*, 2014).

The radial footprint of the CRP is reliant on the neutron's ability to travel hundreds of meters from their source, due to the neutrons scattering in the air (Kohli *et al.*, 2015). Hence the scattering properties of air significantly affect the diameter of the footprint (Jiao *et al.*, 2014). When the CRP is placed in a static position a few meters above the ground, it has a radial footprint of 670 meters in diameter at sea level (Zreda *et al.*, 2008). The radial footprint size is inversely proportional to the air density. At high altitudes, the air pressure is lower, which results in a larger footprint. The measurement diameter slightly decreases with increasing soil moisture and with increasing atmospheric water content (Jiao *et al.*, 2014).

The effective depth is the thickness at which 86% of counted neutrons arise, which depends strongly on the soil moisture content (Ochsner *et al.*, 2013). The measurement depth is inversely proportional to the soil moisture content. A measurement depth of 0.72 m is obtained in dry soil and a depth of 0.12 m is obtained in wet soil, so that the effective measurement depth decreases with increasing hydrogen. (Zreda *et al.*, 2008). The decrease in measurement depth according to an increase in soil moisture is nonlinear and the measurement depth is independent of the air density.

Due to the fact that neutrons react with any source of hydrogen near the earth's surface, the measured neutron intensity represents the total reservoir of neutrons present within the probe's sensing distance (Ochsner *et al.*, 2013). This includes snow, lattice water, water in soil organic matter, water in vegetation and atmospheric water vapour (Ochsner *et al.*, 2013). The measurement footprint and depth is shown in Figure 2.3.

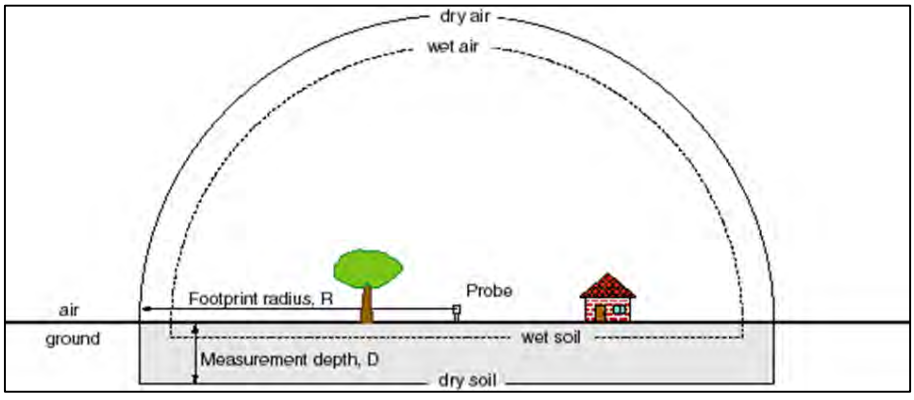

Figure 2.3 Measurement area and depth of CRP (Ochsner *et al.*, 2013)

The CRP can be used either in a fixed position or in a moving vehicle. The fixed position is used to obtain continuous measurements of an area, whilst the roving method can be used for mapping large areas (Dutta and D'este, 2013). The technique functions, as the neutron fluxes are a great proxy for land surface water (Desilets *et al.*, 2010). Along with the neutron count rate, the CRP also measures the internal temperature, relative humidity within the logger enclosure and external barometric pressure (Franz *et al*., 2013).

2.2.5 Advantages of the cosmic ray probe method

The CRP method has several advantages (Zreda *et al.*, 2008; Desilets *et al.*, 2010; Franz *et al.*, 2012b; Franz *et al.*, 2012a; Zreda *et al.*, 2012; Desilets and Zreda, 2013; Franz *et al.*, 2013; Jiao *et al.*, 2014), including:

Table 2.1 Advantages of the CRP

Advantages
The method is passive and non-contact (non-invasive)
The system is easily automated
The CRP is portable
It has minimal power requirements
Applications not limited to soil moisture (can be used to estimate above-ground biomass and snow depth)
The measurement footprint is at an intermediate scale
The measurement depth ranges from 0.12 m to 0.72 m
The method allows for continuous measurements to be obtained
The instrument is easily installed above-ground
The CRP provides excellent data sets
The CRP requires low data processing and transmission
The method is less affected by the presence of vegetation
The method is insensitive to soil texture, bulk density or surface roughness

The CRP is a fairly recent instrument used to obtain soil moisture estimates and seems to have no major limitation associated with it. However, the measurement depth and the calibration procedure could be potential limitations of the technique. The measurement depth is not set by the user, but is dependent on the soil moisture status of the measurement area. The measurement depth of the CRP is generally between 0.12 and 0.72 meters, therefore the CRP technique is limited to measuring soil moisture between this depth range. The calibration procedure is time and labour consuming and it needs to be done correctly in order to provide reliable soil moisture estimates.

The CRP calibration procedure is performed by obtaining corresponding measurements of area-averaged soil moisture and neutron intensity. The area-averaged soil moisture is obtained from many ground-based point measurements, by collecting several soil samples within the CRP measurement area and determining the average gravimetric soil moisture per calibration. The measured neutron intensities need to be adjusted and corrected for variations in location, incoming high-energy particles, atmospheric pressure, absolute humidity and changes in biomass (Franz *et al.*, 2015).

It is recommended that a calibration procedure is carried out for both the dry season and the wet season (Dutta and D'este, 2013). Representative soil samples of the measurement area are required to be analysed, to correct the calibration function for lattice water and water in organic matter (Ochsner *et al.*, 2013).

The potential applications of the CRP make it appealing to scientists in various fields, such as agricultural and ecological monitoring, streamflow forecasting, climate science, drought and flood forecasting, as well as slope stability (Desilets *et al.*, 2010). It should also be noted that the discipline of remote sensing can benefit greatly from this innovative technology, by using CRP measurements for both the calibration and validation of sensors and data products, as it overcomes the spatial limitations of conventional *in-situ* soil moisture estimates (Desilets *et al.*, 2010). The use of the CRP across different continents results in measurement technique consistency, which would reduce the uncertainties related to *in-situ* measurements that use a variety of probe types/methods (Kim *et al.*, 2015).

There have been a limited number of studies using the CRP, as the technique is fairly new. A summary of these studies is presented below:

i. Zreda *et al.* (2008) conducted a study in Arizona, USA, on the use of cosmic ray neutrons to estimate soil moisture at an intermediate spatial scale. The study concluded that the CRP permits high resolution long-term monitoring and the large radial measurement footprint makes the CRP method suitable for climate and weather applications, as well as for satellite sensor calibration.

ii. Desilets *et al.* (2010) looked at implementing the CRP in two ways. The CRP was used to provide stationary measurements in south-eastern Arizona and was used to provide roving measurements in Hawaii. The study concluded that both methods can be implemented with confidence.

iii. Desilets and Zreda (2013) investigated the lateral footprint of the CRP, using a combination of neutron transport simulations and the diffusion theory. The study concluded that the measurement footprint is linearly proportional to the sensor height above the ground and inversely proportional to the air density.

iv. Hawdon *et al.* (2014) conducted a study, which looked at the set-up and field calibration of the CRP at nine locations across Australia. The nine locations had contrasting soil types, land covers and climates. The results of the study indicated that the generalized calibration function is suitable for relating neutron counts to soil moisture and that it holds for all soil types, except for very sandy soils with lower water contents.

3. REMOTE SENSING OF SOIL MOISTURE

Remote sensing is currently used to measure various parameters of the hydrological cycle, such as rainfall, evaporation and soil moisture. Remote sensing is seen as a promising technique for soil moisture estimation, as it aims to address the spatial and temporal variability of soil moisture (Zhao and Li, 2013). It has the advantages of being able to measure large scale soil moisture, the data obtained has periodic data updates, its ability to monitor soil moisture in remote areas, its usability and its cost (Sabins, 2007; Mekonnen, 2009; Lakshmi, 2013). The major limitation to the implementation of remote sensing in critical hydrological application is its coarse resolution. The following section gives an overview of the common remote sensing of soil moisture products. This is followed by an analysis and evaluation of the current downscaling techniques that have been developed to obtain soil moisture at a finer spatial resolution.

3.1 Overview of Remote Sensing of Soil Moisture

There are several remote sensing techniques that have been developed and applied, which include gamma radiation, thermal infrared, near infrared and microwave radiation techniques (Albergel *et al.*, 2012). Each technique measures a different land surface quantity, uses a different range of the electromagnetic spectrum and has its own unique advantages and limitations (Mekonnen, 2009). From past research studies, it is evident that the microwave radiation technique, which consists of both active and passive methods, can be considered as the most promising technique for the remote sensing of soil moisture. This is due to its advantages over the other techniques, such as its all-weather capability, large spatial coverage, temporal resolution, measurement depth and vegetative penetration (Wagner, 2008; Wang and Qu, 2009; Guillem, 2010).

Microwave radiation remote sensing observes the large contrast in the dielectric properties of soil particles and water, as well as the dielectric constant increases, as the soil moisture increases (Mekonnen, 2009; Wang and Qu, 2009). Remote sensing does not measure the soil moisture content directly, therefore mathematical models that describe the association between the measured signal and the subsequent soil moisture need to be derived (Wang and Qu, 2009). Over the past few decades, active and passive microwave remote sensing has provided the unique ability to obtain estimates of soil moisture on a global scale (Brocca *et*

al., 2013). The L-band range (1 to 10 GHz) is preferably used, as higher frequencies are more affected by perturbation factors, such as vegetation cover and atmospheric effects (Albergel *et al.*, 2012). There have been many research studies on microwave remote sensing products over the past few decades. These products include Soil Moisture and Ocean Salinity (SMOS), the Advanced Microwave Scanning Radiometer (AMSR2), European Remote Sensing Satellite (ERS-1/2) and Advanced Scatterometer (ASCAT) (Dorigo *et al.*, 2011).

The remote sensing of soil moisture has advanced and the product user's trust in the remote sensing data has increased, as there has been continuous improvements to sensors and the algorithms used to estimate soil moisture (Brocca *et al.*, 2013). The launch of the SMOS satellite, which was the first satellite radiometer dedicated to measure soil moisture over land, emphasized the increased need for the measurement of soil moisture. This is further highlighted by the anticipated launch of the Soil Moisture Active Passive (SMAP) satellite in 2014 (Jackson *et al.*, 2010; Lakshmi, 2013; Song *et al.*, 2013; Fang and Lakshmi, 2014).

Currently, there are several remote sensing soil moisture products. The two most frequently utilized products that appear in recent research literature, are the AMSR/AMSR-E (predecessors of the AMSR2) and SMOS soil moisture products (Brocca *et al.*, 2013). These two products will be detailed in the subsequent sections.

3.2 AMSR2

The global change observation mission (GCOM) is a project for the global long-term monitoring of the earth's environment. The GCOM consists of two satellites, namely, the GCOM-W and GCOM-C. The GCOM-W1 satellite was launched on the 18th of May 2012 and is equipped with the AMSR2 sensor (Kim *et al.*, 2015). The AMSR2 sensor on the GCOM-W1 satellite, as seen in Figure 3.1, is the successor to the AMSR sensor on-board the ADEOS-II satellite, which has been operational from December 2002 to October 2003 and the AMSR-E sensor, on-board the AQUA satellite, which has been operational from May 2002 to October 2011 (JAXA, 2013a). The basic performance of AMSR2 will be similar to that of AMSR-E, based on the minimum requirement of data continuity (Imaoka *et al.*, 2010).

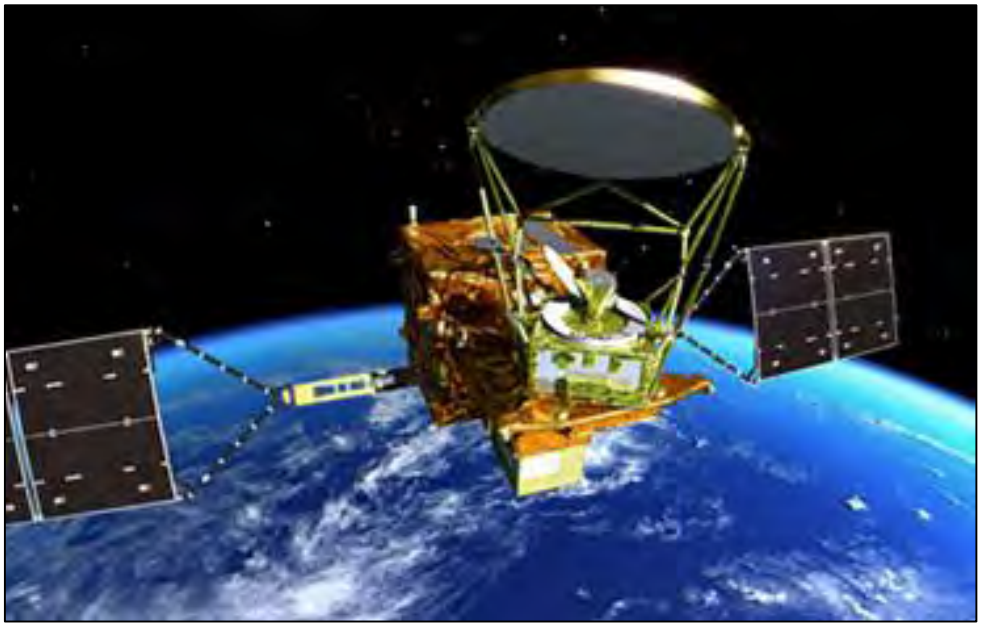

Figure 3.1 AMSR2 sensor on-board the GCOM-W1 satellite

The AMSR2 sensor is a passive microwave scanning radiometer that makes observations at multiple polarizations (both horizontal and vertical) and seven frequency bands, ranging from 6.9 GHz to 89 GHz (Kim *et al.*, 2015). It obtains multi-band observations from the C, X and K bands (Lu *et al.*, 2014). The waves observed are weak and are radiated from the atmosphere and the earth's surface. It orbits 700 km above the earth's surface and has a swath of 1450 km. Its antenna rotates once every one and a half seconds, which creates a conical scan pattern, with a scanning interval of 10 km. The scanning method is capable of making one day (ascending) and one night (descending) observation, covering more than 99% of the earth's surface in two days (Lu *et al.*, 2014).

The AMSR2 sensor estimates several of the parameters, which are predominantly linked to the energy and water cycles, such as precipitation, water vapour, sea-surface temperature, soil moisture and snow depth. The AMSR2 sensor is more advanced than its predecessors (AMSR and AMSR-E). It has a larger main reflector with a 2.0 m antenna diameter, which results in a finer spatial resolution, the addition of a new 7.3 GHz channel to eliminate electro-magnetic wave interference, an upgraded calibration system and it has intensive sunlight shielding, to avoid calibration uncertainties (Imaoka *et al.*, 2010; JAXA, 2013a; Kim *et al.*, 2015)

According to JAXA (2013b), the AMSR2 Level Two soil moisture product uses auxiliary data in the form of global vegetation coverage ratios. It also uses AMSR2 Level One products, which include 10.6 GHz brightness temperatures (horizontal and vertical polarisations), 36.5 GHz brightness temperatures (horizontal polarization), latitude and longitude and observation date.

The AMSR2 Level Two algorithm uses a simple radiative transfer model. The satellite observed brightness temperature (TB) at the 10.7 GHZ and 36.5 GHz channels, measures the natural microwave emissions from the land surface (Kim *et al.*, 2015). The algorithm assumes that the soil temperature is equal to the vegetation canopy temperature and a constant value of 293 K is used throughout the year (Kim *et al.*, 2015). The AMSR2 soil moisture algorithm assesses the vegetation effects on microwave emissions paths. This is important, as vegetation holds a large amount of moisture and thus needs to be evaluated in order to estimate soil moisture from satellite data. The soil moisture algorithm uses the polarization index and the index of soil wetness, obtained from TB, to simultaneously estimate soil moisture and vegetation moisture. With regards to vegetation, the algorithm uses a look-up table method, where a linear relationship between vegetation water content and optical depth is applied (Kim *et al.*, 2015). A dielectric mixing model is used in the algorithm to convert the dielectric constant into soil moisture content (Kim *et al.*, 2015).

3.3 SMOS

The SMOS satellite system, which is illustrated in Figure 3.2, was launched in November 2009 and consists of a space-borne passive microwave L-band (1.4 GHz) interferometric radiometer (Albergel *et al.*, 2012). The overall aim of SMOS is to provide global surface soil moisture maps with an accuracy of 4% at a 35 – 50 km spatial resolution (Parrens *et al.*, 2012). The SMOS satellite has the ability to obtain measurements at multiple angles, which allows for the retrieval of additional parameters (Kerr *et al.*, 2012). The SMOS system is a Y-shaped instrument, which consists of 69 antennae. The antennae are equally spaced along three arms and view the surface of the earth either through full, or two polarized radiances, in order to provide a full image (Gruhier *et al.*, 2011).

Figure 3.2 SMOS satellite

SMOS operates by measuring the phase difference of radiation from various incident angles, so that the earth's surface is frequently viewed at different angles and polarizations (Fang and Lakshmi, 2014). The SMOS soil moisture product has an average spatial resolution of 40 km; however, this varies from 30-50 km due to, the target area being viewed from multiple angles (Kerr *et al.*, 2010). SMOS has a sun-synchronous orbit at an altitude of 757 km, consequently, the entire earth is covered at least twice in three days, with orbit overpasses at 6:00 (ascending) and 18:00 (descending) local standard time (Leroux *et al.*, 2013; Qin *et al.*, 2013).

L-band radiometry has a high potential for the estimation of surface parameters and has been recognised as the most promising technique to monitor soil moisture over land surfaces and at a global scale (Kerr *et al.*, 2012; Parrens *et al.*, 2012). The L-band is the optimum wavelength range to observe soil moisture, as higher frequencies are more affected by perturbing factors, including atmospheric effects and vegetative cover (Parrens *et al.*, 2012; Mecklenburg *et al.*, 2013). The microwave signal at L-band frequency is primarily driven by surface soil moisture (top 5 cm), effective surface temperature and vegetative opacity, with smaller effects from the atmosphere and surface characteristics, such as bulk density, soil texture and surface roughness (Kerr *et al.*, 2012; Leroux *et al.*, 2013). The soil moisture retrieval algorithm needs to account for all these effects (Kerr *et al.*, 2012).

The SMOS Level Two retrieval algorithm is physically-based and complex. It uses the polarizations and multi-angular information derived by the SMOS satellite and involves the use of decision trees and direct model inversions (Parrens *et al.*, 2012). The retrieval algorithm was designed to be easily improved and uses SMOS Level 1C data as input and uses two types of auxiliary data, namely, static data (soil texture) and dynamic data (temperature) (Kerr *et al.*, 2012). SMOS provides multi-angular microwave polarimetric brightness temperature (T_B), from which a surface soil moisture product is derived (Parrens *et al.*, 2012).

The L-band microwave emission of the biosphere model, which simulates the microwave emission at L-Band range from the soil-vegetation layer is a key component of the retrieval algorithm (Parrens *et al.*, 2012). This is important, as the major difficulty in the estimation of soil moisture, using microwave radiometry is due to the presence of dense overlying vegetation, which attenuates the soil emission and adds its own emission (Parrens *et al.*, 2012).

The retrieval algorithm is based on an iterative approach. The aim of the algorithm is to reduce a cost function, the focal constituent of which is the sum of the squared weighted difference between measured T_B and Modelled T_B for a collection of incidence angles (Kerr *et al.*, 2012). In order to reduce this cost function, the most suitable set of parameters needs to be determined and used to drive the T_B model.

Current remote sensing soil moisture products have a spatial pixel grid between 10 to 50 km. The major issues in the calibration and validation procedure, when using *in-situ* point measurements, are the vertical and horizontal scaling issues. The vertical scaling issues occur when remote sensing soil moisture (top 0.05 m) is calibrated and validated against *in-situ* soil moisture measurements (0.00 to 2.00 m) (Jackson *et al.*, 2010). Therefore, the measurements are at different depths, which is a problem, as soil moisture varies with depth. The horizontal scaling issues occur when a point measurement is used to validate a remote sensing area-averaged value. The assumption that the point is representative of a large area can be conceded to be incorrect, due to the spatial variability of soil moisture (Gruber *et al.*, 2013). Therefore, there needs to be a shift to area-averaged *in-situ* methods, to validate and calibrate remote sensing data.

There have been numerous studies on passive microwave remote sensing for soil moisture estimation. The AMSR-E product is a frequently-used product in past studies. Research studies that have evaluated surface soil moisture derived from AMSR–E, have shown promising results (Koike *et al.*, 2004; Draper *et al.*, 2009; Zhang *et al.*, 2011; Qin *et al.*, 2013). Previous literature has mentioned the launch of the SMOS satellite and how it emphasizes the value of soil moisture estimation in the science field. SMOS data have been used in studies which have shown its potential for accurately obtaining soil moisture measurements (Gruhier *et al.*, 2011; Merlin *et al.*, 2012; Wagner *et al.*, 2012; Mecklenburg *et al.*, 2013; Qin *et al.*, 2013). Over the past few decades, there have been many studies involving both the calibration and validation of remote sensing soil moisture products to *in-situ* soil moisture measurements (Jackson *et al.*, 2010; Brocca *et al.*, 2011; Fang and Lakshmi, 2014). The following are some of the remote sensing based soil moisture product studies:

i. The AMSR2 soil moisture product has been used in a recent study by Lu *et al.* (2014), which presented a revised soil moisture retrieval algorithm of AMSR2 and aimed at improving the soil moisture estimates in dry regions. The study concluded that the revised algorithm is effective in overcoming the over-estimation of soil moisture in desert regions.

ii. A recent study by Kim *et al.* (2015) assessed two versions of the AMSR2 soil moisture product. The AMSR2 product from the Japan Aerospace Exploration Agency (JAXA) and Land Parameter Retrieval Model (LPRM) from the VU University Amsterdam, were used and compared on a global scale against field measurements. The study used CRP measurements from the COSMOS. It concluded that the JAXA AMSR2 product has a relatively better performance under dry conditions; however, the JAXA algorithm generally under-estimates the ground soil moisture. It also indicated that there is a need to improve both the algorithms and that a combined product could provide better estimates of soil moisture.

iii. A study by Leroux *et al.* (2013), compared the SMOS, AMSR-E and ASCAT soil moisture products over four watersheds in the United States for the year 2010. The study concluded that the SMOS product correlated the closest to ground

measurements, the AMSR-E product gives reasonable results in terms of correlation and the ASCAT product was unstable.

iv. A study conducted by Albergel *et al.* (2012) evaluated the ASCAT and SMOS products against *in-situ* soil moisture observations from over 200 stations across the world for the year 2010. A similar study was conducted by Brocca *et al.* (2011), which evaluated the ASCAT and AMSR-E satellite-based soil moisture products around Europe. The main purpose was to evaluate the potential of different ASCAT and AMSR-E products in obtaining reliable estimates of soil moisture. The study concluded that the AMSR-E LPRM provided the best results.

3.4 Downscaling Techniques

Microwave remote sensing is extensively used to obtain regional soil moisture estimates, although its application is greatly restricted by its coarse resolution (Zhao and Li, 2013). There have been several research studies undertaken to downscale satellite-based soil moisture estimates for use in hydrological applications (Song *et al.*, 2013). Downscaling is relevant, as the coarse resolution is at tens to hundreds of kilometres, whereas hydrological processes occur at spatial scales of centimetres to kilometres (Shin and Mohanty, 2013).

Satellites have the capability to observe and monitor large areas. The subsequent observational spatial resolution is dependent on the microwave frequency used, the dimensions of the antenna and the height of the satellite above the earth's surface (Piles *et al.*, 2011). There is a trade-off between the temporal and spatial satellite resolution; as the sensor height decreases, the spatial resolution increases and the temporal resolution decreases (Merlin *et al.*, 2012).

Over the past decade, a number of downscaling techniques, with varying degrees of complexity, have been researched and developed (Merlin *et al.*, 2008). An extensive research paper by Lakshmi (2013) outlines the key publications on current methods used to downscale passive microwave remote sensing soil moisture products. These studies have reviewed downscaling procedures, with the use of MODIS sensor-derived parameters, including surface temperature, vegetation and other ground surface parameters.

The consistent theme, with regards to downscaling procedures, which is identified in these key publications, is the combined use of passive microwave data with fine-scale optical data (surface temperature and vegetative indexes). The overall aim of these downscaling techniques are to provide soil moisture estimates at the same accuracy as the input remote sensing soil moisture product, but at the spatial resolution of the optical data used. These key downscaling publications are evaluated and summarized in Table 3.1 below.

Table 3.1 Evaluation of downscaling techniques

Author	**Merlin *et al***	**Piles *et al***	**Merlin *et al***	**Merlin *et al***
Year	2012	2011	2010	2009
Region	Yanco, South-eastern Australia (2010)	Yanco, South-eastern Australia (2010)	Yanco, South-eastern Australia (2006)	Yanco, South-eastern Australia (2006)
Input data	MODIS (LST, emissivity, NDVI and Albedo)	MODIS VIS/IR data (LST and NDVI)	MODIS (LST, red and infrared reflectance and NDVI)	Wind speed, MODIS data (surface temperature, NDVI), ASTER (radiometric surface temperature)
Product	SMOS	SMOS	SMOS	Simulated SMOS
Output resolution (km)	1	10 and 1	4	0.5
Methodology	sequential model	Build model between NDVI, LST and soil moisture	Relationship between soil moisture and soil evaporative efficiency	sequential model
Results	R^2 = 0.70-0.85 in summer, however very poor results obtained in winter	R^2 of 0.14-0.21, RMSE is between 0.9-0.17	Mean slope between simulated and observed is 0.94, with an error of 0.012	R^2 of 0.68, RMSE of 0.062, bias of 0.045

The evaluation of the abovementioned methods highlights significant limitations, which hinder the successful application of the various downscaling procedures that have been developed. These include (a) observational days have to be cloud-free, to avoid obscurities in data retrieval; (b) the presence of vegetation interferes with land surface temperature retrieval; (c) there is a difference in the input data sensing depth; and (d) the model assumptions may not be valid in heterogeneous areas (Merlin *et al.*, 2008; 2009; 2010; Piles *et al.*, 2011).

From the evaluation of these downscaling techniques, several comparisons can be made. Firstly, all of the downscaling research studies were conducted in the same region; this simplifies the evaluation process between the different techniques used. It can be noted that the technique used by Piles *et al*. (2011) requires the least data input, while the technique used by Merlin *et al*. (2009) requires the most input data. All the techniques use SMOS data or a simulated SMOS data set, as the SMOS satellite is the most recent soil moisture satellite. The evaluation between the methods is enhanced due to the common aspects of the research studies.

The differences in the evaluated techniques can be seen in their methodologies, output resolutions and results. Merlin *et al*. (2012) had an output resolution of 1 km and showed good results in summer; however, the technique performed very poorly in winter, when compared to *in-situ* soil moisture data. Piles *et al*. (2011) had an output resolution of 1 and 10 km, but performed poorly, when compared to *in-situ* soil moisture data. The Merlin *et al*. (2010) resulted in the best correlation between observed and simulated soil moisture. Merlin *et al*. (2009) showed good correlation and had the finest resolution.

The limitations of the downscaling process can be summarized as follows:

i. The accuracy of the soil moisture product may decrease as the spatial resolution increases (there is a trade-off between obtaining accurate data and obtaining fine resolution products);
ii. The process requires input data, which may not be freely or readily available;
iii. The technique may be site-specific;
iv. The complexity of the algorithms used; and
v. Cloud-free images are required, if MODIS products are used.

In recent years, the need for fine resolution soil moisture products has resulted in numerous downscaling research studies being conducted. The main publications in this field have been studies conducted by Merlin *et al*. (2009; 2010; 2012) and Piles *et al*. (2011). In addition to these, more recent studies have been conducted, which are based on the same principles of the key techniques. However, there are slight variations, in order to improve and build upon these key approaches. The new studies include:

i. A study conducted by Zhao and Li (2013) aimed to develop a downscaling method to improve the spatial resolution of the AMSR-E derived soil moisture product. The approach was based upon the conventional method of the microwave-optical synergistic technique, which uses LST, vegetative indexes and albedo. This approach replaces LST with two temperature temporal variation parameters. The study was conducted in the Iberian Peninsula for the year 2007. The results showed an improvement in the approach (R^2 increased by 0.08), when the new approach was compared to the conventional method.

ii. A recent study by Ruiz *et al.* (2014) was conducted on combining SMOS visible and near infrared satellite data for high resolution soil moisture over a two-year period in the REMEDHUS network in Spain. The study used a new downscaling algorithm, based on a relationship between LST, NDVI and brightness temperature. The study aimed to obtain a downscaled image with the same accuracy of SMOS, but at the spatial resolution of MODIS (500 m). The best result obtained was a correlation with the *in-situ* measurements of 0.72.

4. METHODS OF MODELLING SOIL MOISTURE

Land surface water and surface energy balance models have been used to estimate soil moisture, as surface soil moisture plays a significant role in controlling the land-atmosphere water and energy fluxes (Walker and Houser, 2000). Several models have been used to obtain soil moisture estimates. These include the Variable infiltration capacity (VIC) hydrological model, the Decision support system for agro-technology transfer crop model (DSSAT), the climate water budget (CWB), the SEBS, PyTOPKAPI and the Surface Energy Balance Algorithm for Land (SEBAL) (Meng and Quiring, 2008; Mengistu *et al.*, 2014). The VIC, DSSAT and CWB are complex models, which require a large amount of input data (Meng and Quiring, 2008). The SEBAL Model is not freely available to apply due to its intellectual property rights (Mengistu *et al.*, 2014).

The following section describes the use of the PyTOPKAPI Model soil moisture product and the SEBS Model to obtain soil moisture estimates. The PyTOPKAPI Model was selected, as it has been used in South Africa. It is able to provide estimates with a fine spatial and temporal resolution and the estimates are readily available. The SEBS Model was selected, as it is an open-source model, it is easy to use and has been validated in several studies internationally and in South Africa.

4.1 Land Surface Model (PyTOPKAPI)

Soil moisture is a significant parameter in the hydrological cycle and is the prime regulator in a catchment's response to precipitation, as it partitions precipitation into infiltration and surface runoff (Vischel *et al.*, 2008). The topographic kinematic approximation and integration (TOPKAPI) model was developed by Liu and Todini (2002). The model is fully distributed and physically-based, as it represents hydrological processes on grid cells, on the basis of soil physics and fluid mechanics (Vischel *et al.*, 2008). The TOPKAPI Model has been adapted to perform simulations in land surface modelling mode and its model code has been adapted, so that it operates as a collection of cells (Sinclair and Pegram, 2010). Each cell is independent of its neighbours and has a plan area of 1 km x 1 km, with a 0.125^{o} grid spacing (Sinclair and Pegram, 2010). Each grid cell comprises of three key reservoirs (soil, overland, channel), as seen in Figure 4.1, which are determined by combing the physically-

based mass and continuity equations under the estimate of the kinematic wave model (Vischel *et al.*, 2008).

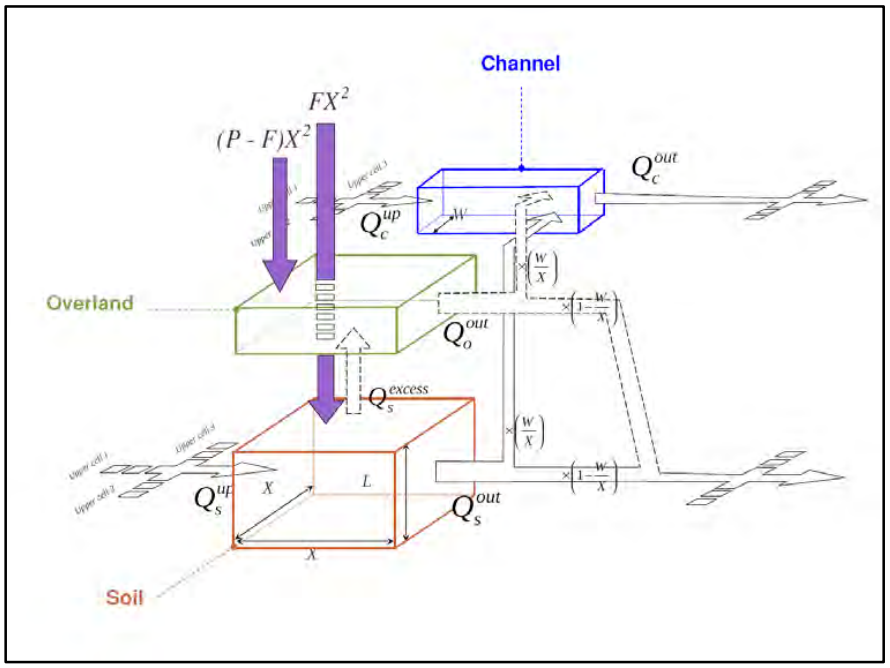

Figure 4.1 A schematic of the water transfer in a typical PyTOPKAPI model cell (Sinclair and Pegram, 2012)

The model is forced by time varying estimates of total evaporation and rainfall for each model cell (Sinclair and Pegram, 2012). The total evaporation forcing is based on the modification of the FAO56 reference crop evaporation, whereas the rainfall forcing is applied in the TRMM 3B42RT product, which is automatically downloaded from the NASA server and processed locally (Sinclair and Pegram, 2010).

There are six fundamental assumptions on which the TOPKAPI model is based on (Vischel *et al.*, 2008):

i. Precipitation is spatially and temporally constant over the integration domain;
ii. Unless the soil is already saturated, all precipitation falling on the soil infiltrates;
iii. The slope of the groundwater table corresponds with the slope of the ground;
iv. The saturated hydraulic conductivity in the soil surface layer is constant with depth;
v. Local transmissivity; and
vi. During the transition phase, the variation in water content in time is constant in space.

The TOPKAPI Model has been adapted to South African conditions. A land surface model was developed, with the final product being the freely available open source software package, known as the PyTOPKAPI (Sinclair and Pegram, 2013). The PyTOPKAPI Model is rainfall-runoff model used to examine the soil moisture dynamics at different scales, ranging from catchment to national scale (Sinclair and Pegram, 2013b).

The PyTOPKAPI Model uses three sets of input data, which consist of the meteorological, static and remote sensing data sets, as seen in Figure 4.2 (Sinclair and Pegram, 2010). The meteorological input data include the calculation of reference crop total evaporation and require parameters, such as relative humidity, temperature, solar radiation flux and wind speed (Sinclair and Pegram, 2010). The static input data required are the digital elevation models, land cover and soil properties. The input remote sensing data required are the rainfall and NDVI products on a three-hour temporal scale. In addition, the solar radiation flux from the meteorological input data is a satellite-based product and can be considered as a remote sensing product (Sinclair and Pegram, 2012).

The PyTOPKAPI is an automated modelling system, which produces national estimates of total evaporation and soil moisture at a three-hour time step over South Africa on a 0.125° spatial grid (Sinclair and Pegram, 2010).

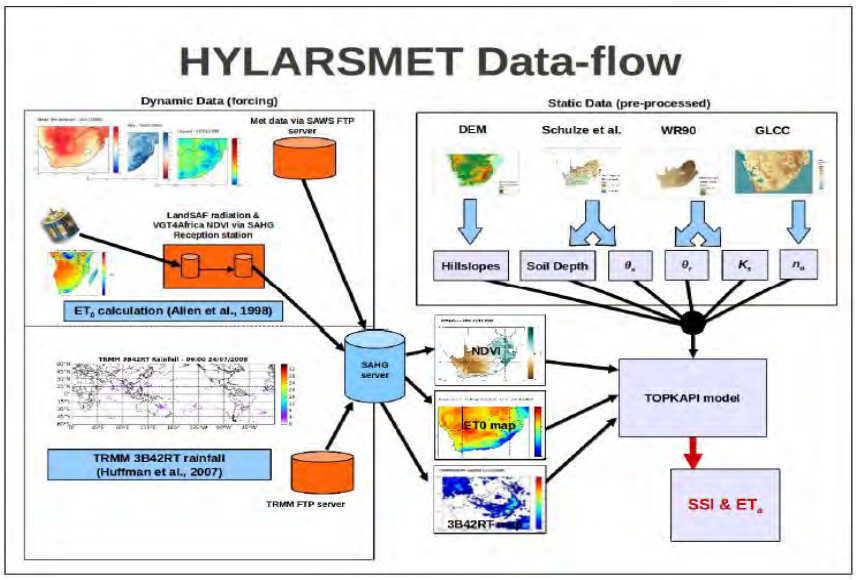

Figure 4.2 Data-flow diagram showing sources of the dynamic and static data to produce the main information streams (Sinclair and Pegram, 2010).

The purpose of the computation is to obtain a Saturated Soil Index (SSI), which is defined as the percentage of the soil voids occupied by water.

$$SSI = 100 * \left(\frac{\theta - \theta_r}{\theta_{sat} - \theta_r}\right) \quad (4.1)$$

Where Θ is the volumetric soil moisture, Θ_r is the residual soil moisture and Θ_{sat} is the saturated soil moisture.

In the original design, Liu and Todini (2002) created the model in such a manner, that whether the soil store was saturated or not, all rainfall during the computational interval was added to the soil store. At the end of the interval, an inventory was made and if the store was full, the excess was assigned to overland and channel stores. Then, based on the content of the soil store, the drainage was sent to the downslope store (Sinclair and Pegram, 2013a). This resulted in two effects: the soil store was always depleted at the end of the computation interval and surface runoff only occurred once the soil store was full, independent of rainfall intensity (Sinclair and Pegram 2013).

In the adaption of the TOPKAPI Model to South African conditions, the first effect was cancelled by modifying the continuity equation, so that there was ponding in the overland store, which resulted in the soil store remaining full after computation (Sinclair and Pegram, 2013a). The second effect was dealt with the introduction of the Green-Ampt infiltration model, which gave the PyTOPKAPI Model the ability to generate rapid overland flows in response to intense rainfall events (Sinclair and Pegram 2013).

The benefits of using this model are that the soil moisture estimates obtained have a temporal resolution of three hours and a spatial resolution grid ≈ 12.5 km. This finer temporal and spatial resolution better accounts for the heterogeneity of soil moisture, compared to the current global remote sensing of soil moisture products.

There have been research studies that reviewed the estimation of soil moisture through land surface modelling.

i. Sinclair and Pegram (2010) conducted a study, which aimed to compare soil moisture estimates from two independent sources over South Africa. The first soil moisture estimate was provided by automated real-time estimates from the TOPKAPI hydrological model. The second set of soil moisture estimates was from the ASCAT remote sensing product.

ii. A similar study was conducted by Vischel *et al.* (2008) in the Liebenbergslvei Catchment in South Africa, which compared soil moisture estimates derived from the TOPKAPI Model with European remote sensing satellite-based soil moisture estimates. Both studies concluded that the modeled soil moisture measurements correlated well, when compared to remote sensing soil moisture measurements.

iii. More recent studies, conducted by Sinclair and Pegram (2013), evaluated the sensitivity of the PyTOPKAPI Model to systematic bias in the variables of soil properties, evapotranspiration and rainfall. This was achieved by analysing 7200 sites within South Africa for a two-and-a-half year simulation period. The study concluded that the model is robust to errors in forcing parameters.

iv. A study conducted by Mengistu *et al.* (2014) involved the validation of variables of the PyTOPKAPI Model. The aims of the study were to provide data for the soil moisture mapping of South Africa, using the PyTOPKAPI Model. The purpose was to provide accurate field and satellite estimates of total evaporation and soil moisture for the calibration of the model and to evaluate the spatial variability of soil moisture at a catchment scale.

4.2 Surface Energy Balance System (SEBS)

Over the past few decades, several methods of estimating evaporation have been developed and implemented (Ma *et al.*, 2012). The SEBS Model was developed by Su (2002) for the estimation of atmospheric turbulent fluxes and surface evaporative fraction, using remote sensing data (Su *et al.*, 2003). The SEBS Model is physically-based, has the advantage of being less site-specific, open-source, it has been applied extensively (especially as an academic tool for research purposes) and does not require subjective intervention by the model user (Gokman *et al.*, 2012).

The model requires three sets of informational input data. The first set comprises of albedo, temperature, leaf area index and vegetation coverage (Su, 2002). In cases where this information is unavailable, the NDVI and the vegetation height are used instead. These informational inputs can be obtained from remote sensing data, in conjunction with additional land surface information. The second set of information comprises the reference boundary layer height (Su, 2002). The third set of input data required is the downward solar and long-wave radiation, which are obtained either from direct measurement, parameterization or model output (Su, 2002).

The SEBS Model consists of numerous individual components, to estimate the net radiation and soil heat flux and to partition the available energy into latent and sensible heat fluxes. The Surface Energy Balance is expressed as follows (Equation 4.2) (Wang and Li, 2011):

$$R_n = G_o + H + \lambda E \quad (4.2)$$

Where R_n = net radiation, G_o = soil heat flux, H = sensible heat flux and λE = latent heat flux.

The considerations of the surface energy balance, at limiting cases, are used to determine the relative evaporation (Wang and Li, 2011). When the dry limit is considered, the latent heat is zero and the sensible heat flux is at its maximum (Wang and Li, 2011):

$$\lambda E_{dry} = R_n - G_o - H_{dry} \equiv 0$$

$$H_{dry} = R_n - G_o \quad (4.3)$$

When the wet limit is considered, evaporation occurs at a maximum rate, whilst the sensible heat flux takes the minimum value (Wang and Li, 2011):

$$\lambda E_{wet} = R_n - G_o - H_{wet} \quad (4.4)$$

The relative evaporation can be expressed as (Su *et al.*, 2003):

$$\Lambda_r = \frac{\lambda E}{\lambda E_{wet}} = 1 - \frac{\lambda E_{wet} - \lambda E}{\lambda E_{wet}} \quad (4.5)$$

By substituting Equations 4.2 – 4.4 in Equation 4.4 and rearranging (Su *et al.*, 2003):

$$\Lambda_r = 1 - \frac{H - H_{wet}}{H_{dry} - H_{wet}} \quad (4.6)$$

Applying the mass conservation principle and integrating with respect to depth and time increments (Su *et al.*, 2003):

$$\int_{z1}^{z2} \theta(z, t2)dz - \int_{z1}^{z2} \theta(z, t1)dz = Q(z1) - Q(z2) \quad (4.7)$$

where θ is the volumetric soil moisture content, t is the time and z is the vertical distance. Applying Equation 4.7 with boundary conditions Q (z1) = P_o + I_o –E at the soil surface and Q (z2) = I_c at the bottom of the rooting zone. The change in soil water content can be expressed as (Su *et al.*, 2003):

$$\Theta(t2) - \Theta(t1) = Po + Io + Ic - E \quad (4.8)$$

where Θ is the volumetric soil water content in the rooting zone, P_o is the precipitation, I_o is the irrigation, I_c capillary flux and E is evaporation. The water balance is then considered at limiting cases. The wet limit is saturation, so that Θ (t1) = Θ_{wet}. At the dry limit Θ (t2) = Θ_{dry}, the evaporation is zero. From Equation 4.8 (Su *et al.*, 2003):

$$\Theta_{wet} - \Theta_{dry} = Ic_{wet} - E_{wet} \quad (4.9)$$

For any time between the two boundary conditions:

$$\Theta - \Theta_{dry} = Ic_{wet} - E \quad (4.10)$$

Manipulating Equation 4.9 and Equation 4.10 (Su *et al.*, 2003):

$$\frac{\Theta - \Theta_{dry}}{\Theta_{wet} - \Theta_{dry}} = \frac{E - Ic}{E_{wet} - Ic_{wet}} \quad (4.11)$$

It is assumed that the capillary flux is linked to the soil texture and is less than that of the uptake of root water ($I_c = I_{wet}$). By defining $R_\theta = \Theta / \Theta_{wet}$ as the relative soil water content and using Equation 4.11 (Su *et al.*, 2003):

$$R_\theta = \frac{\Theta}{\Theta_{wet}} = \frac{\lambda E}{\lambda E_{wet}} \tag{4.12}$$

This inverse relationship is often used in hydrological modelling and can be expressed as:

$$\frac{\lambda E}{\lambda E_{wet}} = f\left(\frac{SM_{actual}}{SM_{field\ capacity}}\right) = \Lambda \tag{4.13}$$

The relative evaporation is therefore calculated as the relative soil moisture contained in the rooting zone. The term f is used as a linear relationship. The $SM_{field\ capacity}$ can be inferred from the soil texture.

An alternative method, which uses an empirical relationship between the evaporative fraction and soil moisture, was developed by Bastiaanssen *et al.* (1997). The equation is based on two large-scale climate-hydrology studies, which investigated the interactions between soil moisture, evaporation and biomass (Scott *et al.*, 2003; Bezerra *et al.*, 2013). The empirical equation was modified by Scott *et al.* (2003), by standardizing soil moisture with saturated soil moisture, to create relative soil moisture content (Scott *et al.*, 2003):

$$\frac{\theta}{\theta_{sat}} = \exp^{[(\Lambda - 1)/0.421]} \tag{4.14}$$

These methods of soil moisture estimation result in a finer spatial resolution than that of current remote sensing soil moisture products, as the remotely sensed data is observed at a finer spatial scale. In addition, the soil moisture being estimated is at a greater depth than that estimated by microwave remote sensing (Bezerra *et al.*, 2013). The limitation of this method is that the observations and measurements are restricted to cloudless days, as retrieval is affected by atmospheric conditions. Therefore, only days which are cloud-free can be used, in order to reduce measurement errors.

The SEBS Model has been applied globally in several studies (Wang and Li, 2011; Gokman *et al.*, 2012; Ma *et al.*, 2012).

i. A study conducted by Su *et al.* (2003) derived a measure for the quantification of drought severity. The study used the SEBS Model, meteorological data and NOAA satellite images to derive relative evaporation in North China. A drought severity index (DSI) was subsequently derived from the relative evaporation. The DSI gives an indication of the soil moisture status, so that a high relative evaporation is associated with a high soil moisture status. The study concluded that the DSI and actual soil moisture measurements show a good comparison.

ii. Studies conducted by Scott *et al.* (2003) and Bezerra *et al.* (2013) evaluated the relationship to calculate soil moisture from remote sensing data. The study conducted by Bezerra *et al.* (2013) was carried out in the Apodi Plateau in Brazil. The study concluded that there was a close correlation between measured and estimated soil moisture value (R^2=0.84).

5. SYNTHESIS OF LITERATURE

The literature review detailed *in-situ*, remote sensing and modelled soil moisture measurement and estimation methods. Soil moisture is an important parameter, which has several implications for a number of applications. Conventional *in-situ* methods have been invaluable in providing validation and calibration data. The major limitation, however, is that the point measurements do not represent the spatial characteristics of soil moisture.

In recent years, the CRP technique has been used to provide continuous measurements of area-averaged soil moisture at an intermediate scale, which bridges the gap between point measurements and large footprints obtained from remote sensing.

Remote sensing of soil moisture is a promising technique, as it accounts for the spatial and temporal characteristics of soil moisture. It has numerous advantages; however, its application is limited, due to its coarse resolution. The product can be downscaled, in order to obtain a spatial resolution applicable for use in hydrological applications. There are several downscaling techniques that vary in complexity and the choice of the downscaling method used will depend on the intended output resolution, the input data available and the general ability of the researcher. Although a finer spatial resolution is favourable, the loss of remote sensing soil moisture product accuracy, due to downscaling, is a concern.

Soil moisture is an important parameter in both the land surface water and land energy balance and can be estimated from modelling. The PyTOPKAPI rainfall-runoff model has been used with confidence to estimate soil moisture across South Africa.

The SEBS Model can also be used to estimate soil moisture. Both models use remote sensing data as input data. The advantage of using models to estimate soil moisture is that the spatial resolution is greater than that of current global remote sensing products.

There needs to be a shift from using point measurements, to using area-averaged soil moisture measurements, to calibrate and validate remote sensing and model products. This will aid in reducing the vertical and horizontal scaling issues. There have been no studies

conducted in South Africa on the comparison of soil moisture estimate methods, using the CRP as validation data for satellite-based soil moisture estimates.

From the literature reviewed, the gaps in past research studies have become apparent. A major gap has been the use of point measurements for the calibration and validation of remote sensing and modelled soil moisture estimates. This has resulted in horizontal and vertical scaling issues, therefore there is a need for a shift towards the use of area-average calibration and validation data, in order to bridge the gap between scales.

Downscaling procedures have not been used in South African case studies; however, they are essential in obtaining remote sensing soil moisture estimates at a fine spatial resolution, which can be used in hydrological applications. Where downscaling has been used, the downscaled estimates were compared to point measurements.

The PyTOPKAPI Model has been implemented in South Africa with confidence; however, its estimates have not been evaluated against area-averaged soil moisture measurements. There have been no South African case studies on the CRP, therefore a comprehensive evaluation of the current methods of soil moisture against the area-averaged soil moisture measurements obtained from the CRP, need to be conducted in South Africa.

6. METHODOLOGY

Several studies referred in the literature review component (chapters two, three and four) have suggested that the current methods of soil moisture estimation do not adequately provide measurements for critical hydrological applications, as each method has its limitations. Although the current methods can provide accurate estimates of soil moisture, the representativeness of these methods may vary at different spatial scales. These methods need to be evaluated and improved, in order to obtain soil moisture data that can be used in critical hydrological applications. Further research is warranted. The following research questions have been formulated to address both the general and specific objectives of the study:

- How suitable is the CRP technique in providing spatial estimates of soil moisture?
- How accurate are the Level Three AMSR2 and SMOS soil moisture estimates?
- How suitable are the PyTOPKAPI Model product and the back-calculation using the SEBS model in providing estimates of soil moisture?
- What are the effects of seasonality on the different methods of soil moisture estimation?

The general objectives of this study were to calibrate and validate the CRP and subsequently use the calibrated CRP soil moisture estimates to validate satellite-based soil moisture estimates. This involved setting up the CRP in Cathedral Peak Catchment VI. The CRP continuously monitored soil moisture at an hourly time-step. During this time, four calibrations were undertaken to determine the representative gravimetric water content of the study area on that calibration day. An *in-situ* soil moisture network was also set up that consisted of TDR and Echo probes. The aim of the *in-situ* soil moisture measurements was to provide data that could be used to create a representative soil moisture dataset of the study area, which could then be used to validate the CRP.

Calibrated CRP estimates were then used to validate satellite-based soil moisture estimates. These consisted of remote sensing products, back-calculated soil moisture using outputs from the SEBS model and modelled soil moisture product from the PyTOPKAPI model. Although the downscaling of remote sensing data was reviewed and evaluated in the literature, the procedure of downscaling remote sensing products did not fall within the scope of this study and therefore, was not applied.

6.1 Study Site

The study site for this research was Cathedral Peak Research Catchment VI. Cathedral Peak was established in 1935, as the chief centre for forest hydrological research in the summer rainfall region (Scott *et al.*, 2000). Its primary purpose was to examine the influences of various management practices on the vegetation and yield of the local mountainous catchments (Everson *et al.*, 1998). Cathedral Peak lies within KwaZulu-Natal, in the Tugela Catchment, as shown in Figure 6.1. It comprises of fifteen gauged catchments that are situated on the little Berg, located below the Drakensberg escarpment, which creates a natural border between the north-eastern side of Lesotho and South Africa (Gush *et al.*, 2002).

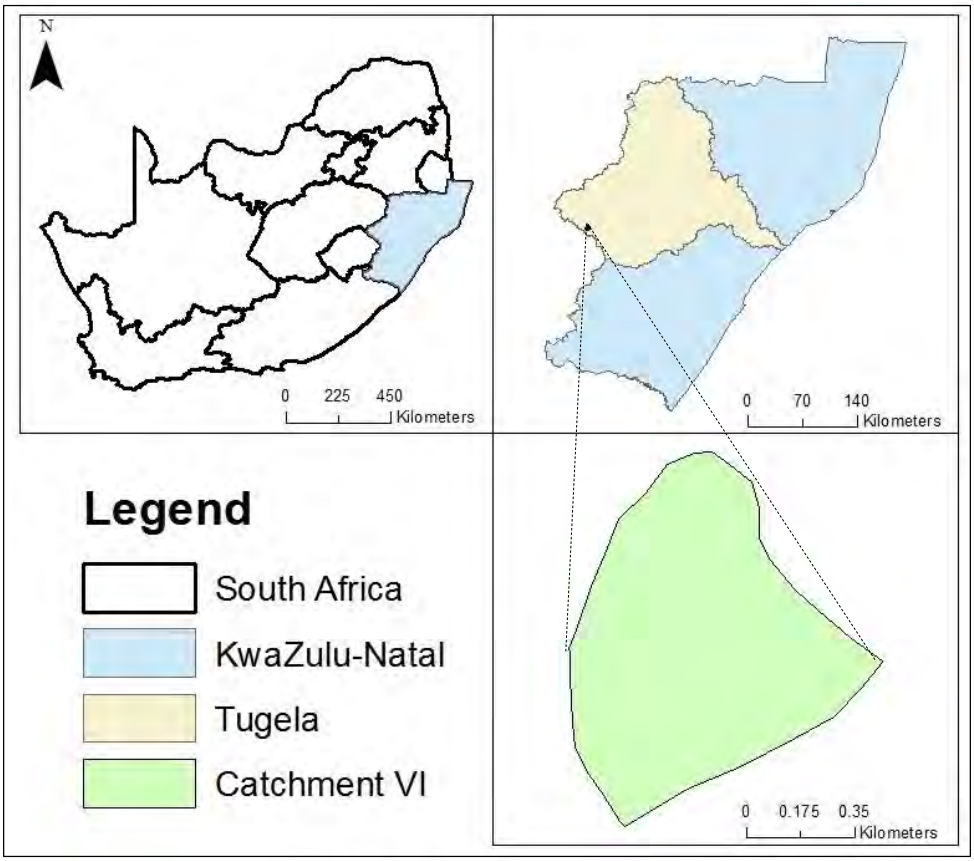

Figure 6.1 Location of Cathedral Peak Catchment VI, within the Tugela catchment, within KwaZulu-Natal

The Drakensberg mountain range is the highest mountain range in South Africa and gives rise to many of the rivers, which are of great economic importance to the country (Everson *et al.*, 1998). The fifteen research catchments (numbered I to XV) received different land

treatments, such as varying burning regimes, grazing, afforestation and protection from burning (Kuenene *et al.*, 2009).

Catchment VI is the focal catchment in this study. It has a catchment area of 0.68 km^2 and is located by latitude of 28.99° S and longitude of 29.25° E. Catchment VI is moderately dissected by streams and has a stream density of 3.25 km/km^2 (Everson *et al.*, 1998). The altitude ranges from 1860 m at the weir (northern-most point of the catchment) to 2070 m at the highest point of the catchment (Kuenene *et al.*, 2009). The average slope of the catchment is 19%. A topographic map of Catchment VI can be seen in Figure 6.2.

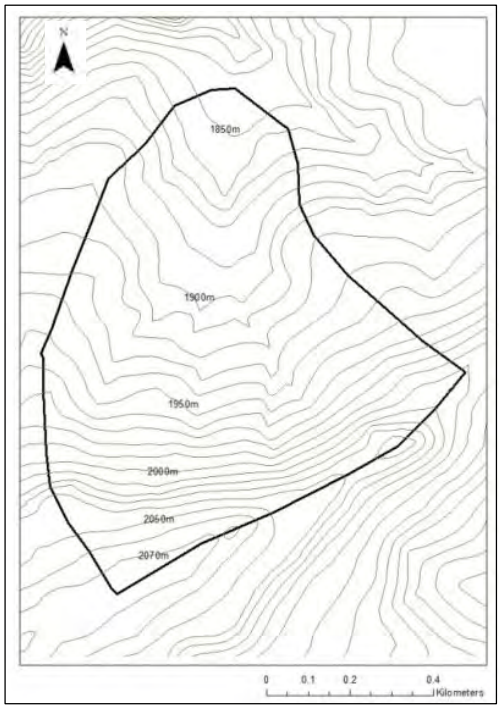

Figure 6.2 Topographic map of Catchment VI

The landcover of Catchment VI is Highland Sourveld grassland (Everson *et al.*, 1998). The soils in the catchments are moderately weathered immature soils, which are primarily derived from basalt (Scott *et al.*, 2000). The soils in the catchment are classified as lateritic yellow and red earths, with heavy black soils occurring in saturated zones and along stream banks (Jarmain *et al.*, 2004). There is a contrast in soil properties among the soil layers. The topsoil has a friable consistency, which results in rapid infiltration, whilst the subsoil has a very high clay content, which results in poor infiltration. The topsoil has a high organic matter content (6-10%), which results in a high water-holding capacity (Kuenene *et al.*, 2009). The region is

characterized climatically by its cold dry winters and hot wet summers. The mean annual precipitation is 1400 mm, with 85% falling between October to March (Gush *et al.*, 2002). Catchment VI has a mean annual precipitation of 1299 mm (Jarmain *et al.*, 2004).

Catchment VI is one of the smallest research catchments in Cathedral Peak. It is 4.027 km south-east of the Mikes Pass weather station and is the most instrumented catchment. It contains the CRP, eddy covariance system, large aperture scintillometer, weather station, a compound V-notch weir and a tipping bucket rain gauge.

6.2 Cosmic Ray Probe

The CRP is a relatively new and innovative *in-situ* instrument used to obtain area-averaged soil moisture measurements.

6.2.1 Set up of the cosmic ray probe

The CRP was installed on the 28th of February 2014 in Cathedral Peak research catchment VI (28.99^{o} S and 29.25^{o} E), as shown in Figure 6.3. The CRP was positioned towards the centre of the catchment and due to its measurement footprint, the soil moisture measurements obtained are assumed to be representative of the catchment area.

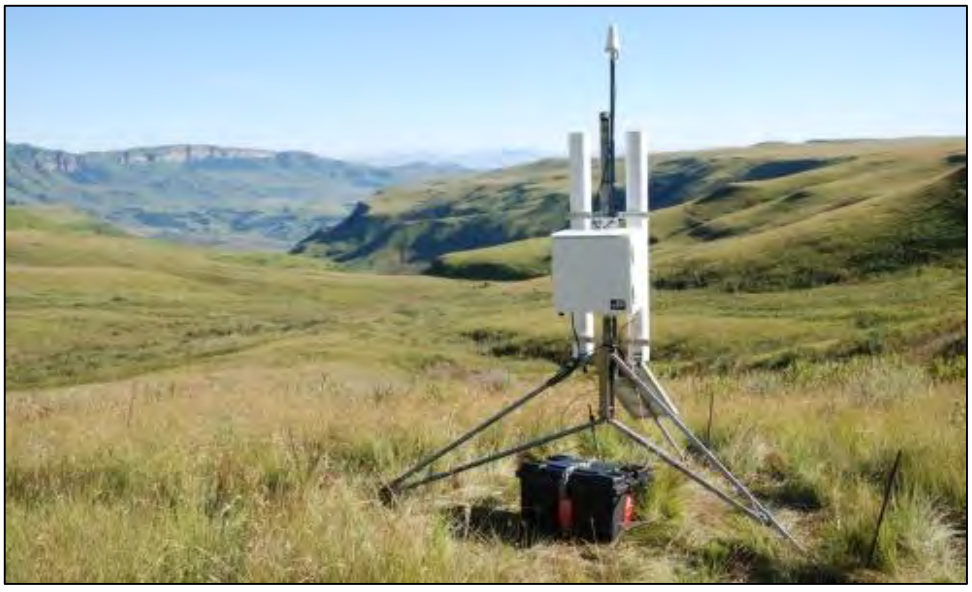

Figure 6.3 CRP in Cathedral Peak Catchment VI

The CRP method requires calibration to obtain accurate soil moisture estimates. The calibration process involves obtaining an estimate of the area-averaged soil moisture content over the CRP measurement footprint by gravimetric sampling. Soil samples were taken at three radial rings, extending outwards from the CRP. The radial rings were situated at a distance of 25 m (A), 100 m (B) and 200 m (C) from the CRP, as shown in Figure 6.4. At each of the three rings, eight points were taken at an equal distance along the circumference of the ring. Therefore, points were taken at 0, 45, 90, 135, 180, 225, 270 and 315 degrees from the CRP.

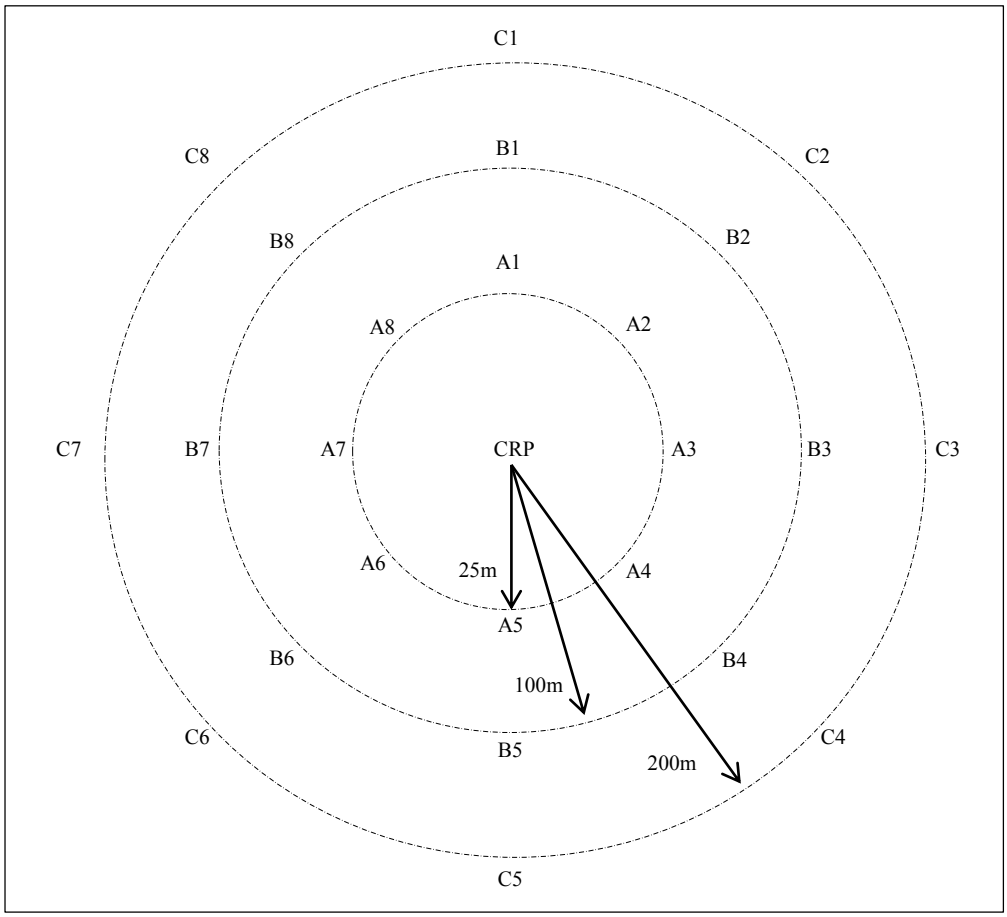

Figure 6.4 Diagram of sampling points

The location of these 24 points (3 rings x 8 points) were mapped, using GIS software and their coordinates were recorded (Table 6.1). These points are located within Catchment VI, as illustrated in Figure 6.5.

Table 6.1 Geographical coordinates of sample points

Sample	Latitude	Longitude	Sample	Latitude	Longitude	Sample	Latitude	Longitude
A1	-28.9929	29.2519	B1	-28.9922	29.2519	C1	-28.9913	29.2519
A2	-28.9929	29.2520	B2	-28.9924	29.2526	C2	-28.9918	29.2533
A3	-28.9931	29.2521	B3	-28.9931	29.2529	C3	-28.9931	29.2539
A4	-28.9932	29.2520	B4	-28.9937	29.2526	C4	-28.9944	29.2533
A5	-28.9933	29.2519	B5	-28.9940	29.2519	C5	-28.9949	29.2519
A6	-28.9932	29.2517	B6	-28.9937	29.2511	C6	-28.9944	29.2504
A7	-28.9931	29.2516	B7	-28.9931	29.2508	C7	-28.9931	29.2498
A8	-28.9929	29.2517	B8	-28.9924	29.2511	C8	-28.9918	29.2504

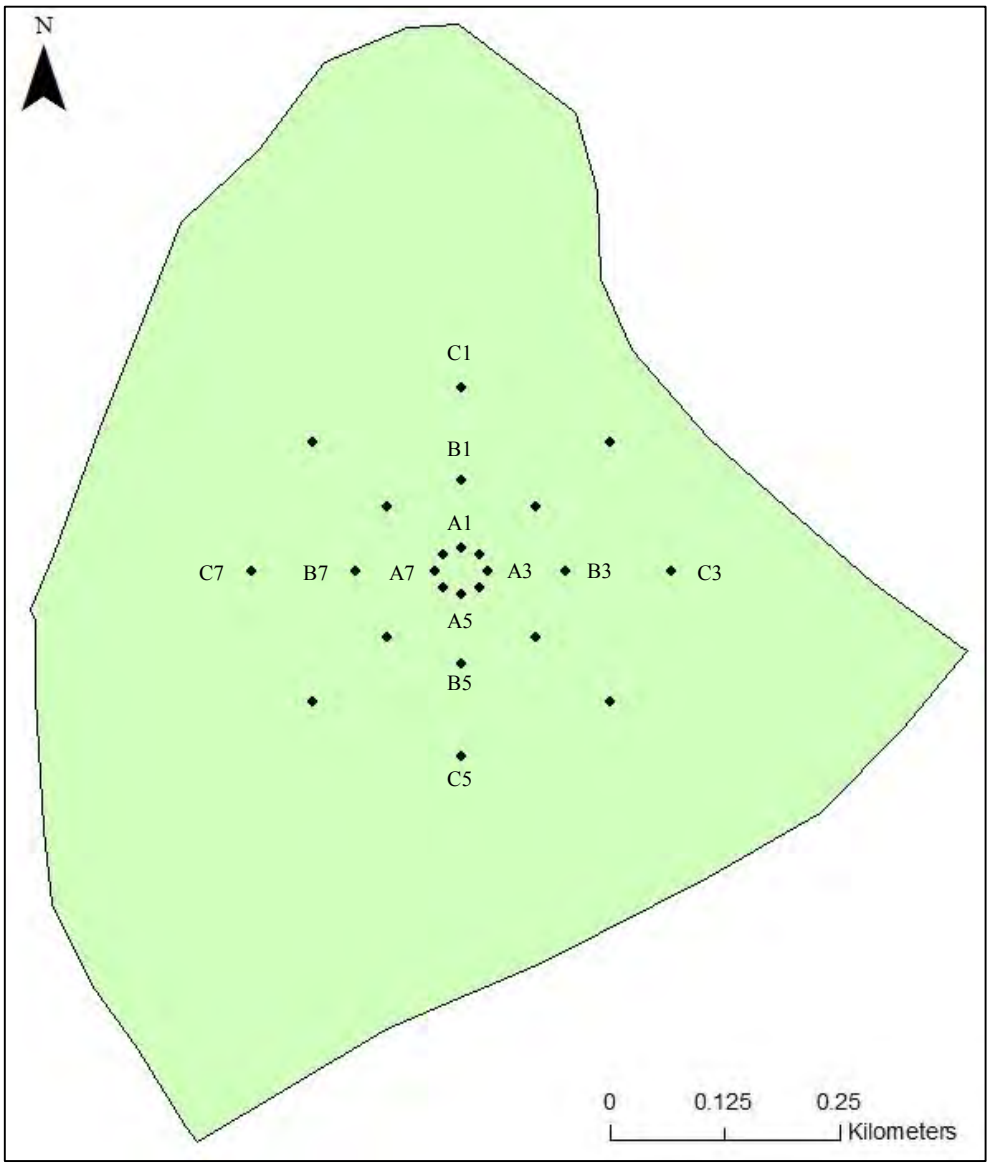

Figure 6.5 Position of calibration sample points within Cathedral Peak Catchment VI

6.2.2 Field sampling

Each sample point was entered and saved in a hand-held GPS system, in order to pinpoint the location of the sample points that had been determined. Once each point was found, they were visually marked, by inserting a metal rod into the ground and tying a piece of hazard tape to the top of the rod. At each point, soil samples were taken and labelled X, Y and Z. At each of these three points, an auger and garden trowel were used to obtain soil samples at depths of 0.05, 0.10, 0.20 and 0.30 m and these were placed in separate plastic bags. The plastic bags were clearly labelled according to the ring (A, B, C), sample point in the ring (1, 2, 3, 4, 5, 6, 7, 8), replicate (X, Y, Z) and depth (5, 10, 20, 30), as seen in Figure 6.6. The soil samples obtained were properly sealed, stored in a box and transported to the laboratory.

Figure 6.6 Field samples contained in plastic bags

6.2.3 Gravimetric water content determination

The determination of the gravimetric soil moisture content of each sample point was required to obtain a representative gravimetric soil moisture content of the study area, for the calibration of the CRP. The soil sample plastic bags were re-opened and a 20 g sub-sample of each sample was weighed, using a mass balance, its weight recorded to three decimal places and placed onto pre-weighed individual foil trays, which were labelled according to the sample (Figure 6.8). The samples were then placed in an oven at 105^{o}C for 24 to 48 hours, after which, the samples were removed from the oven, weighed and recorded once more. The

gravimetric water content was then calculated on a wet basis, using the gravimetric water content:

$$\text{Gravimetric water content} = \frac{\text{Wet mass} - \text{Dry mass}}{\text{Dry mass}} \times 100 \qquad (6.1)$$

Figure 6.7 Weighing the soil samples and placing them in the oven

Four calibrations were carried out over a period of eight months. The calibration dates were the 9th of July 2014, the 28th of August 2014, the 2nd of December 2014, and on the 22nd of January 2015.

6.2.4 Creating a soil moisture network

It was essential to create a soil moisture network comprising of *in-situ* soil moisture measurement instruments at several locations within the CRP measurement area. This was required in order to obtain data that could be used to validate the CRP measurements. There were three sets of measurement instruments installed between the 9th and 10th of July 2015. A soil pit was dug and TDR probes were inserted horizontally at depths of 0.05, 0.10, 0.15, 0.20 and 0.30 m, as illustrated in Figure 6.7 (a). Five wireless TDR sensors (0.12 m) were inserted vertically into the soil surface at sample points A5, B5, C5, A7 and B7, as illustrated in Figure 6.7 (b). Shallow soil pits were dug at A1, B1, C1, A3, B3, C3, B7 and C7, and Echo probes were inserted horizontally at a depth of 0.10 m (Figure 6.7 (c)). The echo probes were buried and their data loggers were attached to the metal rod at the subsequent sample points (Figure 6.7 (d)).

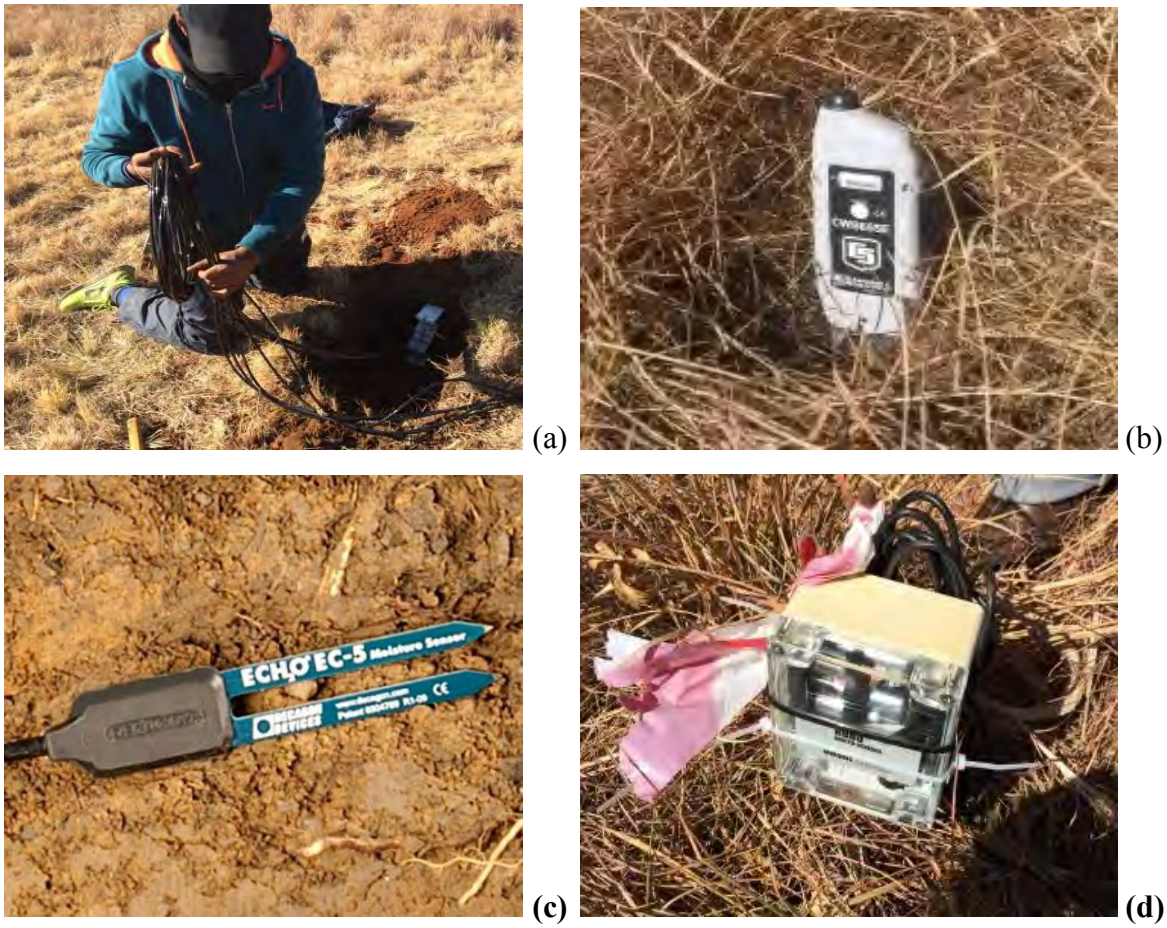

Figure 6.8 (a) Setting up the TDR pit, (b) Wireless TDR, (c) Echo probe and (d) Data Hobo Onset logger for the Echo probe

The wireless TDR sensors, which were placed on the 10th of July 2014 at points A7, A5, B5, B7 and C5, were removed on the 28th of August 2014 to check a problem with the data logging program.

6.2.5 Catchment burning

Catchment VI is subjected to prescribed burning for fire protection and management purposes, as it reduces the amount of groundcover vegetation during the drier (cooler) months and decreases the risk of wildfires. These wildfires could cause greater damage later on in the season. Without fire, grasslands could transform into shrub-lands or forests. Prescribed burning is different to wildfires and has less of an environmental impact. Prescribed burning is undertaken by a team of skilled and equipped laborers, who use firebreaks to control the burning stretch. There are three main types of burning strategies used:

i. Back-burning is the technique of setting small fires along a fire-break and burning back to the main fire front. This burning type is usually against the ground-level winds and often downslope, which results in a lower intensity fire that moves at a slower speed, which makes the fire easier to control.
ii. Head-burning is the technique of burning with the ground-level wind direction and is usually upslope. This burning type has a high intensity and moves at a faster rate, which makes it harder to control.
iii. Flanking is the technique of setting a fire, which moves parallel to and into the wind. This burning type is used to supplement the other two burning techniques.

The hydrological consequences of fire include the removal of vegetation cover and the direct effect of the fire heating the soil (Scott, 1994). The removal of the vegetation cover could have an impact on the soil moisture status, as the soil surface has greater exposure to atmospheric conditions. This could lead to increased soil evaporation, which could result in drier topsoils (Stoof *et al.*, 2012). Conversely, there could be an increase in soil moisture in the subsoils, due to a reduction in transpiration (Stoof *et al.*, 2012). The removal of vegetation may also result in increased erosion and sedimentation, due to an increased exposure of the soil surface to raindrop impact (Scott, 1994). There is a possibility of post-fire pore-clogging by infiltrated ash, which leads to reduced infiltration rates and causes an increase in overland-flow (Stoof *et al.*, 2012). There could also be the development of soil water repellency during and after the fire.

Although these hydrological consequences have been reported, the effects of fire on hydrological responses at a catchment scale are minor, as these fires are generally prescribed burns and the issue of scale plays a significant role in the overall change detection of the hydrological system (Scott, 1994).

On the 5th of September, a scheduled burning from an adjacent Catchment (VII) spread and caused the unscheduled burning of Catchment VI. As a result of the fire, the Echo probe soil moisture sensors were destroyed. However, the data from the hobo loggers were retrieved (Figure 6.9). The larger equipment in Catchment VI were not harmed due to the fire breaks, as seen in Figure 6.10. Due to the loss of the echo probe sensors, the wireless TDR sensors had to be placed, to best represent the catchment. This was done by identifying the wet,

intermediate and dry areas of the catchment, by using the soil moisture map obtained from the first calibration.

Figure 6.9 Data retrieved from burned echo probe data loggers

Figure 6.10 Protection of equipment by fire breaks in Catchment VI

6.2.6 Bulk density determination

The gravimetric determination technique was used for the calibration of the CRP. The gravimetric soil moisture content is expressed, by weight, as the ratio of the mass of water present to the dry weight of the soil sample (g/g). The CRP, however, measures the volumetric soil moisture content, which is expressed, as the ratio of volume of water to the total volume of the soil sample (cm^3/cm^3). This is further expressed as volumetric water content in percentage.

The calibration of the CRP requires a representative bulk density value, to convert the gravimetric soil moisture content to volumetric water content. In order to convert gravimetric soil moisture into volumetric soil moisture, the gravimetric water content is multiplied by the bulk density. The bulk density determination was carried out on the 2nd of December 2014. Undisturbed soil cores were taken at three locations in the catchment, corresponding with three sample points (C1, CRP and C5) and at three depths (0.00 – 0.05 m, 0.05 – 0.10 m and 0.10 – 0.15 m). These sites were selected to best represent the catchment.

At each of the three sites, steel cylindrical cores were inserted vertically into the soil. Starting with the 0.00 – 0.05 m measurement, the steel core was placed on the surface of the soil. A wooden board was placed on the top of the core and the core was hammered down into the soil. The wooden board was used to distribute the force of the hammer on the steel core, so that the core moves down equally. Once the steel core had reached its intended depth, the soil around the core was loosened and removed carefully. The steel core was then removed, clearly labeled and its ends tightly sealed. The same procedure was then carried out at 0.05 – 0.10 m and 0.10 – 0.15 m depths.

The soil cores were then transported to the laboratory, where they were opened carefully. A knife was used to trim the excess soil of the ends of each side of the core, so that the volume of the soil equaled the volume of the core. The soil cores (steel core and soil) were oven-dried at 105ºC for 48 hours. The mass of the soil cores were weighed and recorded after oven drying (refer to Figure 7.14). The mass of the cylindrical steel cores were recorded and subtracted from the soil core mass, to obtain the mass of dry soil. The volumes of the soil cores were determined by the dimensions of the cylindrical steel cores. The volume of the steel core is the volume of the soil.

The bulk densities were calculated, using Equation 6.2:

$$\text{Bulk Density (g/cm}^3) = \frac{Dry\ Mass\ of\ soil\ (g)}{Total\ Volume\ (cm^3)} \qquad (6.2)$$

The calculated bulk densities of each sample point and depth along with the variables used to calculate them are illustrated in Table 6.2.

Table 6.2 Variables required in obtaining the bulk density

Sample	Depth (m)	Ms (g)	Volume (cm^3)	Bulk Density (g/cm^3)
C1	0.05	38.863	98.175	0.396
C1	0.10	50.404	98.175	0.513
C1	0.15	56.127	98.175	0.572
CRP	0.05	55.45	98.175	0.565
CRP	0.10	60.359	98.175	0.615
CRP	0.15	65.143	98.175	0.664
C5	0.05	60.253	98.175	0.614
C5	0.10	65.194	98.175	0.664
C5	0.15	71.86	98.175	0.732

It can be seen that, as the depth increases, the bulk density increases. The calculated bulk density values were low. This can be attributed to the soil cover, organic matter content, soil structure, porosity and the lack of compaction, as the catchment is situated in an undisturbed area. Initially, the calibration involved a depth weighting soil moisture procedure. Therefore, the average bulk density per depth was required. The new and current calibration procedure does not involve a depth weighted soil moisture, thus one representative bulk density value was required and was calculated by averaging all the bulk density values. The average measured bulk density was thus 0.593 g/cm^3.

6.3 Calibration

In total, four calibrations were completed. Two of the calibrations were completed in the "dry" period and two were completed in the "wet" period. Subsequently, one "full" calibration and one "partial" calibration were completed in each period. The partial calibrations were the result of limited field time. The calibrations, number of samples and depths obtained, are shown in Table 6.3. The full calibrations (1 and 3) have a large number of samples, due to all 24 points being covered. Furthermore, three replicate samples were obtained at each point, at each depth. The first calibration involved collecting samples from a depth of 0.30 m; however, the CRP did not measure the soil moisture at a depth greater than 0.20 m, due to the relatively high soil moisture in the "dry" period. Therefore, this depth was discontinued for the subsequent calibrations.

Table 6.3 Information regarding the calibration sampling

				Depth Measured (m)			
Calibration	**Date**	**Period**	**No. of samples**	**0.05**	**0.10**	**0.20**	**0.30**
1 (Full)	July 9, 2014	Dry	288	x	x	x	x
2 (Partial)	August 28, 2014	Dry	36	x	x	x	-
3 (Full)	December 2, 2014	Wet	216	x	x	x	-
4 (Partial)	January 22, 2015	Wet	36	x	x	x	-

For the purpose of the calibration of the CRP, an average (one single) soil moisture value per calibration is needed, thus a representative soil moisture value was determined for each calibration.

Soil moisture maps of each calibration were created by averaging the depths of each sample point and using the kriging interpolation technique to create soil moisture maps between the sample points obtained. These maps were not required for the calibration procedure, but were created to show the spatial characteristics of soil moisture in the research area. The soil moisture map values are in percentage volumetric content.

Calibrations one and three are more detailed, as they have more points. Calibrations one and two were done in the dry period (Figure 6.11 and Figure 6.12). Calibrations three and four where done in the wet period (Figure 6.13 and Figure 6.14). From these soil moisture maps, general trends can be seen. The soil moisture is lowest in the south (upslope) and the highest in the north (downslope). It can be seen that topography affects the soil moisture content, as the soil moisture content generally increases as the altitude decreases along the north-south transect. The change in soil moisture in the research area, illustrates the limitation of using *in-situ* point measurements due to the spatial variability of soil moisture.

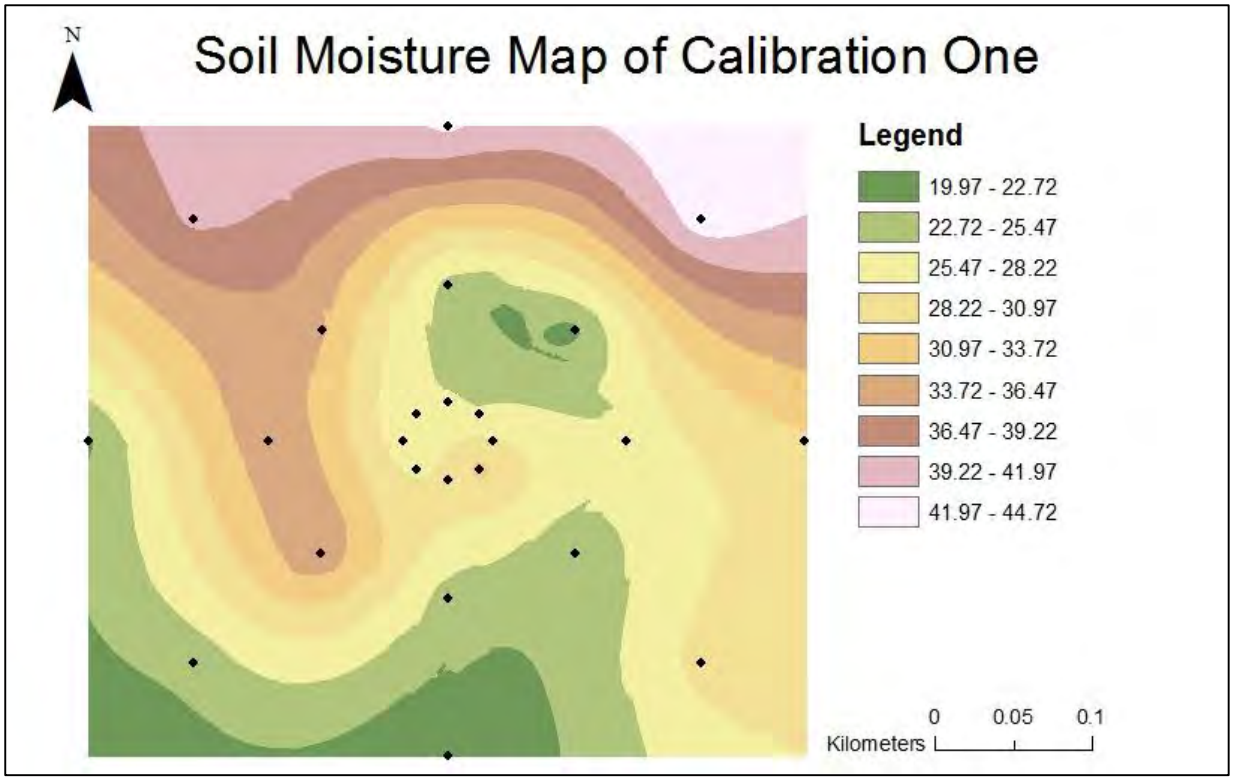

Figure 6.11 Soil moisture map of the first calibration (9th of July 2014)

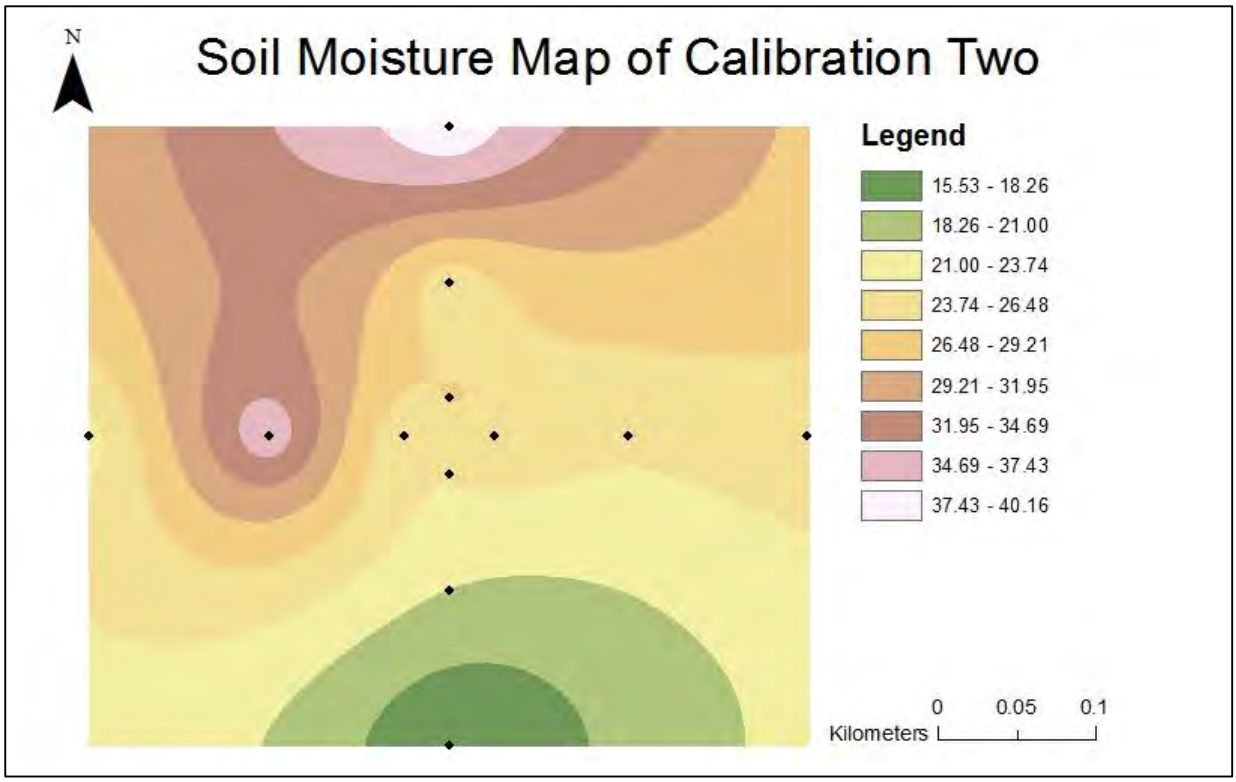

Figure 6.12 Soil moisture map of the second calibration (28th of August 2014)

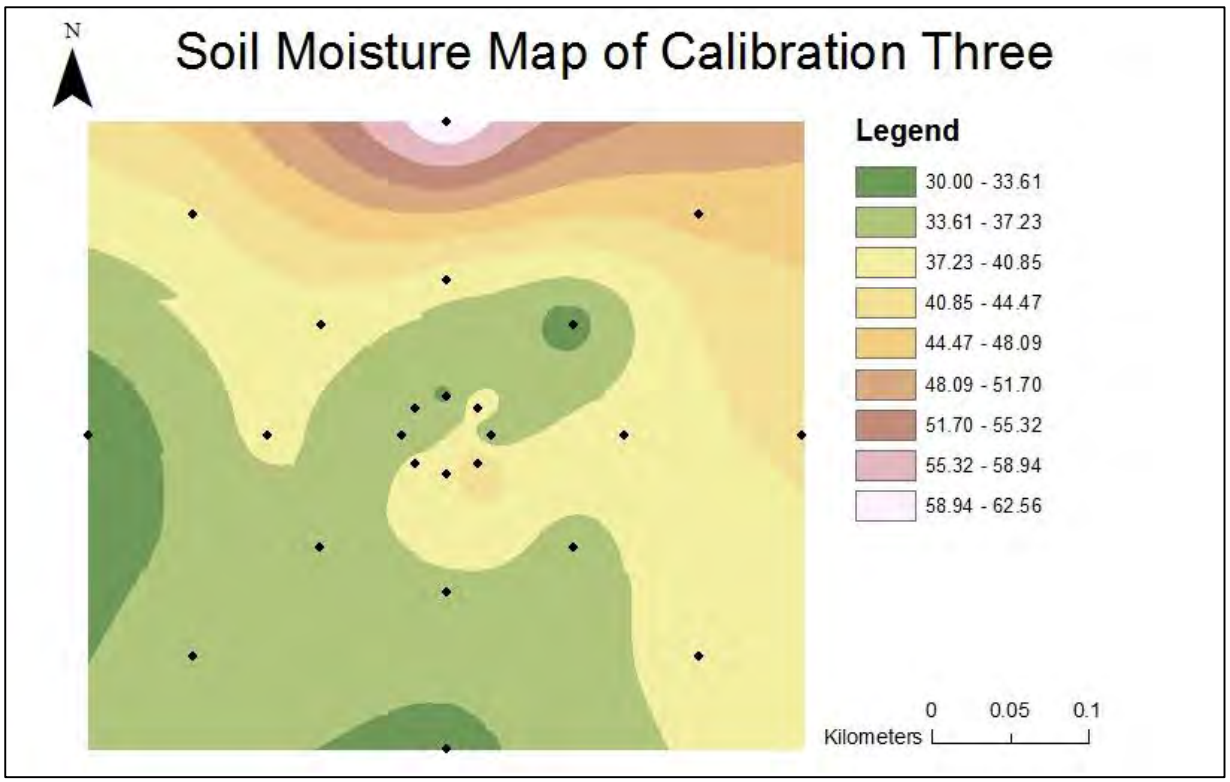

Figure 6.13 Soil moisture map of the third calibration (2nd of December 2014)

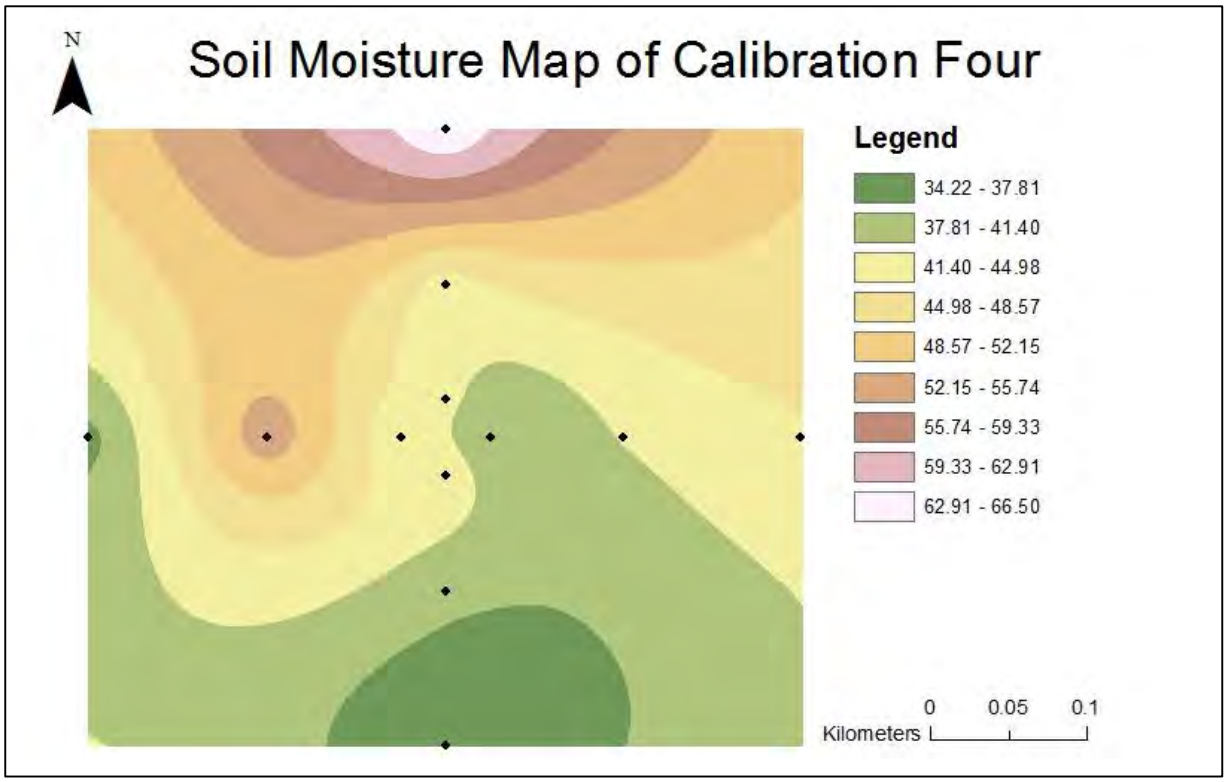

Figure 6.14 Soil moisture map of the fourth calibration (22nd of January 2015)

Soil moisture varies both spatially and temporally. With regards to its spatial variability, soil moisture varies horizontally, as well as vertically. The horizontal and vertical spatial variability can be due to several factors, such as topography, rainfall distribution, soil characteristics and vegetation. If calibration one is considered, for each site (A1, A2, A3, etc.), three auger points were taken, so that there are three replicate samples at each sample point. The data of sample point A1, from calibration one, is depicted in Figure 6.15. From Figure 6.15, it can be seen that soil moisture varies with depth. In general, the soil moisture increases with depth. It is also evident that, although the three auger points were not more than one meter apart from one another, there was a noticeable change in the soil moisture content.

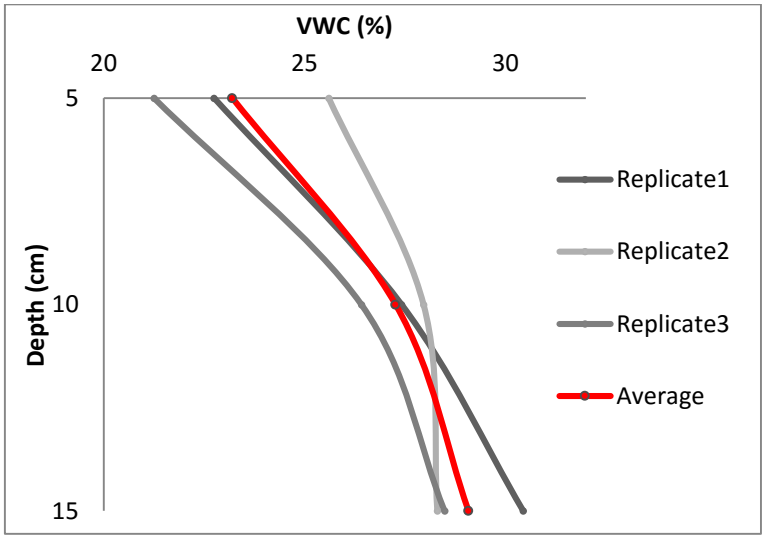

Figure 6.15 Volumetric water content against depth for each replicate at one sample point

The averages of all 24 soil sample points, for calibration one, are plotted against depth on the same graph. In Figure 6.16, it is evident that the change in soil moisture content is not constant. In general, the soil moisture seemed to increase with depth. The 24 plotted points show the variability of soil moisture of the area. The graph also shows the variability of soil moisture with depth, as some curves show a noticeable change in soil moisture with depth, whilst others have a fairly constant soil moisture content down a profile.

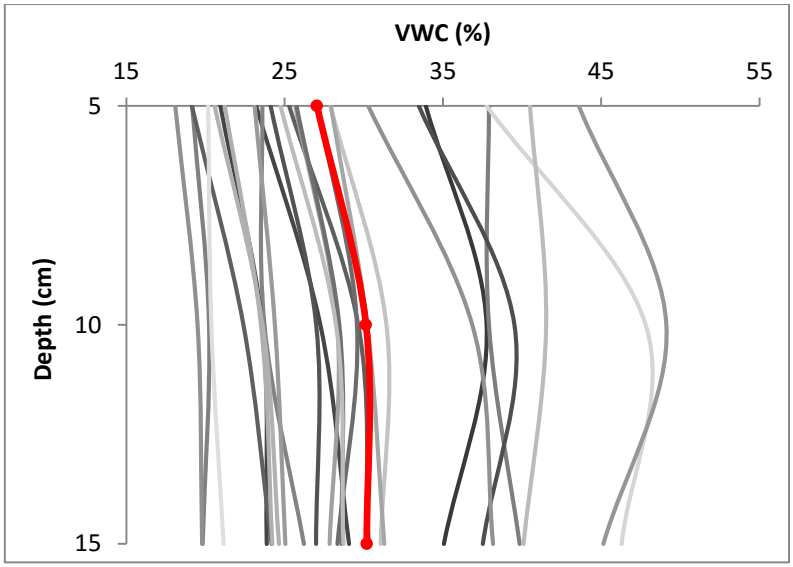

Figure 6.16 Volumetric water content against depth for all 24 sample points

The calibration procedure was carried out once all four calibrations had been completed. The aim of the calibration was to determine the average N_o value, by averaging the N_o value determined for each calibration. The data from the CRP is sent, via satellite link, to the COSMOS server: http://cosmos.hwr.arizona.edu/Probes/probemap.php. The data is available at three levels. Level one data comprises of raw counts of fast and thermal neutrons. Level two data is quality controlled, uses level one data and subsequently converts it into a suitable format to determine soil moisture. Level three data takes level two data and converts it directly to measurements of soil moisture. The calibration procedure outline that was followed is that of Franz (2014) and Franz *et al.* (2015).

The first step in the calibration procedure was to correct the neutron counts. This involved determining the neutron correction factors, using the following equations (Franz, 2014):

$$N = \frac{N' * CP * CWV}{CI * CS} \qquad (6.3)$$

where N is the corrected neutron counts per hour, *N'* is the raw moderated neutron counts, *CP* is the pressure correction factor, *CWV* is the water vapour correction factor, *CI* is the high-energy intensity correction factor, and *CS* is the scaling factor for geomagnetic latitude (Franz, 2014).

$$CP = \exp\left(\frac{P_i - P_o}{130}\right) \quad (6.4)$$

$$CI = \frac{N_H^i(t)}{N_H^o} \quad (6.5)$$

$$CS = f(x, y, z, t) \quad (6.6)$$

Where *x*, *y*, *z*, is location and elevation, and *t* is time.

$$CWV = 1 + 0.0054\left(\rho_v^i(T, P, RH) - \rho_v^o(T, P, RH)\right) \quad (6.7)$$

where r_v^i is the absolute humidity of the air (g/m^3), r_v^0 is the reference absolute humidity of the air (g/m^3), T is air temperature in (^{o}C), *P* is pressure (mb), and *RH* is relative humidity (%) (Franz, 2014).

For the calibration procedure, the level two data was used, which has already been corrected for CP, CI and CS. If level one data were used, then the original equation and all the corrections are required. The revised neutron count correction equation:

$$N = N' * CWV \quad (6.8)$$

Therefore, when using level two neutron counts, only the correction for absolute water vapour (CWV) is required. The absolute water vapour calculation was obtained, using the following equations (Franz, 2014):

$$es_o = 611.2 * \exp\left(\frac{17.67 * T}{243.5 + T}\right) \quad (6.9)$$

Where es_o is the saturated vapour pressure at surface (Pa) and *T* is air temperature (^{o}C) (Franz, 2014).

$$e_o = \frac{RH}{100} * es_o \quad (6.10)$$

Where e_o is actual vapour pressure at surface (Pa) and *RH* is the relative humidity (%) (Franz, 2014).

$$\rho_v = \frac{e_o}{Rvap*(T+273.15)} * 1000 \qquad (6.11)$$

Where r_v is the absolute humidity of air (g/m^3), $R_{vap} = \frac{R}{0.001 M_{vap}}$ is the gas constant for water vapour (J/K/kg), R is universal gas constant (= 8.31432 J/mol/K), M_{vap} is the molar mass of water vapour (= 18.01528 g/mol = 0.01801528 kg/mol), and T is air temperature (^{o}C).

These equations require hourly temperature and relative humidity data for the same time period as the level two neutron count data (hourly). The data set required covered the period of March 2014 to March 2015. Although the CRP system does measure temperature and pressure, the sensors are inside the data logger casing, which results in the measurement of the loggers conditions. The primary data set used was from the eddy covariance system; however, this only had data from the 12th of July 2014 and there were a few gaps in the data set, which are illustrated by the vertical red arrows, as seen in Figure 6.17. This data alone could not be used in the calibration, as the time period that it covers is not adequate and the gaps are problematic.

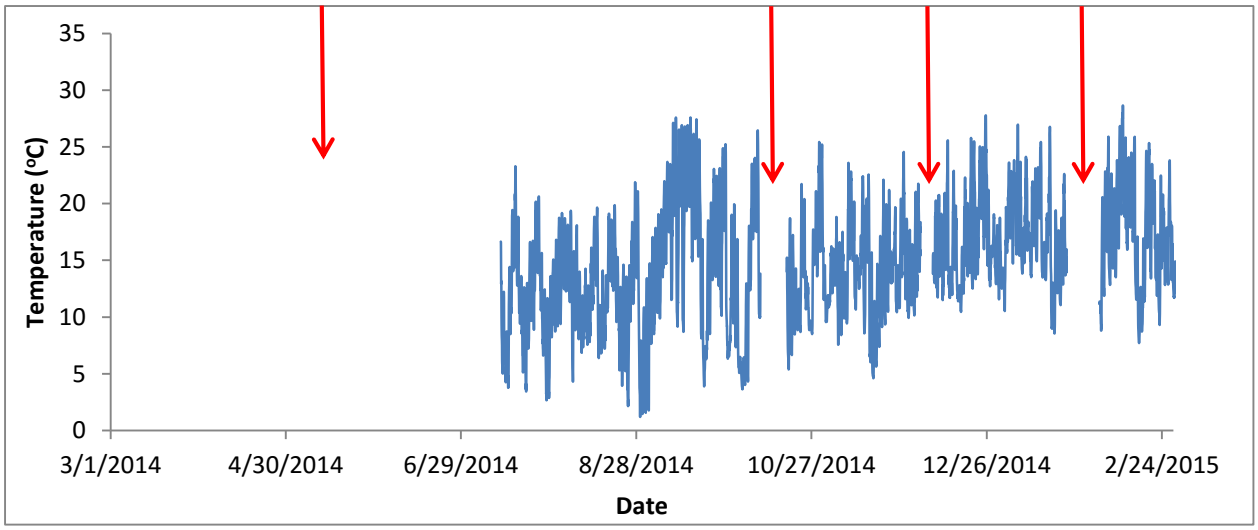

Figure 6.17 Hourly temperature (The same data gaps present in the relative humidity dataset)

In order to calibrate the CRP, a complete and reliable temperature and relative humidity data set was required. Therefore, the data from the eddy covariance system was in-filled and patched with data from the nearby Mikes Pass weather station (refer to Figure 6.18). The Mikes Pass weather station had the hourly temperature and relative humidity for the period required.

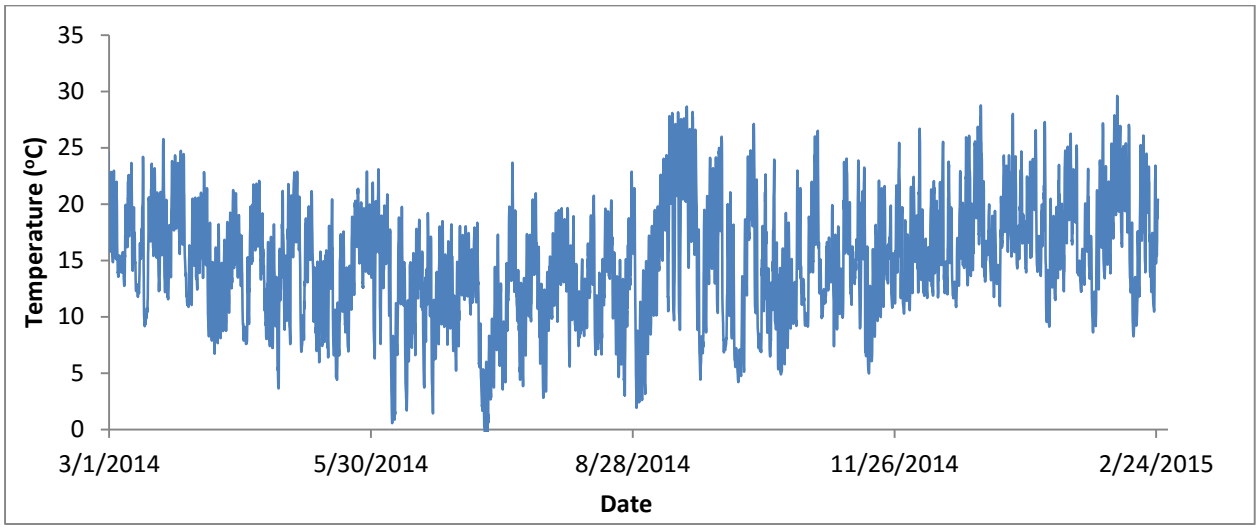

Figure 6.18 Complete daily air temperature data for Cathedral Peak Catchment VI

Once the hourly CWV values were determined, the corrected neutron count rates were determined. The following calibration function was then used to determine the N_o value for each calibration (Franz *et al.*, 2015):

$$(\theta_P + \theta_{LW} + \theta_{SOC})\rho_{bd} = \frac{0.0808}{\frac{N}{N_o} - 0.372} - 0.115 \qquad (6.12)$$

Where q_p is pore water content (g/g), q_{LW} is lattice water content (g/g), $q_{SOC_{eq}}$ is soil organic carbon water content (g/g), r_{bd} is dry soil bulk density (g/cm^3), N is the corrected neutron counts per hour, and N_0 is an instrument specific calibrated parameter that represents the count rate over dry silica soils.

$$\theta_{SOC} = \left(TC - \frac{12}{44} CO_2\right) 0.5556 \qquad (6.13)$$

Where *TC* is the soil total carbon (g/g), CO_2 is the soil CO_2 (g/g), 12/44 represents the stoichiometric ratio of carbon to CO_2, and 0.5556 is the stoichiometric ratio of H_2O to organic carbon (assuming organic carbon is cellulose $C_6H_{10}O_5$).

θ_{soc} was not determined, but was given a value of 0.01 g/g.

θ_{lw} was determined to be 0.15433 g/g. A 50 gram representative soil sample was sent to Activation Laboratories in Canada for θ_{lw} determination.

There is a need to correct for biomass (Franz *et al.*, 2015)

$$(\theta_P + \theta_{LW} + \theta_{SOC})\rho_{bd} = \frac{0.0808}{\frac{N}{N_o(BWE)} - 0.372} - 0.115 \quad (6.14)$$

where BWE is the biomass water equivalent (mm). The biomass calculation is done for vegetation types, whose biomass changes with their growing stage. Due to the vegetation of Catchment VI being grassland, the biomass did not change much and the change in biomass was therefore insignificant and a biomass correction was not required. The burning of the catchment affected the biomass content greatly. This issue was resolved by performing a calibration before (calibration two) and a calibration after (calibration three) the burning.

The neutron count (N) for each calibration was determined to be the average neutron count, during which the soil samples for that calibration were obtained (Table 6.4). For the "full" calibration, the duration was ≈ six hours. The duration of the "partial" calibration was ≈ three hours

Table 6.4 The gravimetric soil moisture, bulk density and Neutron count

Calibration	Gravimetric Soil Moisture (g/cm^3)	Bulk density (g/cm^3)	Neutron Count (count/hr)
1	0.490	0.593	1731.684
2	0.438	0.593	1761.408
3	0.647	0.593	1652.600
4	0.741	0.593	1611.059

The CRP data prior to calibration (blue), with the calibration points (red), were plotted against time:

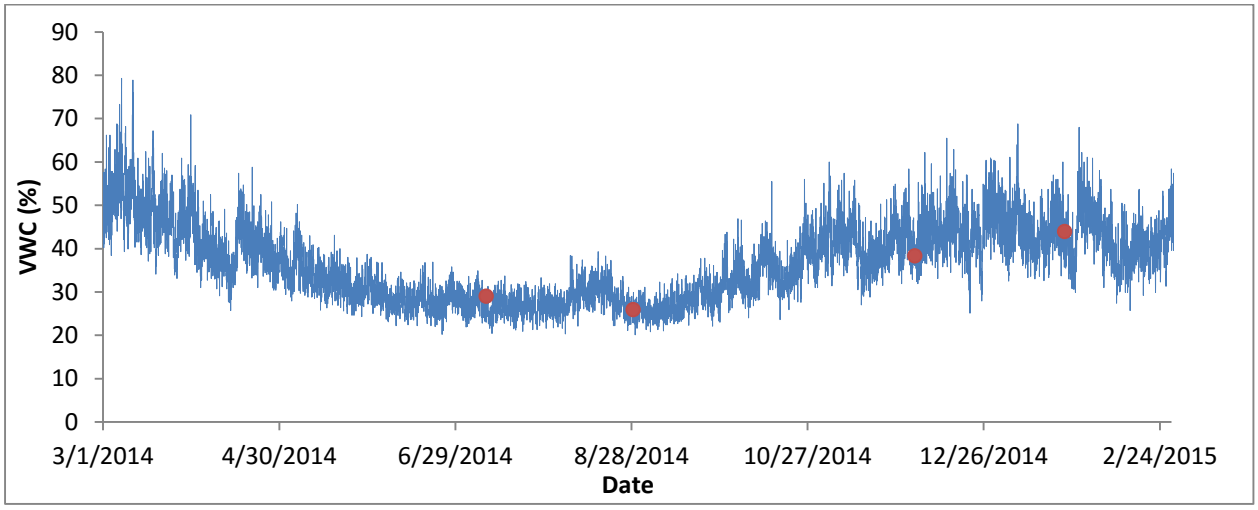

Figure 6.19 CRP soil moisture estimates prior to calibration, with calibration points

From Figure 6.19, it can be seen that the soil moisture calibration values correlate well with the soil moisture estimates of the CRP. This is the result of the uncalibrated N_o value being relatively close to the actual N_o value. The uncalibrated N_o value (3000) was set by the developers of the probe.

The calibration equation (Equation 6.12) was used to determine the N_o value for each calibration, which are shown in Table 6.5.

Table 6.5 Date and calculated N_o value for each calibration

Calibration	Date	N_o
1	09 July 2014	3250.573
2	28 August 2014	3242.507
3	02 December 2014	3255.973
4	22 January 2015	3248.243

The average N_o value for the calibrations was calculated to be 3249.324. This calculated N_o value was then used in the calibration function equation (Equation 6.12), to determine the volumetric soil moisture content.

The calibration function was used to determine an hourly $(\theta_p+\theta_{lw}+\theta_{soc})\rho_{bd,}$ by using a constant N_o and the hourly corrected N values. The lattice water and soil organic carbon water $(\theta_{lw}+\theta_{soc})$ were subtracted from $(\theta_p+\theta_{lw}+\theta_{soc})\rho_{bd}$ to determine the Volumetric Water Content (VWC) (calibrated CRP dataset). The hourly calibrated VWC from the CRP was plotted against time, as shown in Figure 6.20.

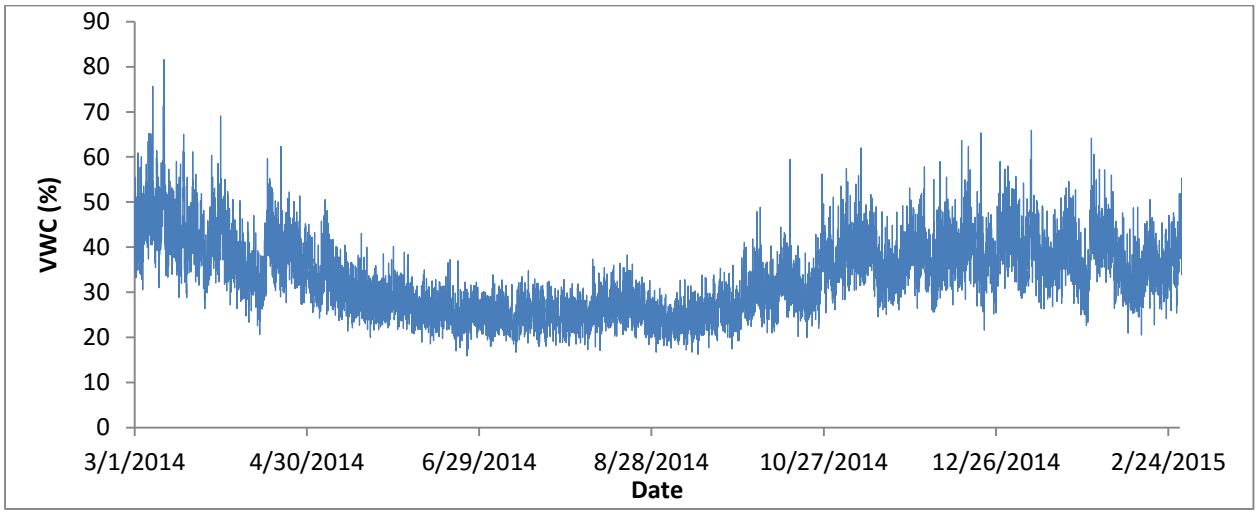

Figure 6.20 Hourly soil moisture estimates of the calibrated CRP

From Figure 6.20, it can be seen that the calibrated hourly CRP follows the same trend as the uncalibrated hourly CRP dataset (shown in Figure 6.24); however, there is a downward shift in the points. The neutron count was then plotted against the calibrated VWC. The exponential function from the graph (Figure 6.21) can be used to determine the VWC from the neutron count measured.

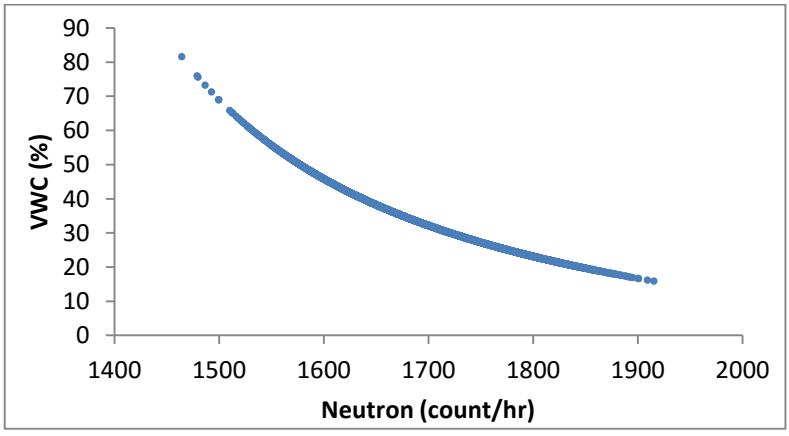

Figure 6.21 Neutron count against volumetric water content

The hourly CRP data was converted into a daily dataset (Figure 6.22). From Figure 6.22, it can be seen that the conversion from hourly to daily data results in a smoother dataset, as the fluctuations are averaged. The soil moisture dataset generally shows that soil moisture is higher in the summer and lower in the winter, as expected in the summer rainfall region of South Africa.

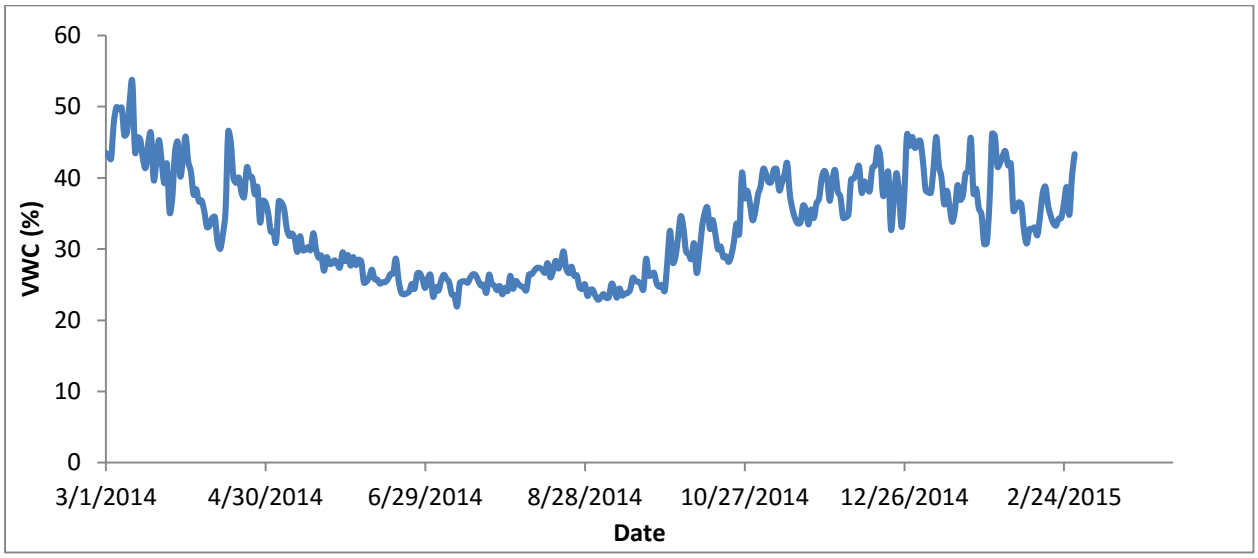

Figure 6.22 Daily calibrated CRP soil moisture measurements in Catchment VI

6.4 Creating an *In-situ* Soil Moisture Dataset

There were three types/sets of *in-situ* soil moisture instrumentation used:

i. 5 TDR (pit) probes at one point placed horizontally at depths of 0.05, 010, 0.15, 0.20 and 0.30 m.
ii. 5 wireless TDR probes (0.12 m) placed vertically at different sites in the catchment.
iii. 8 echo probes placed horizontally at a depth of 0.10 m at different sites.

The TDR pit had the most complete data set out of all the *in-situ* instrument sets, as it has a continuous record from the 11th of July 2014 to March 2015. The wireless TDR probes have data from the 11th of July to March 2015; however, there are numerous gaps in the data set, due to the erratic operation of all five TDR probes. The echo probes have the shortest data record from the 9th of July 2014 to the 4th of September 2014. They were problematic and were destroyed in a catchment fire on the 5th of September 2014.

Although the study period of the research extends from March 2014 to March 2015, the validation of the CRP was for the period 11th of July 2014 to the 20th of March 2015, as this is the corresponding period for *in-situ* measurements.

In order to validate the CRP, a representative *in-situ* soil moisture data set is required. The TDR pit, wireless TDR and ECHO probe datasets were converted from an hourly time-step to a daily time-step, as a daily time-step was used in this research project.

The soil moisture from the TDR pit at five different depths in the profile is plotted against time, as shown in Figure 6.23. The soil moisture at different depths followed the same wetting and drying trends; however, the change in soil moisture, with depth was observed (Figure 6.23). In general, the soil moisture increased with depth. In the "dry" period, the soil moisture values were relatively constant. In the "wet" period, the temporal variation in soil moisture was a result of more rainfall (input) and higher rates of total evaporation (output).

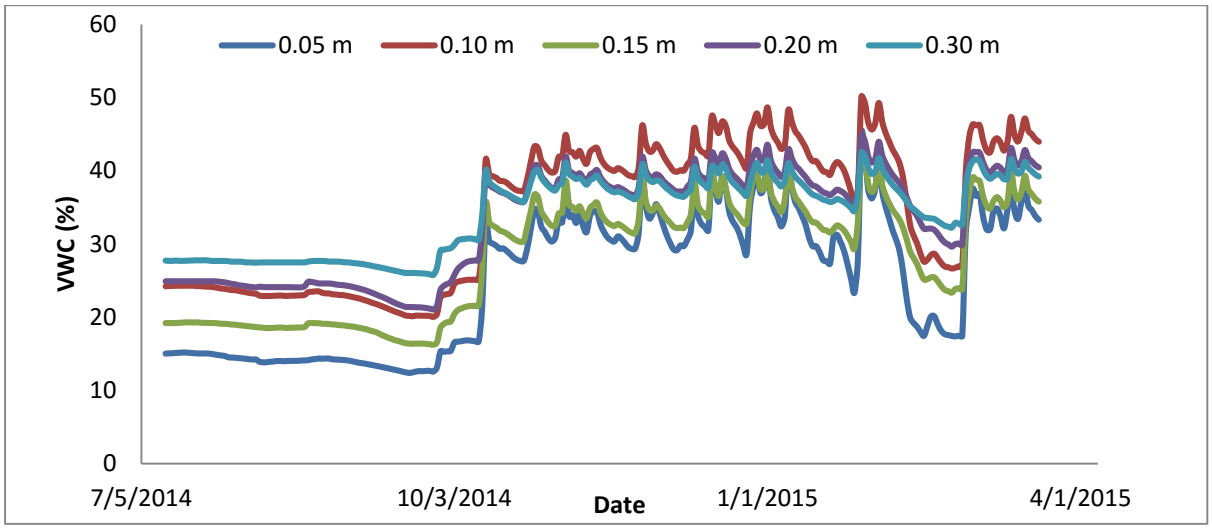

Figure 6.23 Daily TDR pit soil moisture measurements in Catchment VI

If we consider the effective measurement depth of the CRP during the one year period between March 2014 and March 2015 (Figure 6.24), it can be seen that the effective measurement depth of the CRP for this period does not exceed 0.15 m, therefore the 0.20 and 0.30 m TDR pit depth measurement data were excluded, when determining the average soil moisture of the TDR pit. The 0.05 m TDR pit depth was also excluded, as the effective depth of the CRP was closer to the 0.10 cm depth than the 0.05 m depth and the other two data

sources had measurements at 0.10 and 0.12 m depths (echo and wireless TDR). The mean effective depth for this period was 0.11 m.

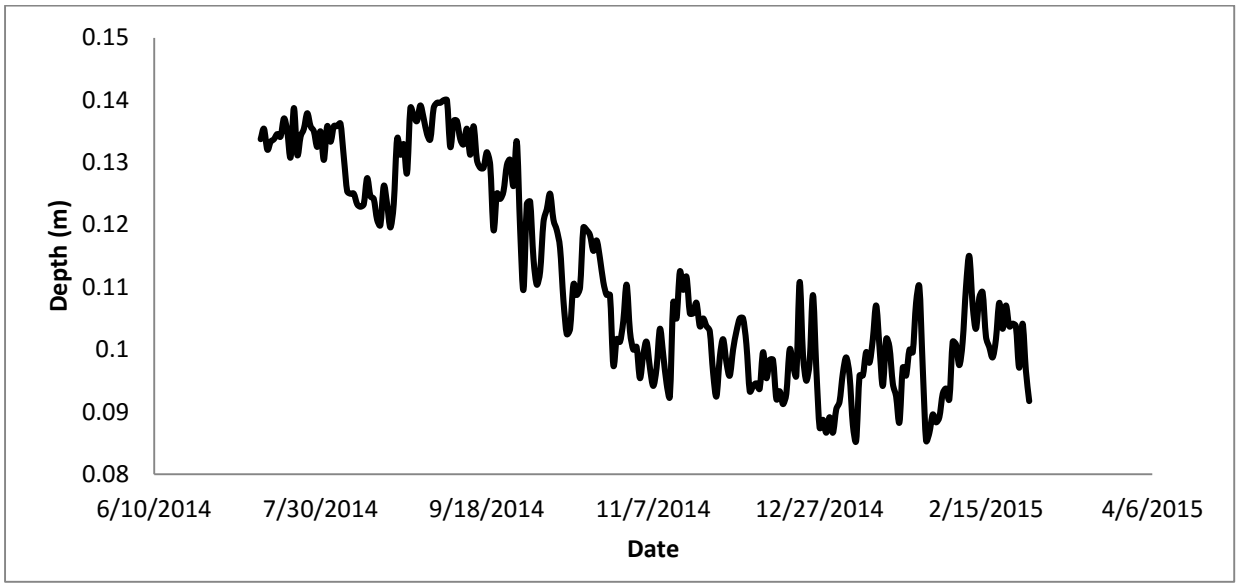

Figure 6.24 The CRP effective measurement depth

The average (0.10 and 0.15 m) daily TDR pit soil moisture was plotted against time (Figure 6.25). From Figure 6.25, it can be seen that the average TDR pit dataset covers the winter and summer period.

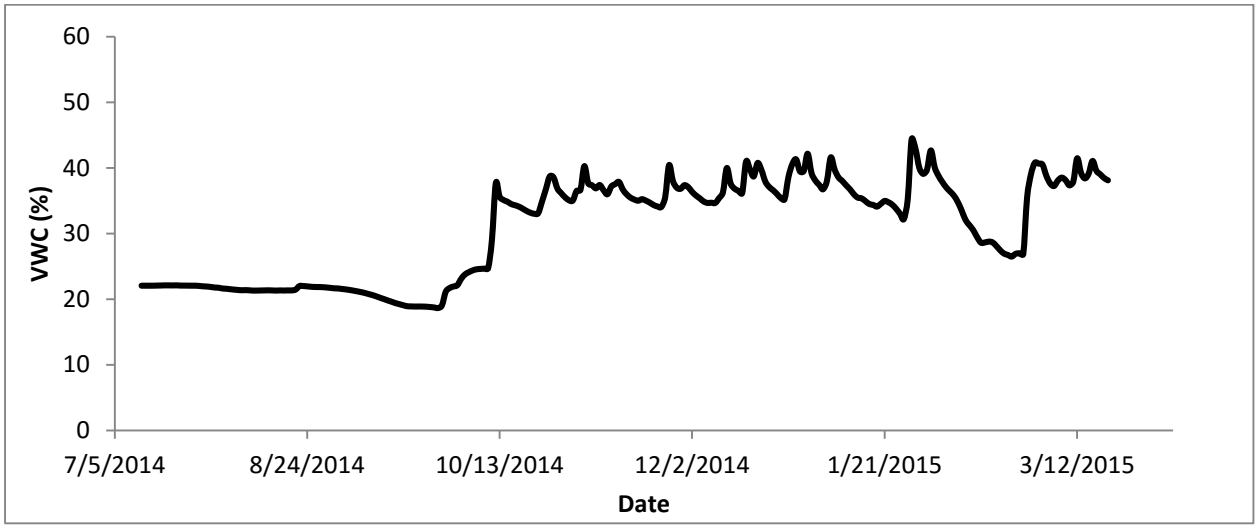

Figure 6.25 The average TDR pit soil moisture measurements in Catchment VI

The daily wireless TDR data was plotted for the measurement period, as shown in Figure 6.26. The wireless TDR data has gaps in the data set. This is due to errors in the data logging programme and faults in the sensors.

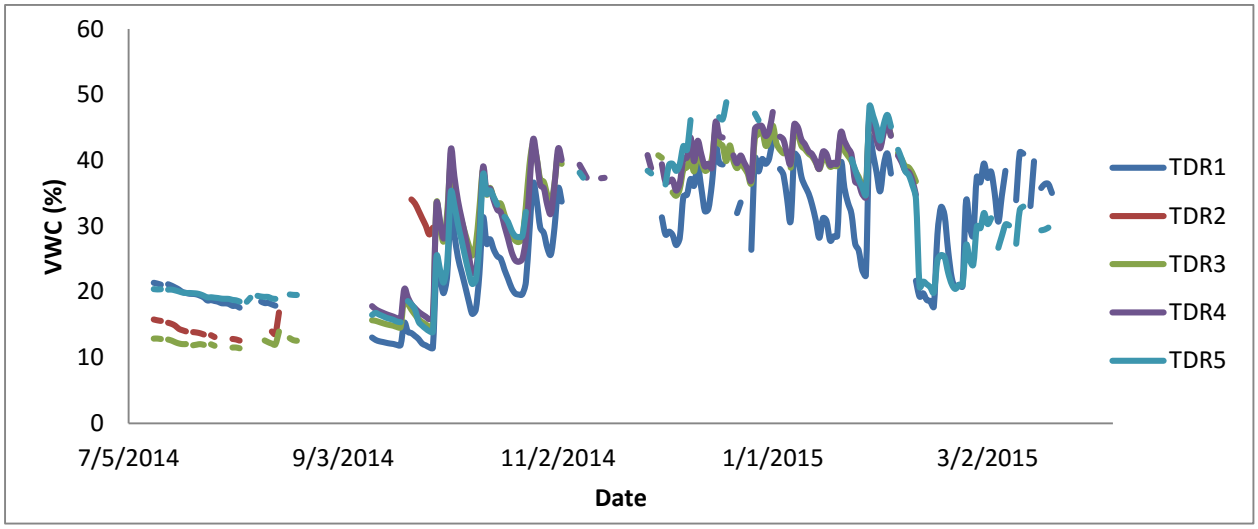

Figure 6.26 Daily wireless TDR data in Catchment VI

The Echo probe data was then plotted against time (Figure 6.27). The echo probe data only covered the dry period, as the fire that burnt Catchment VI, also destroyed the sensors, which could not be used again in this study.

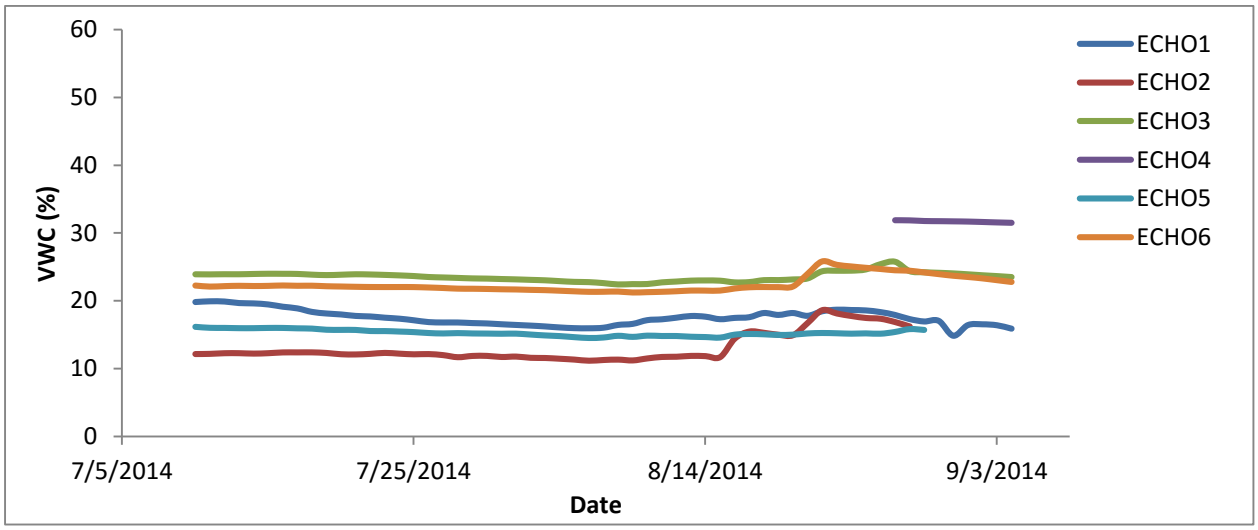

Figure 6.27 Daily echo probe data in Catchment VI

All three (TDR pit, wireless TDR and echo probe) sets of data were merged by weighting each point within the catchment equally, to create a representative *in-situ* soil moisture estimate (Figure 6.28), which shows the merged dataset. This dataset weighted each sensor, in each sample point equally.

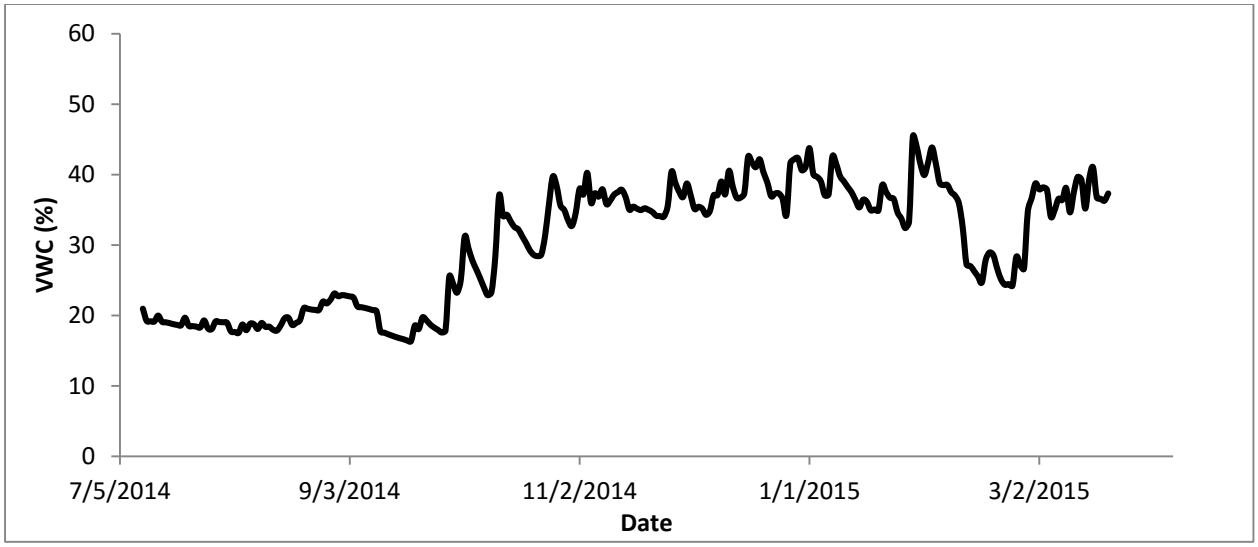

Figure 6.28 Representative soil moisture measurements

6.5 Acquisition and Processing of the AMSR2 Soil Moisture Product

This section describes the methodology adopted to obtain the AMSR2 remote sensing soil moisture product. The AMSR2 sensor estimates several parameters, which are predominately linked to the energy and water cycles, namely, precipitation, water vapour, sea-surface temperature, soil moisture and snow depth. The AMSR2 soil moisture product was obtained from the JAXA website: http://sharaku.eorc.jaxa.jp/. The data is freely available; however, a relatively short registration was required, in order to gain access into the GCOM-W1 Data Providing Service.

Level Two and Level Three soil moisture data sets are available from July 2012 to present day. The Level Two data is available on a 25 km spatial resolution grid, whilst the Level Three data is available on both 10 km and 25 km spatial resolution grids. The Level Three soil moisture product uses Level 1B brightness temperature and Level Two soil moisture data and averages both of them spatially and temporally, with respect to predefined lattice grid points on the earth's surface.

The 10 km and 25 km Level Three AMSR2 products are presented in Figure 6.29 and illustrates the significance of spatial resolution. The 10 km spatial resolution is much finer and therefore has a lot more detail, compared to the coarser 25 km resolution. The need for finer spatial resolution data is to capture spatial heterogeinity and accurately represent processes occuring at particular scales. The 10 km product results in a pixel area of 100 km^2, whilst the 25 km product results in a pixel area of 625 km^2.

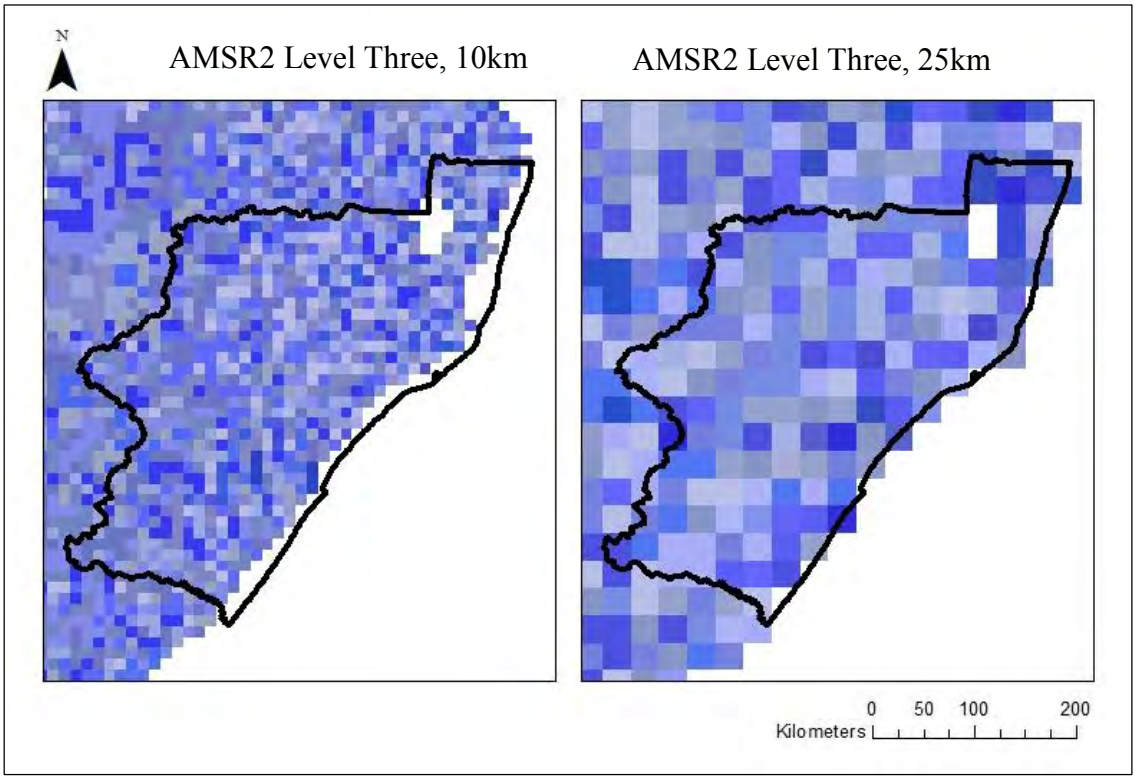

Figure 6.29 Comparison of spatial resolution of AMSR2 10 km and 25 km Level Three soil moisture products

The Level Three soil moisture product at a 10 km spatial resolution was selected to be used in this study. Once the Level Three 10 km soil moisture product is selected, the data type and observation period needs to be specified, before specifying the search area. Once all the specifications have been made, the data can be searched for and subsequently downloaded. The data format is then specified and there is an option to leave the data in its original format or convert it to HDF5, Geotiff of NetCDF. The conversion to Geotiff was chosen, as this data format is compatible with ArcGis 9.3.

The data can now be ordered. Once ordered, an order acceptance email, which contains an ftp and URL site link to directly download the data. The data was then opened in ArcGis 9.3. The data was defined on the WGS 84 geographic coordinate system and no projection or transformation was required. There were two files per day, as each day had an ascending and descending orbit.

Due to the nature of satellite orbits, on some days, the catchment area was covered by:

i. An ascending orbit;
ii. A descending orbit;
iii. An ascending and descending orbit;
iv. Neither.

The catchment shape file was overlaid onto the AMSR2 soil moisture raster image, as seen in Figure 6.30. The pixel value that was covered by the catchment was determined. The pixel values ranged from 0 to 600. The pixel values were multiplied by a scaling factor of 0.001, to obtain the soil moisture in g/cm^3. The density of water is assumed to be 1.0 g/cm^3 and the volume of 1.0 g of water is 1.0 cm^3. Therefore, the VWC in percentage was obtained by multiplying the scaled pixel value by 100.

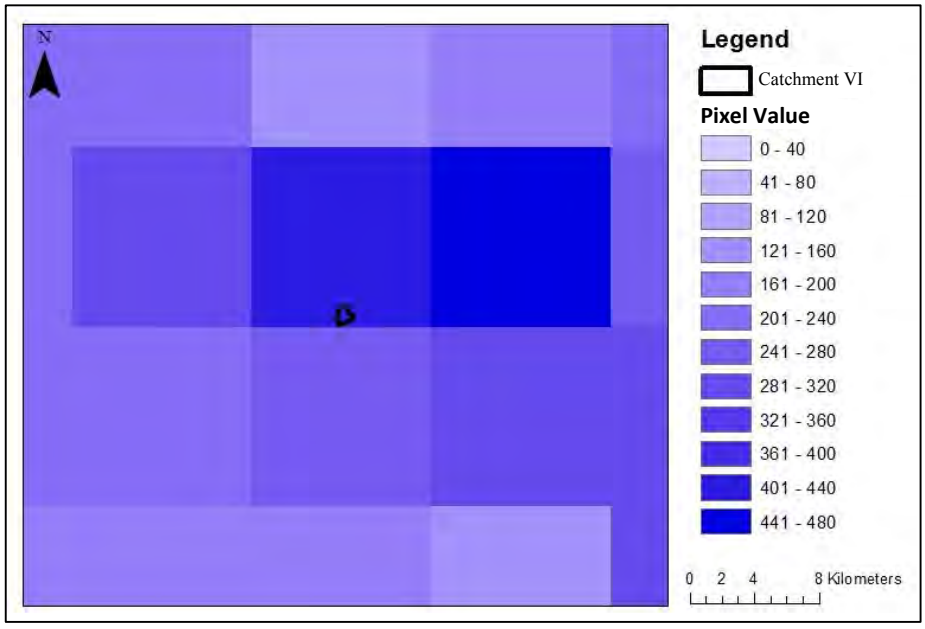

Figure 6.30 The Catchment VI shapefile overlaid over the AMSR2 soil moisture product to obtain the volumetric water content

6.6 Acquisition and Processing of the SMOS Soil Moisture Product

This section describes the methodology adopted to obtain the SMOS remote sensing soil moisture product. Level Two and Level Three SMOS soil moisture products are available. The Level Two soil moisture products are at a 30-50 km spatial resolution and can be obtained from the ESA website: http://eopi.esa.int/. The data is freely available from the Eoli-sa catalogue. The Eoli-sa catalogue gives users access to European Space Agency (ESA) Earth Observation data products.

The Level Three SMOS soil moisture products are available from the national French and Spanish processing entities, namely, the CATDS (Centre Aval de Traitement des Donnees SMOS) and SMOS CP34-BEC (SMOS Barcelona Expert Centre). The BEC-34 was used, as it was more user-friendly and the site was a lot easier to navigate. The BEC is an ESA expert support laboratory committed to the ongoing analysis and development of new algorithms to improve the baseline SMOS Level Two products.

The SMOS Level Three soil moisture products are computed from Level Two soil moisture user data products, which consist of geophysical parameters, a theoretical estimate of accuracy, flags and product descriptors. First, the Level Two soil moisture user data products are filtered and combined into maps with the same spatial resolution. Next, the quality flags and product descriptors are used to discard unreliable soil moisture values. The final soil moisture product is a global daily soil moisture map on a 25 km spatial resolution grid.

The Level Three SMOS BEC-34 data was obtained from http://cp34-bec.cmima.csic.es/. This site is the SMOS-BEC data distribution and visualization service. A short registration procedure is required before the data can be accessed from the site's THREDDS service, which provides netCDF data files. The SMOS soil moisture products fall under the Land category. The BEC land near real-time (0.25 x 0.25 degree resolution) was selected, as the other two options had fine resolution soil moisture, which only covered the Iberian Peninsula. The option selected was a global dataset. There are numerous soil moisture products at different intervals. The one-day global soil moisture product was chosen. For each day, there are two files, the ascending and descending orbits. Figure 6.31 shows the navigation through the THREDDS service.

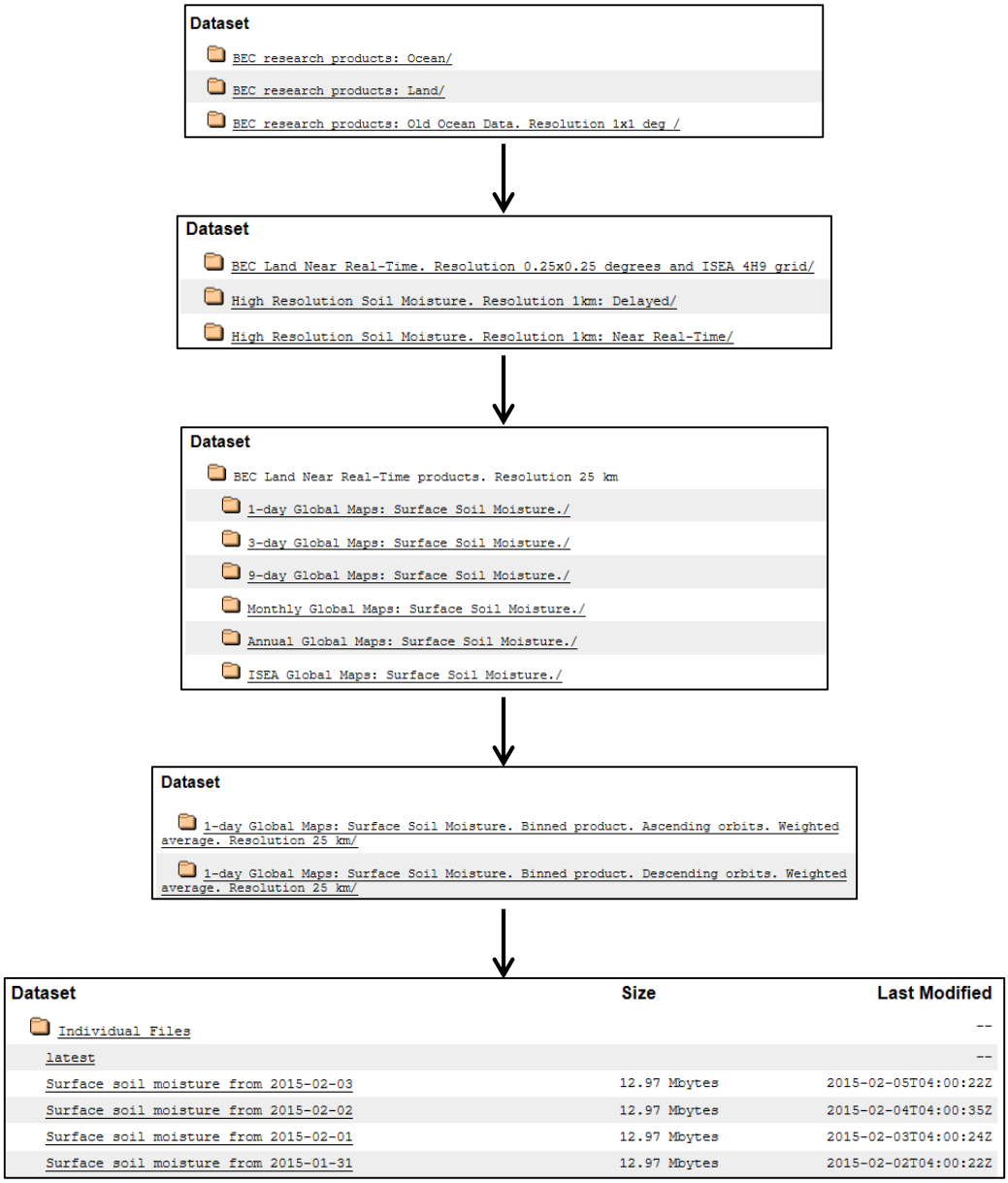

Figure 6.31 Navigation through the THREDDS service

The soil moisture product files can either be directly downloaded or viewed, using one of the data viewers on the site. The viewers include NetCDF-Java ToolsUI, Integrated Data Viewer and the Godiva2 online tool. The Godiva2 online visualization tool was used to obtain the soil moisture data (Figure 7.32).

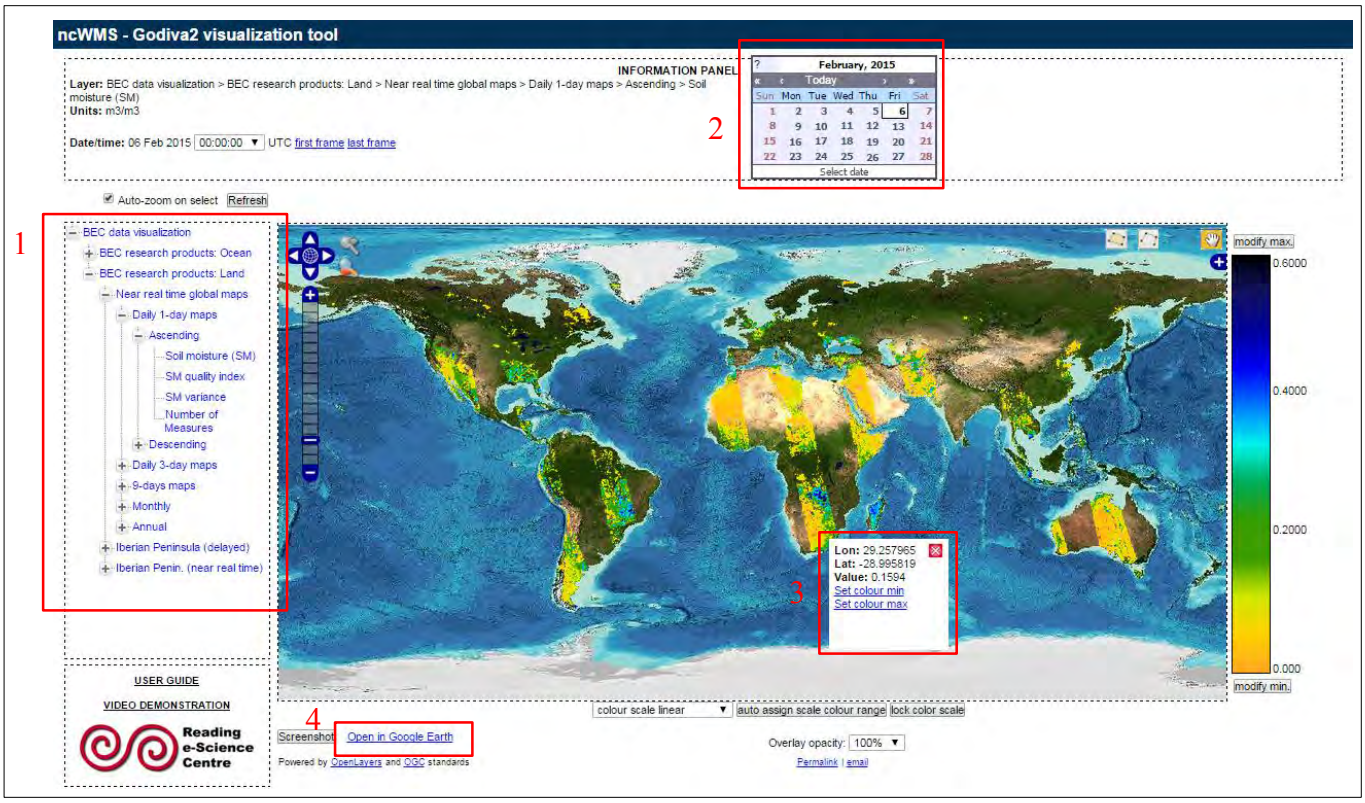

Figure 6.32 Layout of the Godiva2 online visualization tool

The Godiva2 visualization tool is very user-friendly and the data was easily obtained. The required data set was viewed by selecting the necessary data requirements (1). The data requirements were selected as follows; the BEC research products land, near-real time global maps, daily one-day maps, choose between ascending and descending (both are required, but are obtained separately) and lastly soil moisture (SM).

Next, the date was specified (2). The data for a specific day is viewed by clicking on the date on the calendar. The transition from day-to-day is quick.

The global map was used to locate the co-ordinates of the area required. The correct pixel was located, which corresponded to the co-ordinates of the catchment. The pixel information, which consisted of its longitude, latitude and soil moisture value, was displayed (3).

A check was done to determine if the catchment was contained in one pixel. This was done by opening the image in Google Earth (4).

Once it was determined that the catchment was completely contained in one pixel (Figure 6.33), the soil moisture data could be obtained by changing the date and obtaining the data by clicking on the corresponding pixel (Figure 6.34).

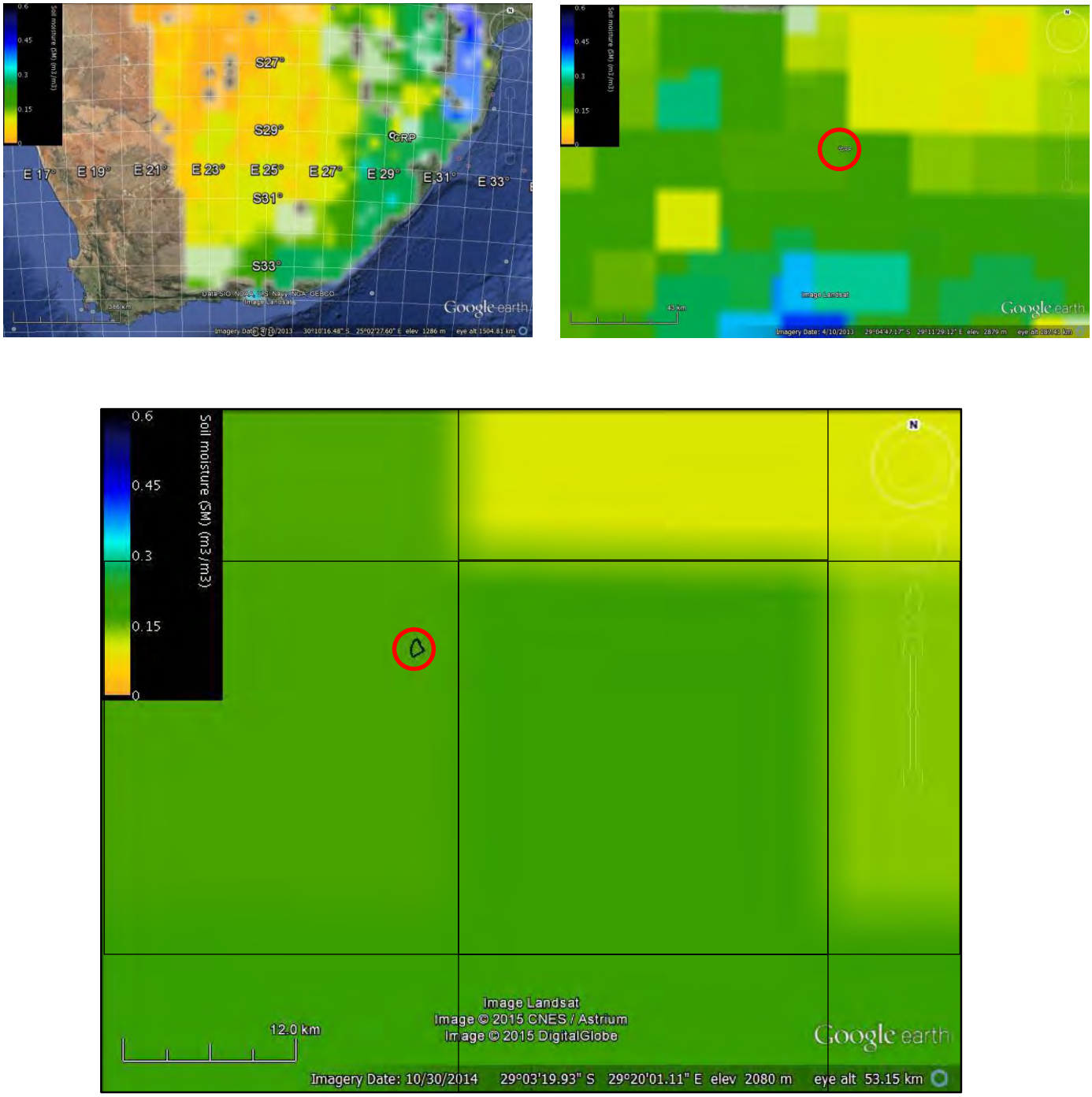

Figure 6.33 The position of the catchment in relation to a single pixel of the SMOS soil moisture product

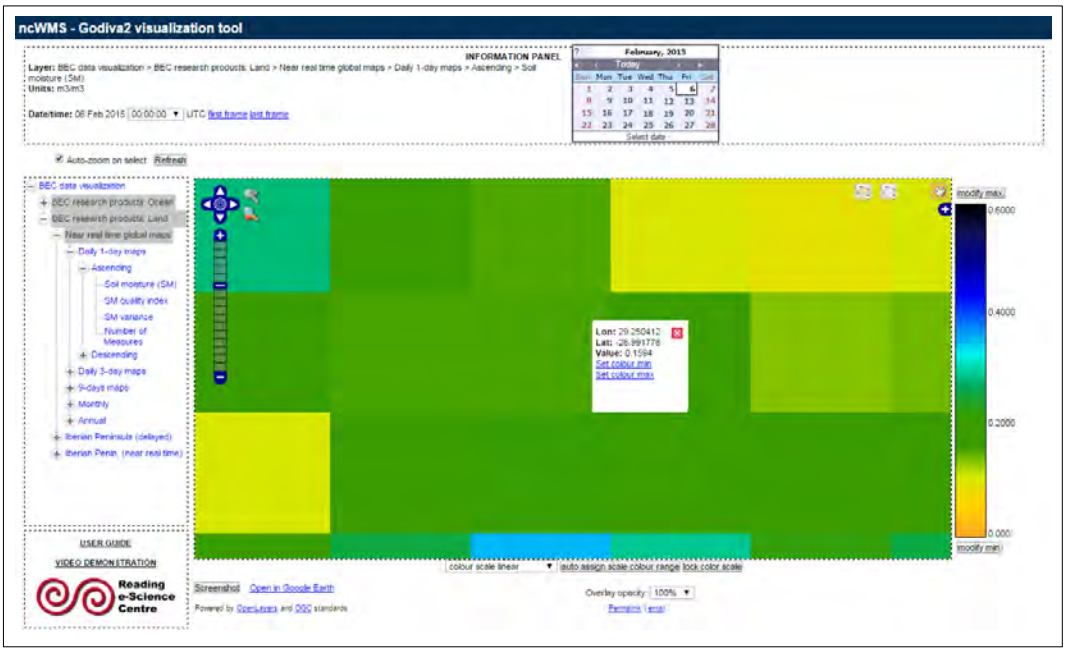

Figure 6.34 Godiva2 visualization tool showing the pixel value for the Catchment VI

This method of obtaining daily soil moisture data was efficient, as the data did not have to be downloaded, stored, opened with the appropriate software, spatially defined and projected, before overlaying the catchment shapefile and determining the soil moisture estimate. This online viewer was more than adequate to obtain the daily soil moisture data for both ascending and descending data sets for a one year period. The images obtained were near-real time, as the present day data was available the following day. The pixel values were in volumetric water content, so no conversion was required.

6.7 Analysis of AMSR2 and SMOS Remote Sensing Data

The AMSR2 and SMOS products are daily soil moisture products; however, there were days in which the study area was not covered by an ascending or descending orbit (missing data). Of the 365 day study period the various days in terms of coverage are presented in Figures 6.35 and 6.36.

From Figure 6.35, it can be seen that AMSR2 data was available for 343 days of the 365 days. There were 22 days which had no data, resulting in a daily annual coverage of 94%. The days with missing data seemed to follow a general pattern throughout the year, as there were similar amounts of missing data each month of the observation period.

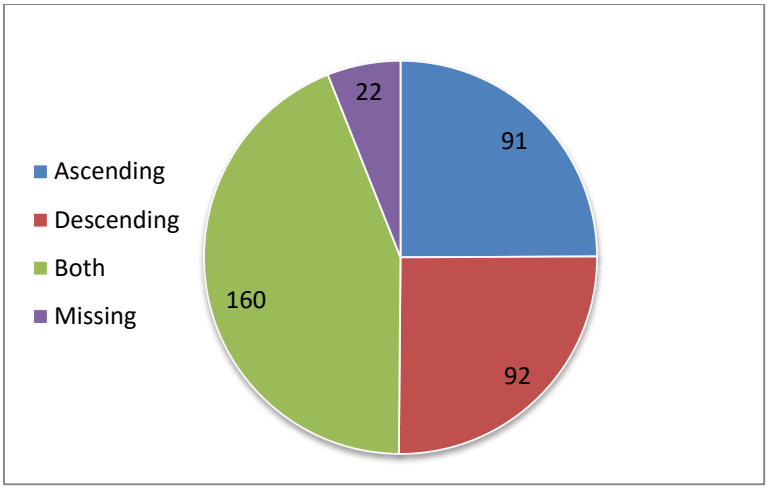

Figure 6.35 AMSR2 data availability for the observation period

From Figure 6.36, it can be seen that of the 365 of days observed SMOS data, 129 days are missing, which results in a daily annual coverage of 65%. Of the total 236 days with data, only 103 of them were covered by both ascending and descending orbits, whilst 66 days had an ascending value only and 67 days had a descending value only.

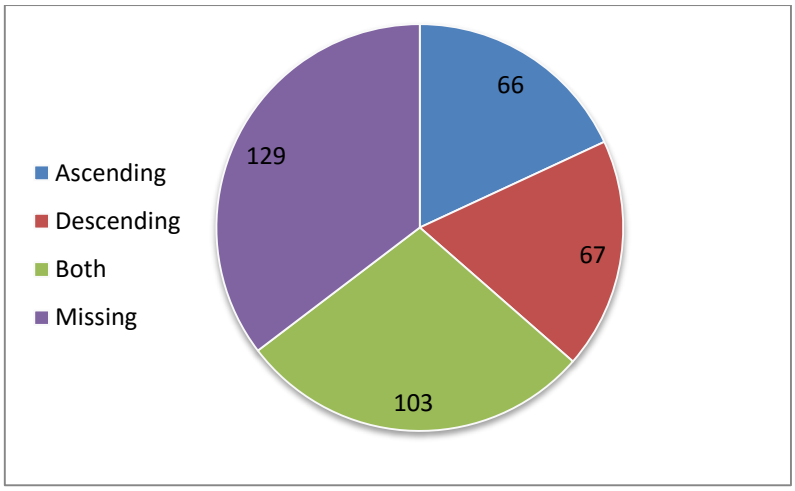

Figure 6.36 SMOS data availability for the observation period

The 160 days for which ascending and descending AMSR2 data was available was plotted against time, as indicated in Figure 6.37. This was done to compare the ascending and descending values of the same day. From figure 6.37, there is very close correlation between the ascending and descending values during the dry period. There is less correlation during the wet periods. Both the ascending and descending datasets follow the same trend.

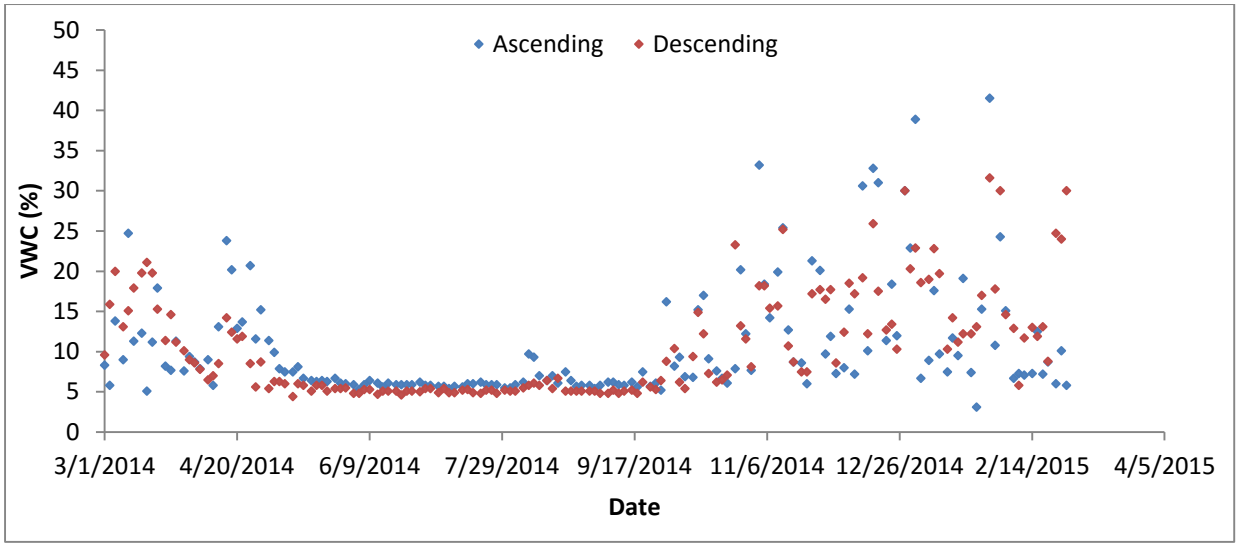

Figure 6.37 Time series analysis of days which have both ascending and descending AMSR2 values

The 103 days for which ascending and descending SMOS data was available was plotted as a time series (Figure 6.38). From figure 6.38, it is evident that both the ascending and descending data follow the same trend. There are differences in values between the two datasets on the same day. These differences are larger in the wetter periods. The differences in ascending and descending values are greater for the SMOS dataset compared to the AMSR2 dataset.

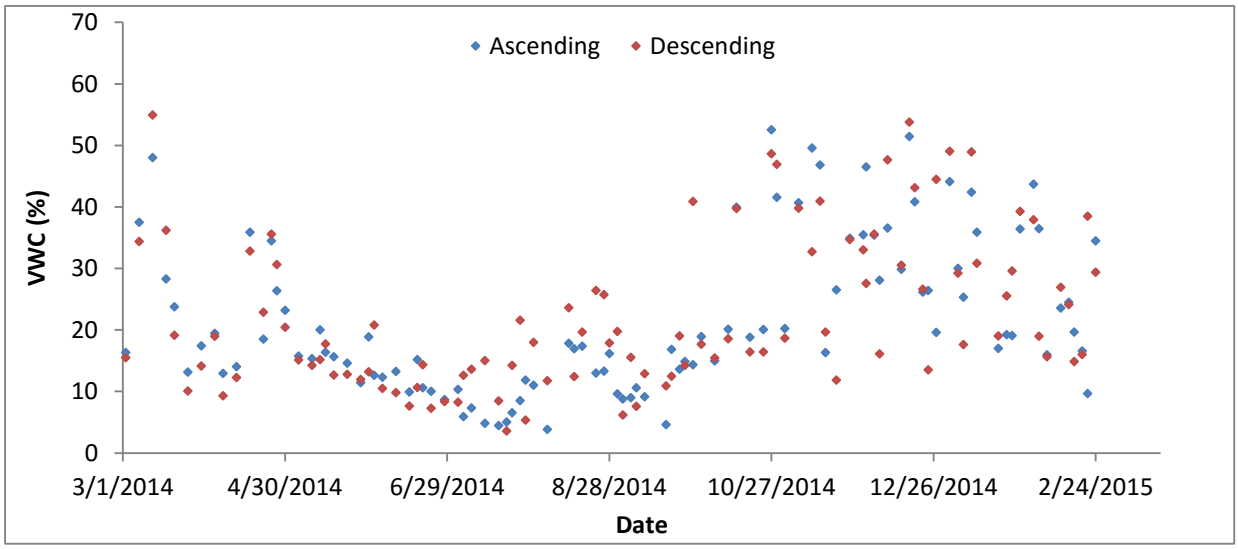

Figure 6.38 Time series analysis of days which have both ascending and descending SMOS values.

The differences observed between the ascending and descending values for the same day and over the time period can be attributed to the temporal variation in soil moisture. The ascending values are obtained at 06:00, whereas the descending values are obtained at 18:00. Therefore, the change in soil moisture during this 12-hour interval could be due to rainfall and total evaporation.

This is further emphasized in the dry period, when rainfall and total evaporation is low. The ascending and descending values correlate well, as the VWC does not change much in the interval. However, in summer, the rainfall and total evaporation rates are high resulting in changes in the VWC between the ascending and descending measurements.

There are expected differences between ascending and descending overpass soil moisture retrievals, due to the difference in geophysical conditions at day time and night time, with night time conditions being more favourable for soil moisture retrieval (Kim *et al.*, 2015). Therefore, should soil moisture studies only use descending values, which would result in more missing data days, but better favourable soil moisture retrieval values.

An alternative is to use only the days which have both ascending and descending values, as this will average the two retrieval values, however, there will also be a large number of missing data days. For this research study, all observation days with ascending, descending and days with both ascending and descending values were used.

6.8 PyTOPKAPI Soil Moisture Product (SAHG)

This section details the acquisition of the PyTOPKAPI modeled soil moisture estimates. The PyTOPKAPI soil moisture product was obtained from the Satellite Applications and Hydrology Group (SAHG) website: http://sahg.ukzn.ac.za/.

The PyTOPKAPI modelled soil moisture product will be referred to as the SAHG soil moisture product. The soil moisture products are freely and readily available. The data has a temporal resolution of three hours and is on a spatial resolution grid ≈ 12.5 km. The data ranges from the year 2008 to the present.

The data was obtained by downloading the SSI (soil saturation index) product in the ascii file format, which can be opened and processed in ArcGis 9, as seen in Figure 6.39. The soil moisture data for each day was available on a three-hour time-step. Therefore, eight files had to be downloaded for each day.

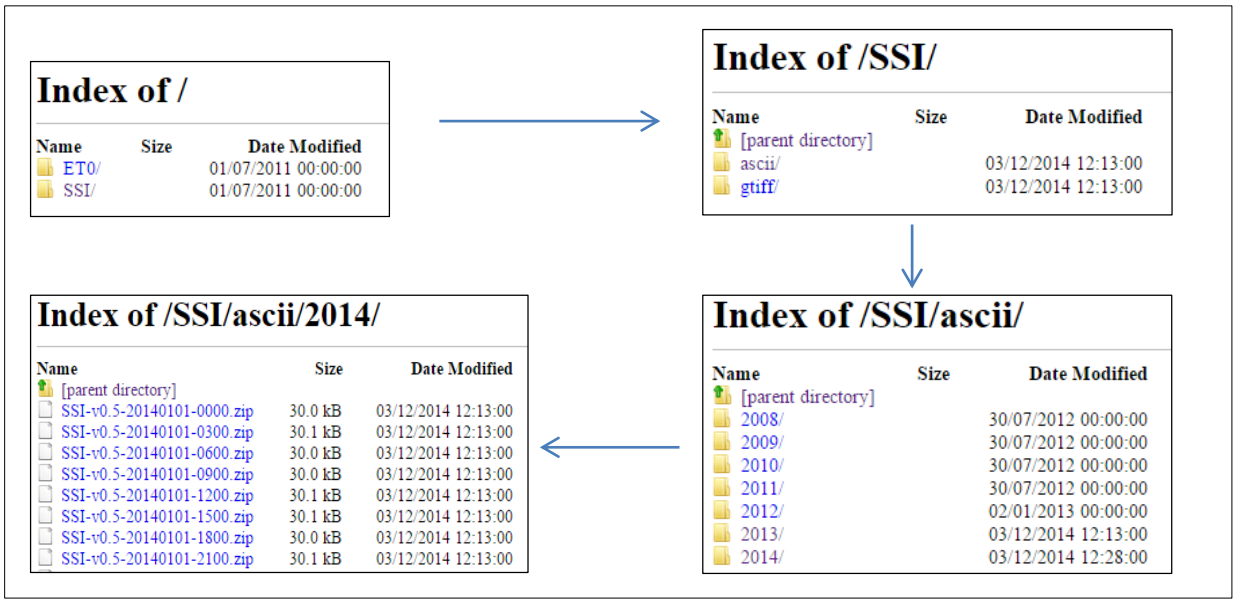

Figure 6.39 Navigation through the SAHG website to download SSI data

The files were then opened in ArcGis 9.3 and the spatial referencing of the data was first checked. The data was defined in the correct spatial reference (WGS 84 geographic co-ordinates) and no defining projections and transformations were required. The soil moisture products were on a three-hour time-step: (i) 00:00, (ii) 03:00, (iii) 06:00, (iv) 09:00, (v) 12:00, (vi) 15:00, (vii) 18:00 and (viii) 21:00 (see Figure 6.40). These eight raster images per day had to be converted into a daily raster image. This was done by using the Mosaic to New Raster option under the Data Management Tools in ArcGIS 9.3.

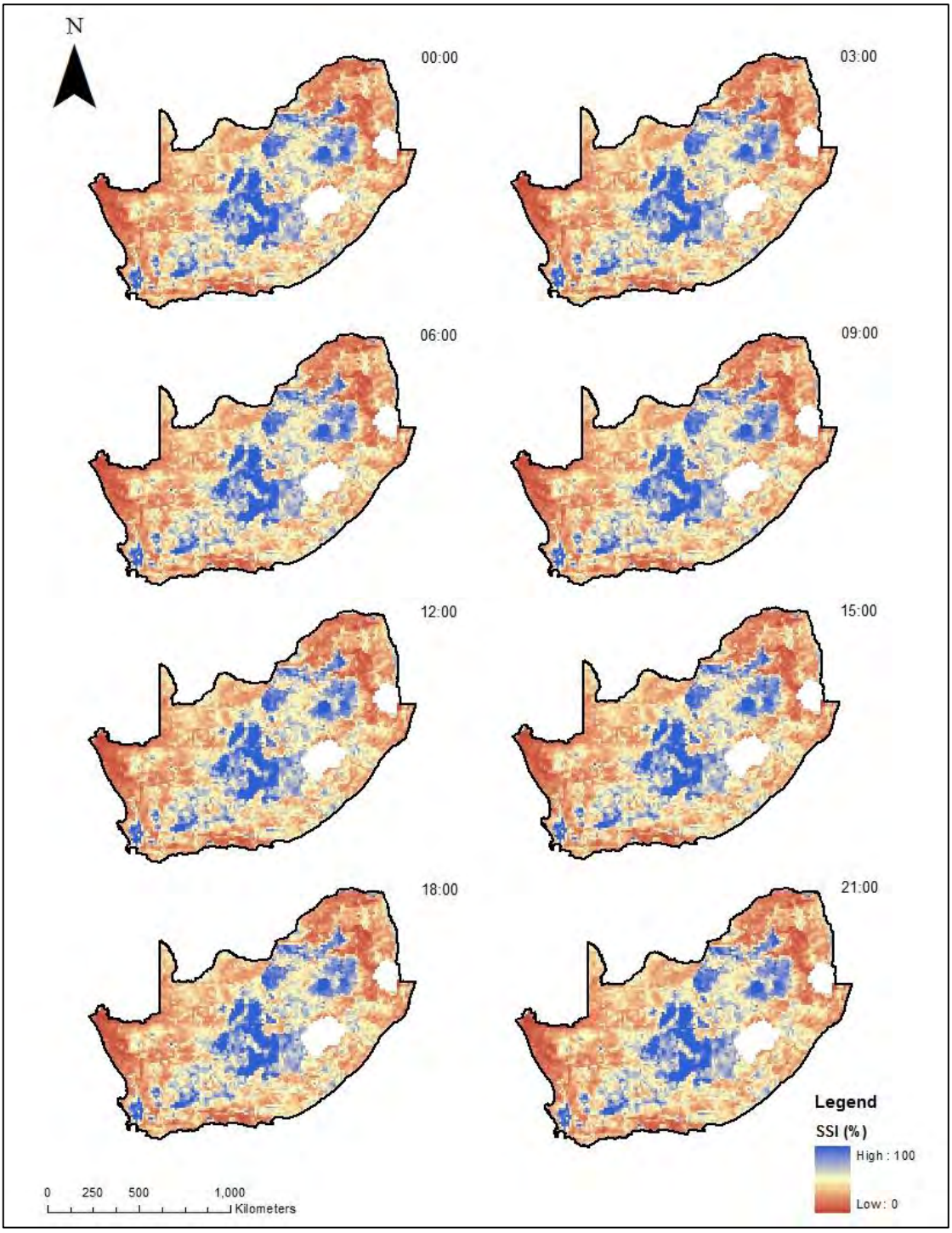

Figure 6.40 One day of SSI data (eight images on a three hour interval)

Once the daily image was created (Figure 6.41), the catchment shape file was overlaid onto it (Figure 6.42). The pixel value was then determined and recorded.

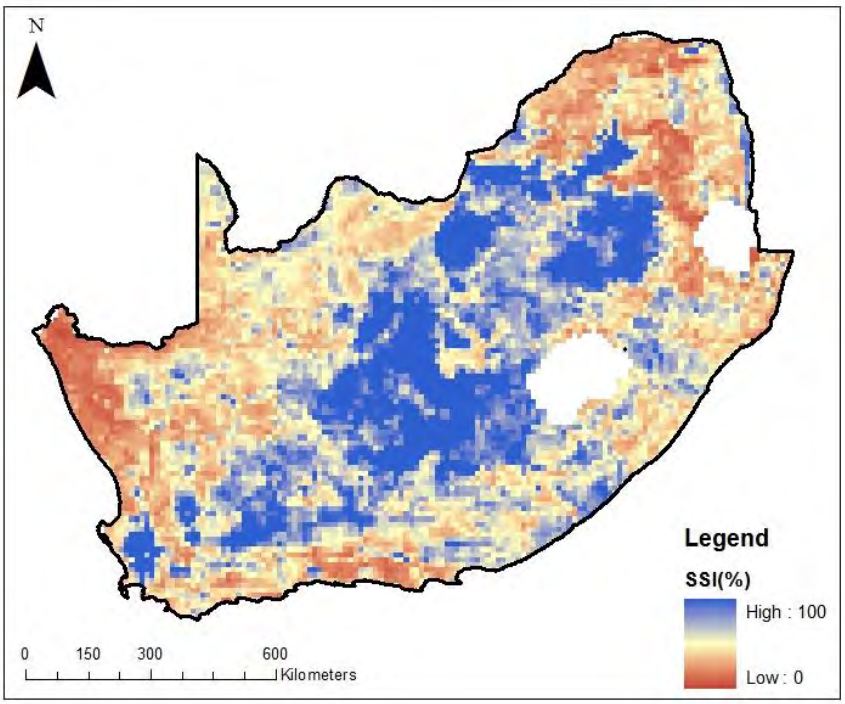

Figure 6.41 Daily SAHG soil moisture product

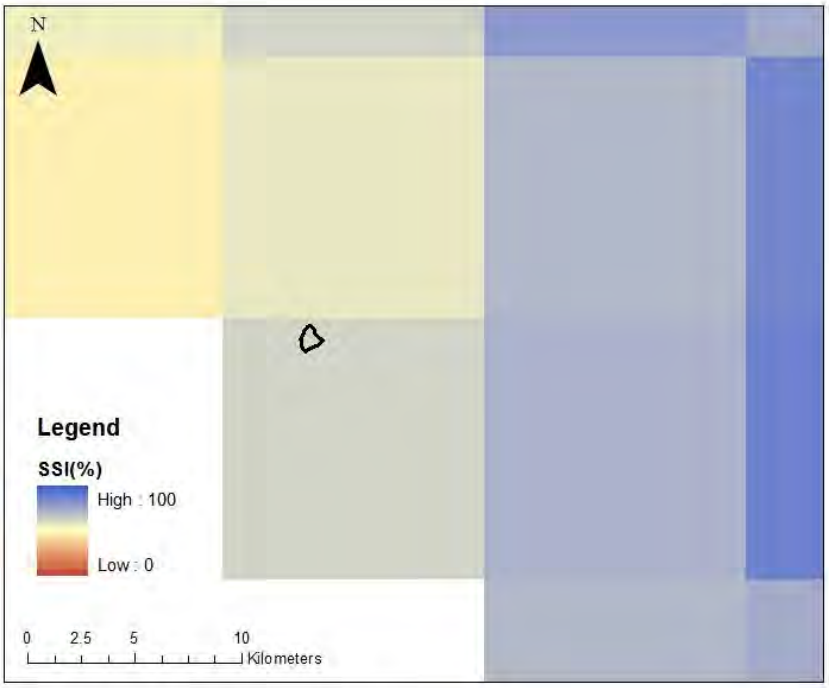

Figure 6.42 Overlay of the Cathedral Peak Catchment VI onto the SAHG soil moisture product

The soil moisture data from the SAHG product is represented as a soil saturation index (SSI), which is expressed as a percentage. The SSI was then converted into a VWC, using the simplified equation.

$$SSI = \frac{VWC}{Porosity} \quad (6.15)$$

The SSI equation (Equation 6.15) can easily be rearranged to solve for VWC:

$$VWC = SSI \times Porosity \quad (6.16)$$

The soil porosity can be determined by measurement or calculation. In order to calculate porosity, the following equation was used:

$$Porosity = 1 - \frac{Pb}{Ps} \quad (6.17)$$

where Pb is the bulk density and Ps is the particle density. The bulk density was determined to be 0.593 g/cm3 and a generic value of 2.65 g/cm3 was used for the particle density (Hillel, 2008).

$$Porosity = 1 - \frac{0.593}{2.65}$$

The porosity was calculated to be 0.77. Therefore, from Equation 6.16, all the SSI values were multiplied by 0.77, to convert them to volumetric water content.

The porosity was determined from the bulk density, which was valid for the top 0.15 m of the soil surface. The PyTOPKAPI soil moisture product is the SSI for the A and B horizon of the soil profile. Therefore, a porosity value that represents the A and B (one meter depth) horizon, needs to be determined. A study conducted by Everson *et al*. (1998), contains soil bulk density values for Catchment VI at depths of 0.20, 0.50, 0.75 and 1.00 m (Table 6.6). The bulk density values used in this study can be incorporated and used to obtain a representative porosity value that covers the A and B horizons. The porosity values should not have changed over the past 16 years, as the catchment is in a protected area.

Table 6.6 The bulk density of Catchment VI, as determined by Everson *et al*. (1998)

Soil Depth (m)	Dry Season		Wet Season		Mean
0.20	0.660	0.786	0.868	0.886	0.800
0.50	0.898	0.899	0.847	0.798	0.861
0.75	0.803	0.757	0.662	0.784	0.752
1.00	0.863	0.799	0.905	0.844	0.853

These bulk density values were incorporated into the values that were obtained in this study and the mean bulk density of the soil profile (0 to 1.00 m) was determined (Table 6.7).

Table 6.7 Mean bulk density according to depth

Soil Depth (m)	Mean Bulk density (g/cm^3)
0.05	0.525
0.10	0.597
0.15	0.656
0.20	0.800
0.50	0.861
0.75	0.752
1.00	0.853
Average	0.720

The average bulk density was 0.720 g/cm3. The average porosity was calculated, using the new bulk density value in Equation 6.12.

$$Porosity = 1 - \frac{0.720}{2.65} \quad (6.12)$$

The average porosity is 0.728. Therefore, the SSI pixel values obtained must be multiplied by 0.728, in order to convert them into VWC (Equation 6.11).

6.9 Surface Energy Balance System (SEBS)

The SEBS Model, developed by Su (2002), was run in the Integrated Land and Water Information System (ILWIS) 3.8.3 for the estimation of relative evaporation and evaporative fraction in Cathedral Peak Research Catchment VI for the period of March 2014 to March 2015. The SEBS Model uses remote sensing and meteorological data sets to estimate heat fluxes.

Landsat 8 images were used for the estimation of relative evaporation and evaporative fraction, using the SEBS Model. The Landsat 8 satellite, as seen in Figure 6.43, is the latest addition to the Landsat series and was launched on the 11th of February 2013 (Markham *et al.*, 2015). Landsat satellites have continuously acquired information of the earth's land surface since 1972, thus the continuation of data acquisition from the Landsat 8 satellite is essential (USGS, 2013). Landsat 8 orbits the earth at an altitude of 705 km, which results in 14 full orbits being completed each day, with every point of the earth being covered once every 16 days. The satellite carries out north to south orbits and has an overpass time of 10:00 (Markham *et al.*, 2015). Landsat 8 carries two push-broom sensors, so that the reflective and thermal bands were split into two instruments (Markham *et al.*, 2015). These two instruments are the Operational Land Imager (OLI) and Thermal Infrared Sensor (TIRS).

Figure 6.43 Landsat 8 satellite

Landsat 8 images were used in this study due to their spatial resolution. It has the ability to estimate relative evaporation and evaporative fraction at a spatial resolution of 30 m, however, it has a temporal resolution of 16 days. The Landsat 8 product consists of several bands (one to eleven), each band having its own spectral characteristics and wavelength range (Table 6.8).

Table 6.8 Characteristics of the various landsat 8 bands (USGS, 2015).

Spectral bands	Wavelength (µm)	Resolution (m)
1- coastal/aerosol	0.43-0.45	30
2- blue	0.45-0.51	30
3- green	0.53-0.59	30
4- red	0.64-0.67	30
5- near IR	0.85-0.88	30
6- SWIR 1	1.57-1.65	30
7- SWIR-1	2.11-2.29	30
8- panchromatic	0.50-0.68	15
9- cirrus	1.36-1.38	30
10- TIRS 1	10.60-11.19	100
11- TIRS 2	11.50-12.51	100

Landsat 8 satellite imagery was freely acquired from the Earth Explorer website: http://earthexplorer.usgs.gov. The area of interest and time period of the data required was specified. Next, the data set that the user requires can be selected from a list of all the available data sets. The data set selected was the L8 OLI/TIRS. The catchment study area fell within one Lesotho image. The Landsat 8 image footprint is very large, as seen in Figure 6.44. Between March 2014 and March 2015, there were a total of 22 images.

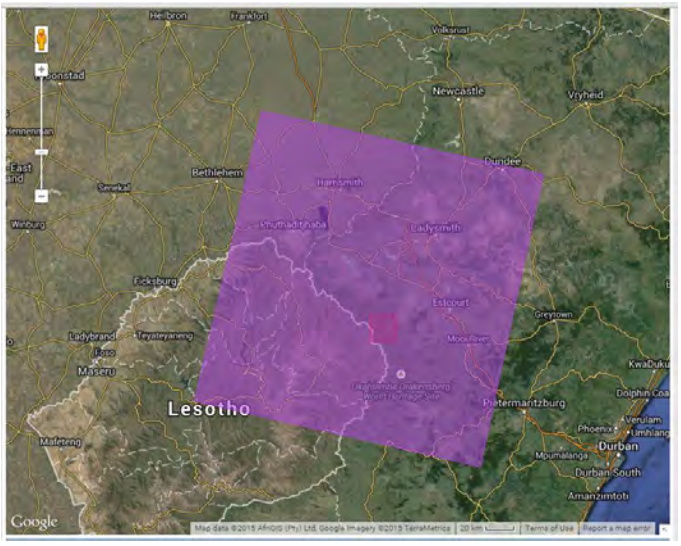

Figure 6.44 Landsat 8 image footprint

Most of the images, which were acquired, were for clear sky conditions. Some images possessed variable cloud cover; however, the area of interest was cloud-free, therefore, the image could still be used. There were six images, which could not be used for the retrieval of the evaporative fraction and relative evaporation, as the image contained cloud cover, which blocked the area of interest. The different cloud-cover conditions are seen in Figure 6.45.

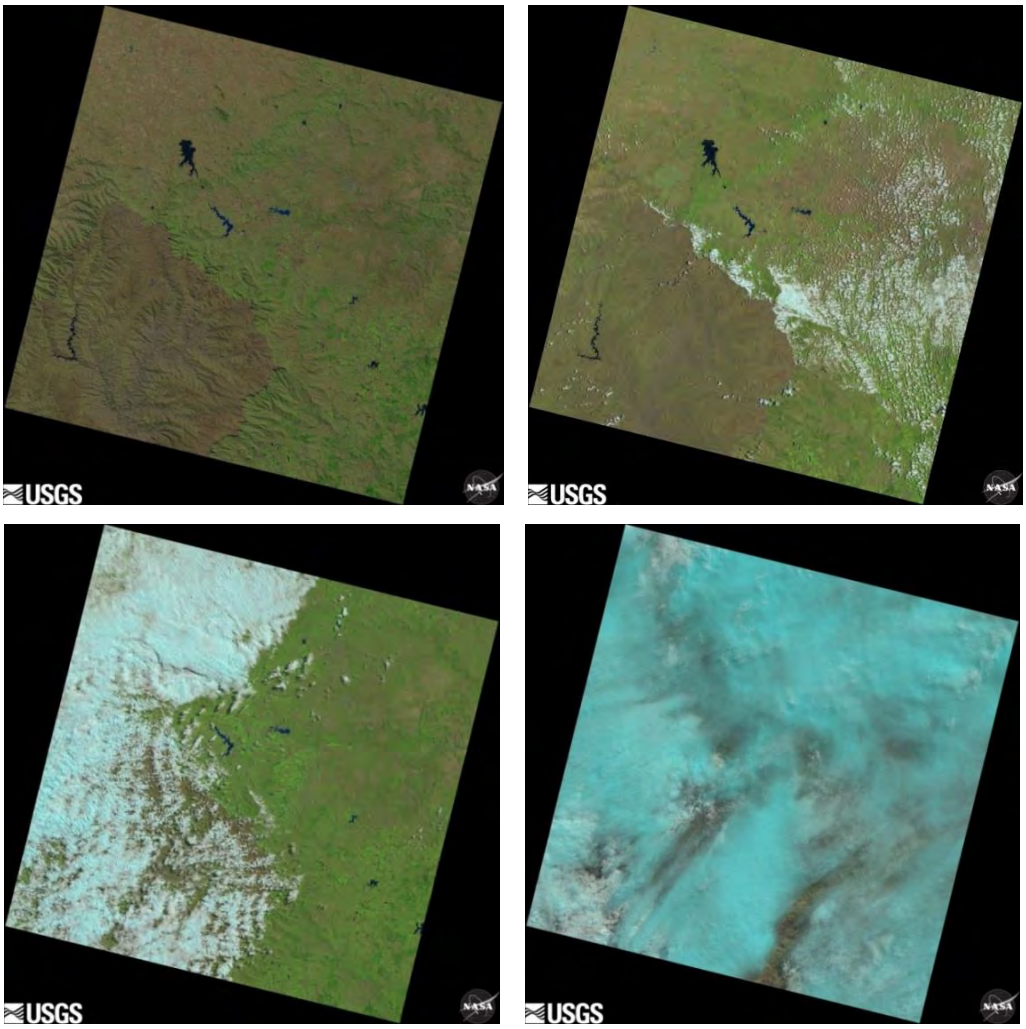

Figure 6.45 Landsat images with different cloud-cover conditions

Of the 22 images available for the study period, only 16 images could be used due to cloud-cover. The 16 images that could be used were downloaded. The Level one Geotiff Data Product was the download option selected. Each Level One Geotiff product contains a Material Library (MTL) file, which contains all the necessary information (metadata) about the images and 12 images, which include images B1 to B11 and BQA, where B1 is band one and B11 is band eleven.

The ILWIS 3.8.3 software was downloaded from http://52north.org/downloads/ilwis/. The images (bands) were imported into ILWIS 3.8.3 as digital numbers (DN). The bands required were 2, 3, 4, 5, 6, 7, 10 and 11. These bands were rescaled to Top of Atmosphere (TOA) reflectance and/or radiance, using the radiometric rescaling coefficients provided in the metadata file. The procedure followed has been outlined by Allen *et al.* (2002) and the USGS (2015). The USGS (2015) provides the necessary equations for the conversion to TOA Radiance, conversion to TOA Reflectance and conversion to TOA brightness temperature. The equations to obtain the inputs into the SEBS Model, such as the albedo, NDVI, surface emissivity and land surface temperature maps are presented in Allen *et al.* (2002). Although the equations in Allen *et al.* (2002) were intended to be used in SEBAL, they can be used in other models, such as SEBS.

Conversion to TOA Radiance

Bands 10 and 11 (TIRS bands) were converted to TOA Radiance, using the radiance rescaling factors provided in the metadata file (USGS, 2015).

$$L\lambda = (M_L * Q_{cal}) + A_L \quad (6.18)$$

where, Lλ is the TOA spectral radiance (Watts/(m^2*srad*µm)), ML is the band specific multiplicative rescaling factor (RADIANCE_MULT_BAND_X) from the metadata file (where X is the band number), Qcal is the quantized and calibrated standard product pixel value (DN) and AL is the band specific additive rescaling factor (RADIANCE_ADD_BAND_X) from the metadata (where X is the band number).

Conversion to TOA Reflectance

Bands 2, 3, 4, 5, 6 and 7 (OLI bands) were converted to TOA planetary reflectance, using reflectance rescaling coefficients provided in the metadata file (USGS, 2015).

$$P\lambda' = (M_P * Q_{cal}) + A_P \quad (6.19)$$

where Pλ′ is the TOA planetary reflectance (without solar angle correction), Mp is the band specific multiplicative reflectance factor (REFLECTANCE_MULT_BAND_X) from the metadata file (where X is the band number) and Ap is the band specific additive rescaling factor (REFLECTANCE_ADD_BAND_X) from the metadata (where X is the band number).

The TOA reflectance was then corrected for the sun angle (USGS, 2015):

$$P\lambda = \frac{P\lambda'}{\sin(\Theta_{SE})} \quad (6.20)$$

where pλ is the TOA planetary reflectance and Θ_{SE} is the local sun elevation (SUN_ELEVATION), which is obtained from the metadata file.

The ESUN values were determined for bands 2, 3, 4, 5, 6 and 7, using the following equations (Allen *et al.*, 2002):

$$ESUN = (\pi * d^2) * \left(\frac{RAD\_MAX}{REF\_MAX}\right) \quad (6.21)$$

Where d is the earth-sun distance, RAD_MAX is the maximum radiance and REF_MAX is the maximum reflectance (all of which are found in the metadata file).

The ESUN values (Table 6.9) are required to create an equation to determine albedo for the TOA (Allen *et al.*, 2002).

$$\alpha_{TOA} = \sum(\omega\lambda * P\lambda) \quad (6.22)$$

$$\omega\lambda = \frac{ESUN\lambda}{\sum ESUN\lambda} \quad (6.23)$$

Table 6.9 Calculated ESUN values

Band	ωλ	Band	ωλ
2	0.300	5	0.143
3	0.277	6	0.036
4	0.233	7	0.012

The ESUN band values change, due to changes in the earth-sun distance (d), maximum radiance and maximum reflectance of each data product. However, the $\omega\lambda$ band value was determined to be the same for each image, as the ratio remains the same.

Albedo is then calculated by correcting TOA albedo, using the following equation (Allen *et al.*, 2002):

$$\propto = \frac{\alpha_{TOA} - \alpha_{Path\_radiance}}{{\tau_{sw}}^2} \qquad (6.24)$$

where $\alpha_{Path\_radiance}$ is 0.03 and τ_{sw} is 0.774 (Allen *et al.*, 2002).

The generated albedo map is illustrated in Figure 6.46. Albedo ranges from 0.0 to 1.0 and is a measure of the reflectivity of the earth's surface. As the reflectivity increases, the albedo value increases. Grasslands generally have an albedo of between 0.15 to 0.25.

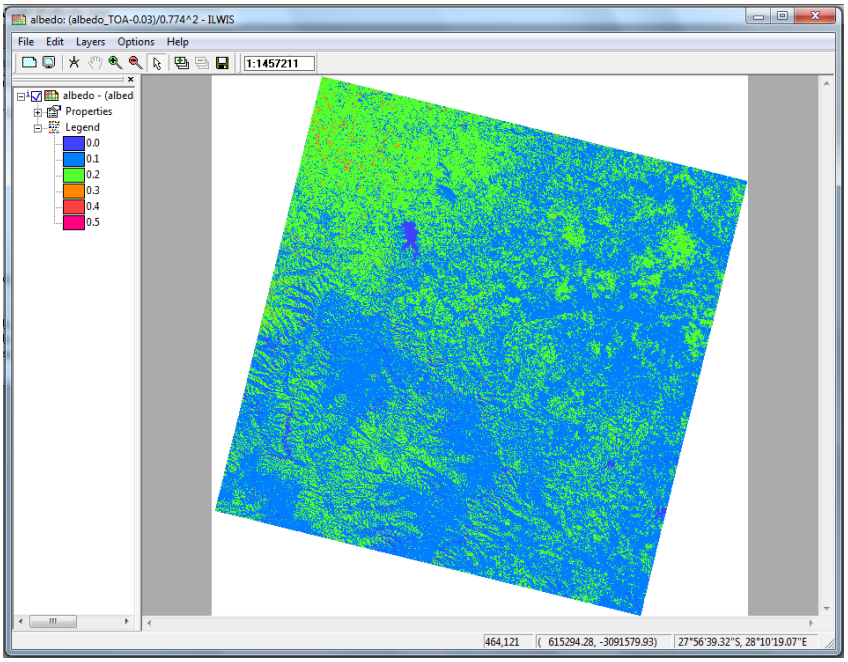

Figure 6.46 Albedo map generated in ILWIS

The normalized difference vegetation index (NDVI) was determined by Allen *et al.* (2002):

$$NDVI = \frac{(P5-P4)}{(P5+P4)} \quad (6.25)$$

where P5 is the corrected reflectance band five and P4 is the corrected reflectance band four. The generated NDVI map is illustrated in Figure 6.47. The NDVI ranges from -1.0 to 1.0. The more vegetation present, the higher the NDVI value. Water bodies have a negative NDVI value.

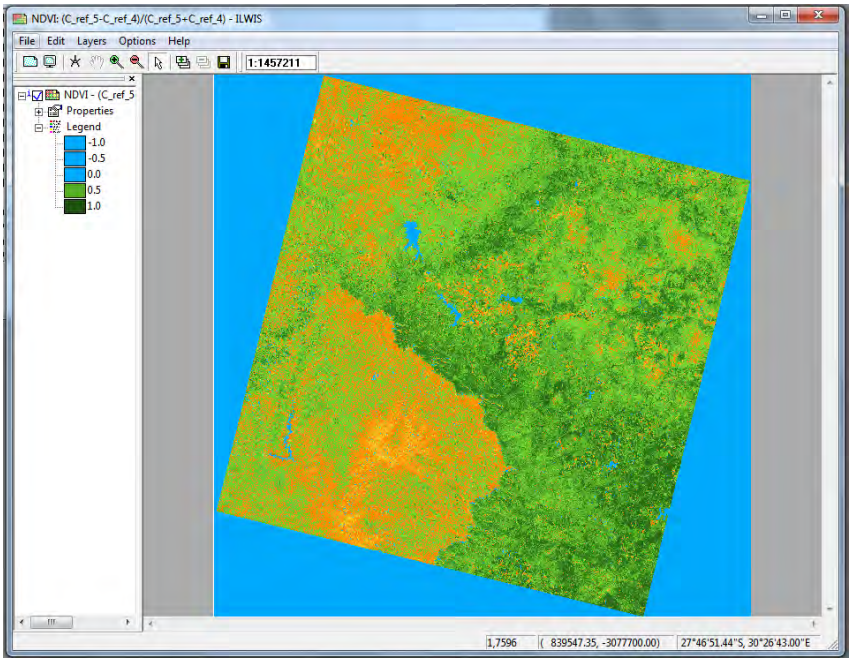

Figure 6.47 NDVI map generated in ILWIS

The surface emissivity (ε_o) was determined using the following equation Allen *et al.* (2002):

$$\varepsilon_o = 1.009 + 0.047 * \ln(NDVI) \quad (6.26)$$

The generated surface emissivity map is illustrated in Figure 6.48. The surface emissivity is 0.999 for NDVI values less than 0.

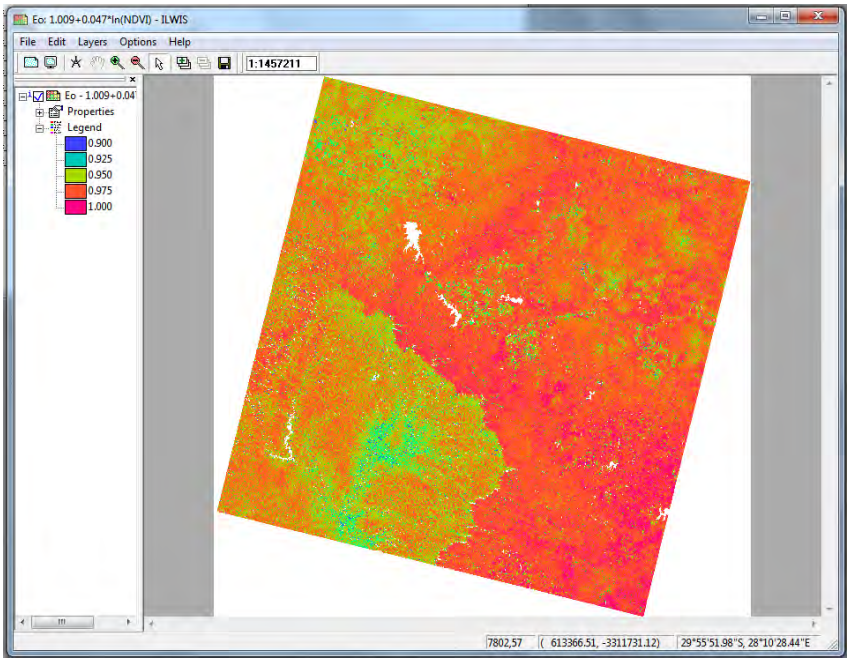

Figure 6.48 Surface emissivity map generated in ILWIS

The TIRS bands (bands 10 and 11) are converted from spectral radiance to at-satellite brightness temperature, using the following equation (USGS, 2015):

$$Tbb = \frac{K2}{ln\left[\frac{K1}{L\lambda}+1\right]} \quad (6.27)$$

Where K1 and K2 are constants, which are found in the metadata file and Lλ is either band 10 or band 11, according to high or low gain conditions. Band 11 was used in this study, as high gain is suited for grassland vegetation.

The Land Surface Temperature (LST) can be determined by Allen *et al.* (2002):

$$LST = \frac{Tbb}{\varepsilon o^{0.25}} \quad (6.28)$$

Figure 6.49 shows the generated land surface temperature map. The land surface temperature is expressed in degrees kelvin.

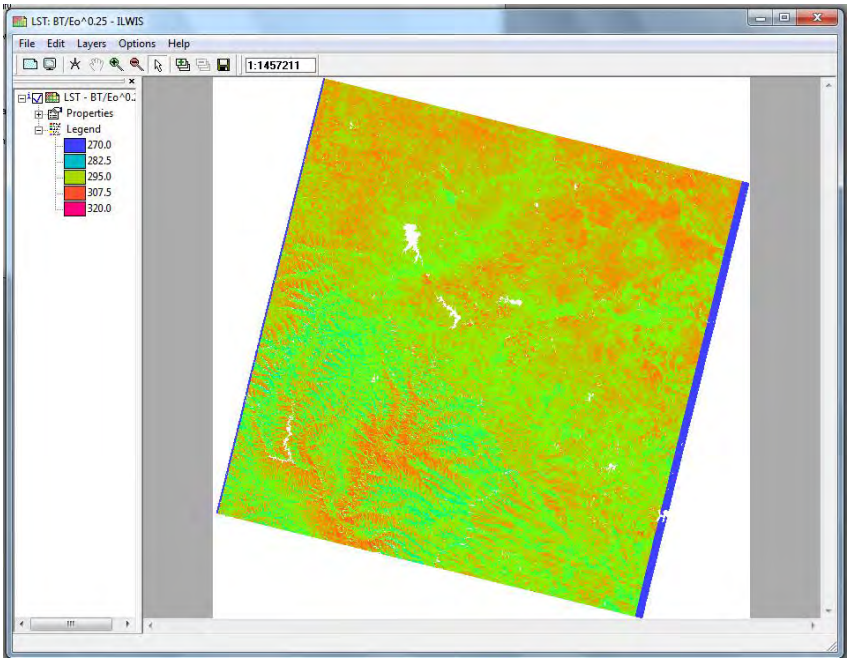

Figure 6.49 Land surface temperature map generated in ILWIS

The SEBS Model requires a digital elevation model (DEM) (Figure 6.50), as input. The DEM of South Africa was obtained http://srtm.csi.cgiar.org. The DEM for each image had to be resampled before it could be used:

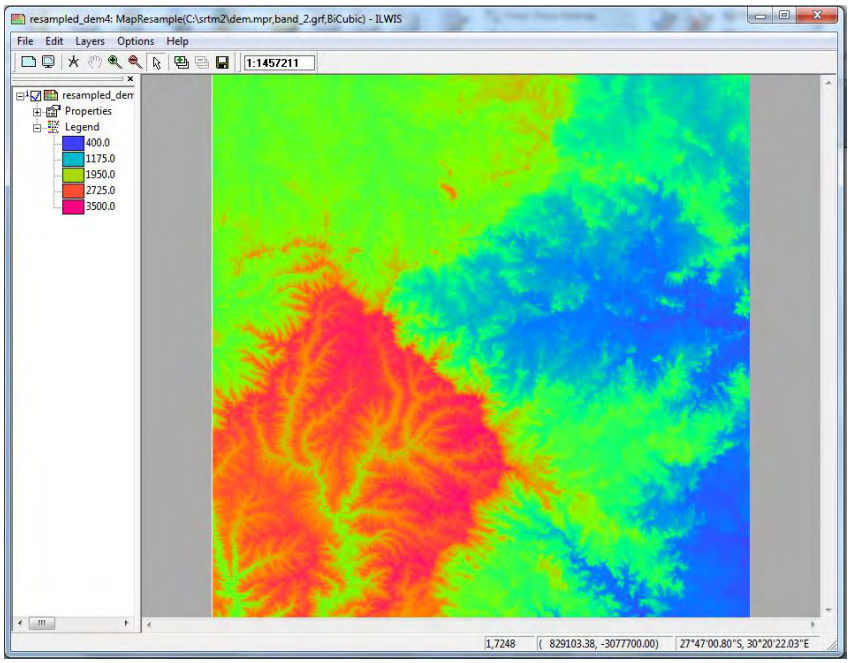

Figure 6.50 DEM map used in ILWIS as an input in SEBS

Once the input maps (albedo, NDVI, surface emissivity, land surface temperature and DEM) had been created, the SEBS Model was run in ILWIS. The meteorological data required to run the model was obtained from the eddy covariance weather data, which is located within Catchment VI. On the days where the eddy covariance weather data was not available, data from the nearby Mikes Pass weather station was used. The data required from the weather station were the instantaneous downward solar radiations, wind speed, air temperature, pressure, mean daily air temperature and sunshine hours. The downward solar radiation, wind speed, air temperature and pressure data were at the time of the satellite overpass (10:00 am).

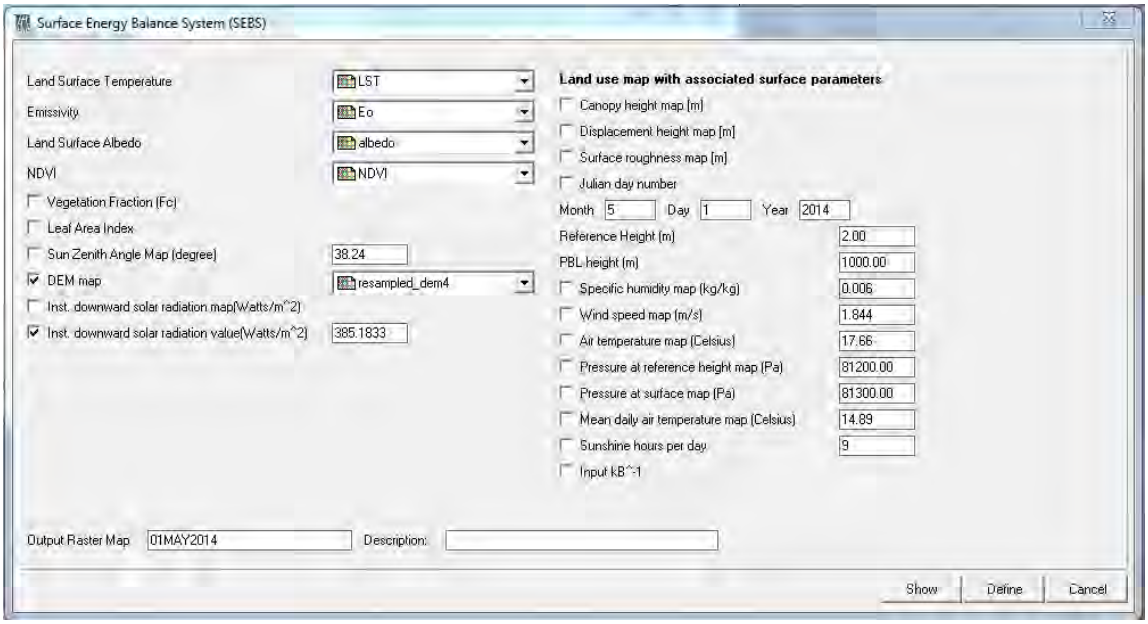

Figure 6.51 The SEBS model in ILWIS

The SEBS Model was run (Figure 6.51) and many outputs were generated. These outputs included daily evaporation, relative evaporation, evaporative fraction, net radiation, soil heat flux, sensible heat flux dry, sensible heat flux wet, sensible heat flux index and leaf area index.

For the purpose of this research, the evaporative fraction (Figure 6.52) and relative evaporation (Figure 6.53) outputs were required.

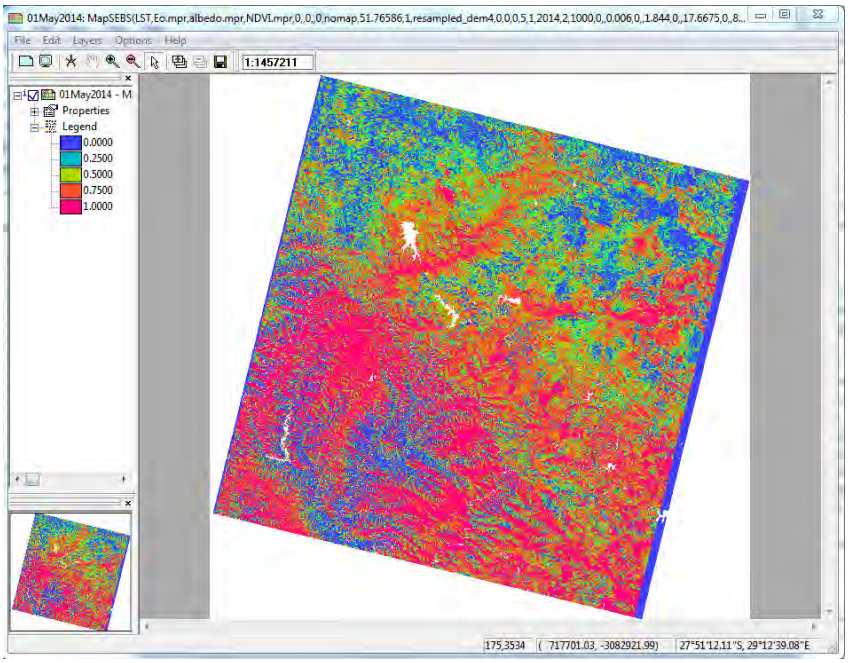

Figure 6.52 Evaporative fraction map generated as an output of the SEBS model in ILWIS

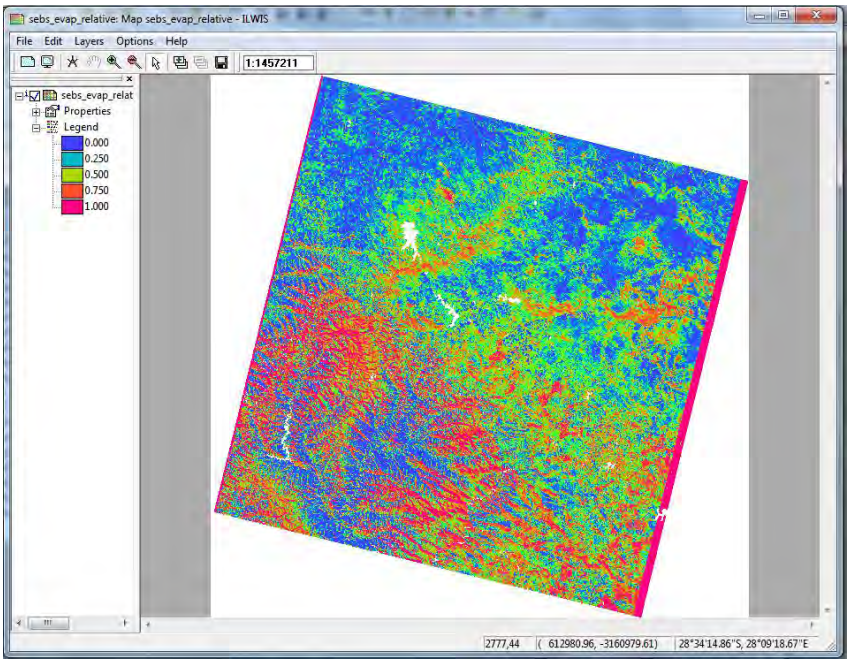

Figure 6.53 Relative evaporation map generated as an output of the SEBS model in ILWIS

The relative evaporation output map (Figure 6.53) was exported as in ASCII format. The output ASCII file was opened in ArcGIS 9.3 (Figure 6.54). The spatial reference of the relative evaporation map was defined as WGS 1984 UTM Zone 35 N. The catchment shapefile was projected to WGS 1984 UTM Zone 35 N and overlaid onto the relative evaporation map (Figure 6.55).

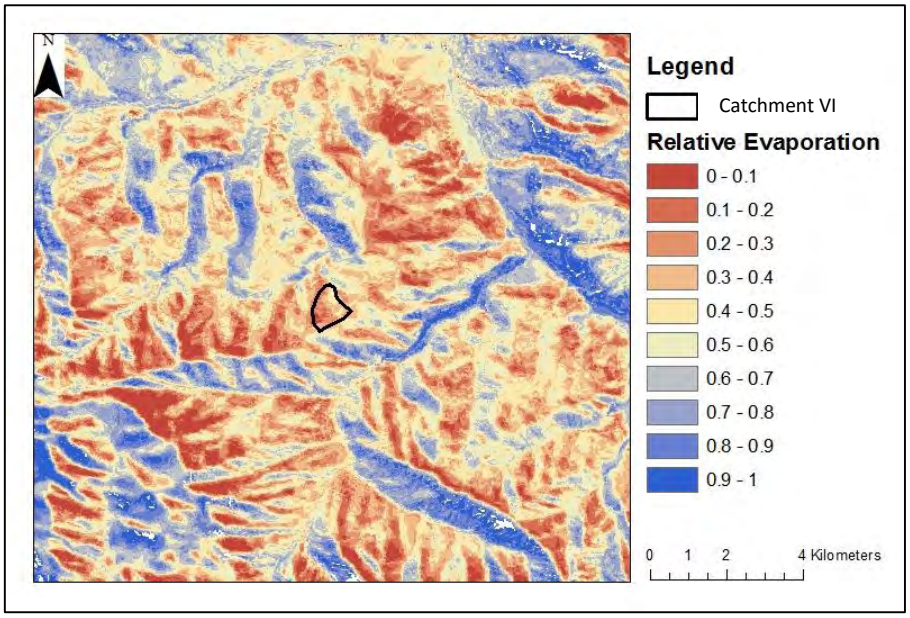

Figure 6.54 Catchment VI shapefile overlaid onto relative evaporation map

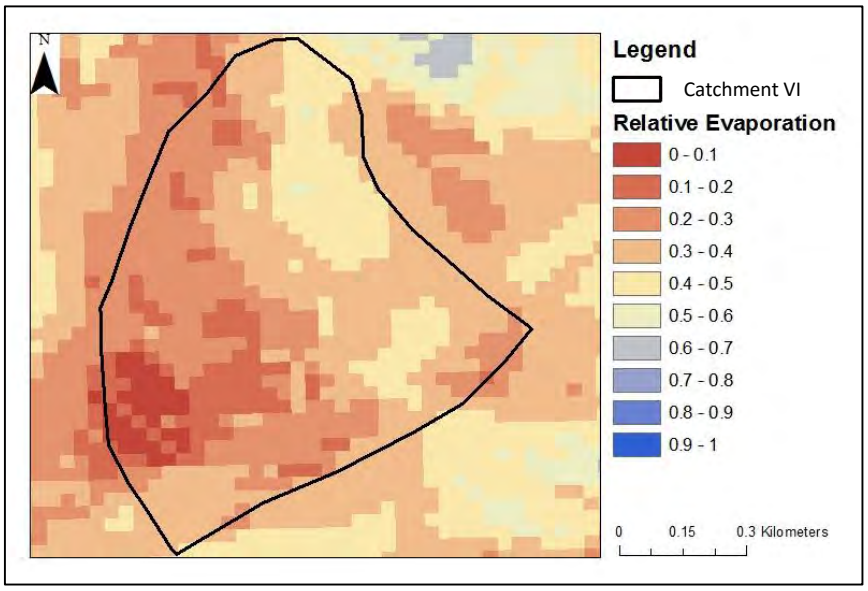

Figure 6.55 The relative evaporation map of Catchment VI

The spatial analyst tool was then used in ArcGIS 9.3 data management tools, to calculate the zonal statistics of the area enclosed by the catchment shapefile. Table 6.10 shows the zonal statistics, it can be seen that the catchment encloses 686 pixels. The mean value is taken from the zonal statistics as the relative evaporation for that image. The same procedure was repeated to determine the evaporative fraction values.

Table 6.10 Zonal statistics of relative evaporation enclosed by catchment VI

Rowid	VALUE	COUNT	AREA	MIN	MAX	RANGE	MEAN	STD	SUM
1	0	686	61740	0.03	0.56	0.527	0.299121	0.104147	205.19701

Once the relative evaporation and evaporative fraction values had been determined, soil moisture was calculated, using two equations, one by Su *et al.* (2003) (Equation 4.13) and the other by Scott *et al.* (2003) (Equation 4.14).

The SEBS process is depicted in the flow diagram (Figure 6.56). It illustrates the various procedures required to obtain relative evaporation and the evaporative fraction, using the SEBS model.

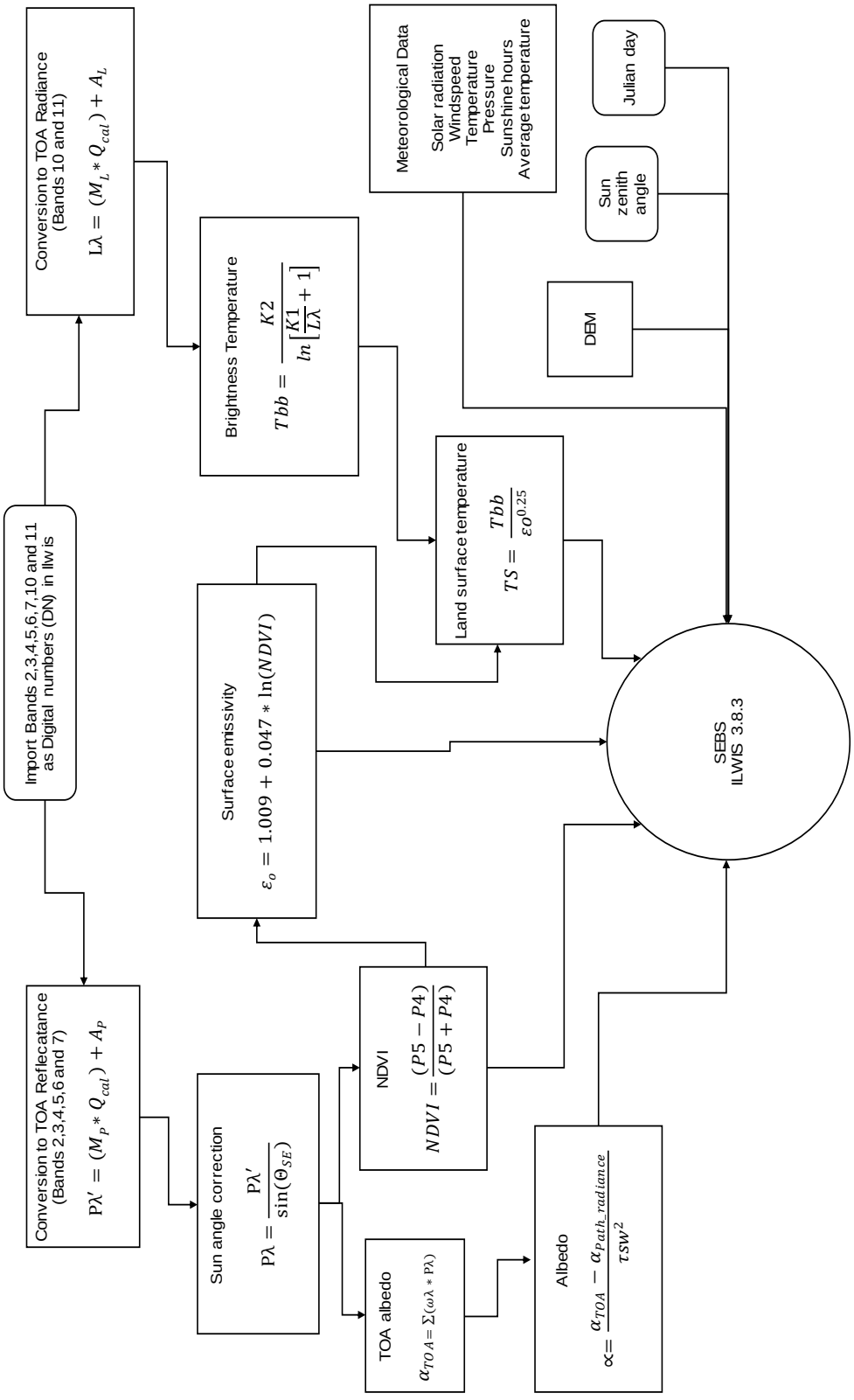

Figure 6.56 Processes used to obtain relative evaporation from Landsat 8 data

7. RESULTS AND DISCUSSION

This chapter presents the results and discussion of the various aspects of the research project. The section will detail the following aspects:

i. The validation of the CRP with a representative *in-situ* soil moisture data set;
ii. The validation of remote sensing soil moisture products (AMSR2 and SMOS) with CRP soil moisture estimates; and
iii. The validation of modelled soil moisture products (SAHG and SEBS) with CRP soil moisture estimates.

The term validation is used in the sense of an assessment, rather than a strict justification to observations. The validation will therefore focus on the comparison of spatial pattern, temporal development and regularity (consistency of estimates produced) amongst the different data sources. The types of analyses implemented in this research study include:

i. Time series analysis;
ii. Correlation coefficient (R) and coefficient of determination (R^2);
    a. The slope of the graph represents the change in y-units per change in x-units (the change of variable two to the change in variable one). The closer the slope value is to 1, the better the datasets correlate to one another;
    b. R^2 is the coefficient of determination and denotes the strength of the linear association between variable x and variable y. R^2 ranges from zero to one ($0 \leq R^2 \leq 1$). The strength of the linear association increase as R^2 becomes closer to one;
iii. Residual analysis; and
iv. Paired t-test.

The statistical analyses selected for this study are amongst the most common analyses used in current satellite-based soil moisture studies. These analyses are considered appropriate to validate the various soil moisture products used in this study, in order to draw reliable conclusions. The above statistical analyses, will not all be used on each validation, but will be selected for use appropriately.

Soil moisture varies both spatially and temporally and fluxes in soil moisture content occur over short time periods. The key input to soil moisture content is rainfall. Therefore, rainfall data is necessary to describe and supplement changes in soil moisture. Rainfall data from a rain gauge situated within Catchment VI was obtained for the one year period from March 2014 to March 2015 on an event basis. This data was then converted to a daily rainfall dataset, as shown in Figure 7.1. The rainfall distribution shows that the majority of the rainfall occurs in the summer months. During winter there are a few small rainfall events, whilst in summer there are several rainfall events, which vary in magnitude.

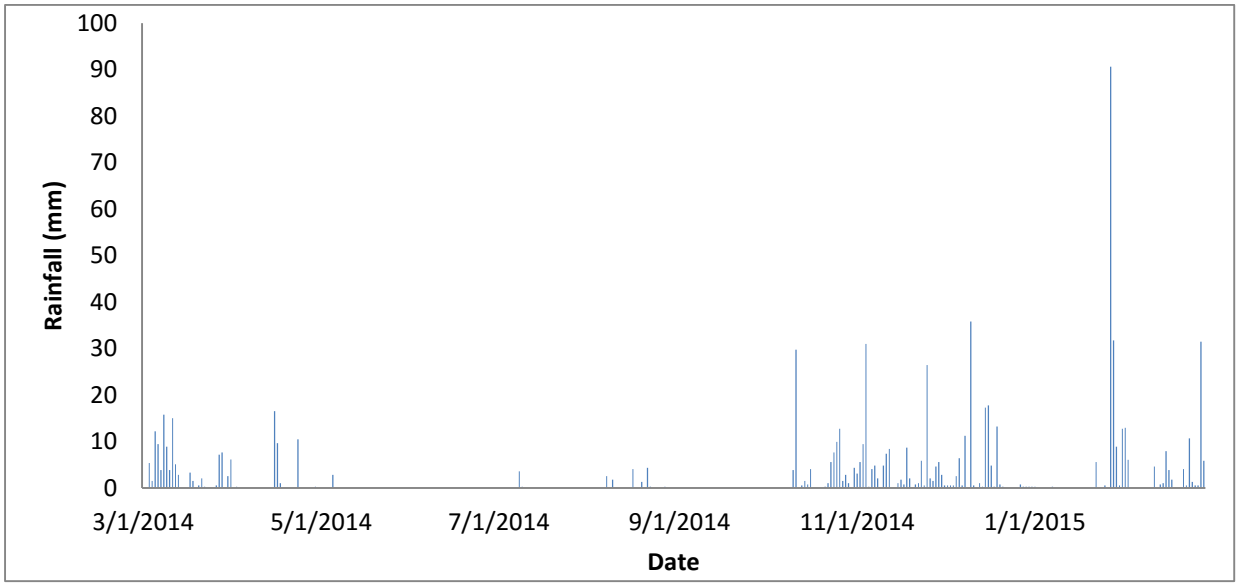

Figure 7.1 Daily rainfall measured at Catchment VI

7.1 Validating the CRP

One of the key objectives of this research project is to test the suitability of the CRP for providing spatial estimates of soil moisture. In order to achieve this, the CRP is validated against a representative *in-situ* soil moisture data set.

A time series analysis was plotted to visually interpret and compare the CRP dataset and the representative *in-situ* data set (Figure 7.2). Although the study period of the research project was from the 1st of March 2014 to the 28th of February 2015 (one year), the time period in which the representative data set was available (12th July 2014 to 28th February 2015) was

used. This time period is considered adequate for the validation procedure, as both the wet (summer) and dry (winter) periods are covered.

As shown in Figure 7.2, the CRP estimates followed the same seasonal trend as the *in-situ* soil moisture data set. The CRP estimates correlated to the *in-situ* soil moisture data set better in the wetter periods, when the soil moisture values were higher (above 30%), compared to the drier periods. The CRP soil moisture estimates were higher than the *in-situ* estimates for the dry period with low VWC values. This could be due to the differences in the measurement depths between the CRP and the representative *in-situ* instruments. Overall, it can be seen that the CRP dataset followed the general trend of the *in-situ* soil moisture variations. The soil moisture fluctuations were dependent on the rainfall input and total evaporation rate, as there were smaller fluctuations in winter, due to less rainfall and a lower total evaporation rate. In summer, the fluctuations in soil moisture were greater, due to more rainfall and a higher rate of total evaporation. There were differences between the datasets, as the CRP dataset was generally slightly higher than the *in-situ* dataset. This difference was more noticable when the soil moisture content was low. Overall, the CRP data seemed to correlate well with the *in-situ* soil moisture dataset.

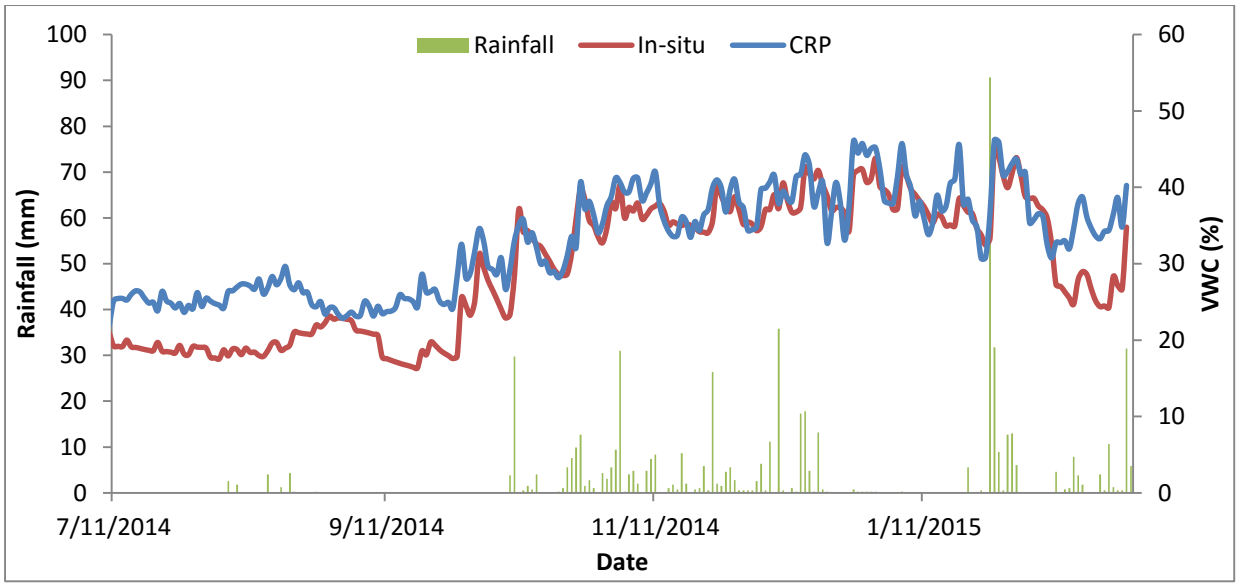

Figure 7.2 Daily *in-situ* and CRP soil moisture estimates for Catchment VI

A graph of correlation coefficients was then plotted with the representative *in-situ* data set on the x-axis and the CRP estimates on the y-axis (Figure 7.3). From Figure 7.3, it can be seen

that the majority of the points are above the 1:1 line (red), however they are in close proximity to the 1:1 line. There seems to be no extreme outliers. The positive y-intercept of 12.024 indicates an over-estimation by the CRP of the lower values (when the soil is drier). The slope is 0.709, which represents the relationship between the variables, with respect to their increases and decreases. This indicates that there is a good correlation between both data sets, as the value is close to 1. The R^2 is 0.845. It is a measure of the strength of the linear association between the datasets.

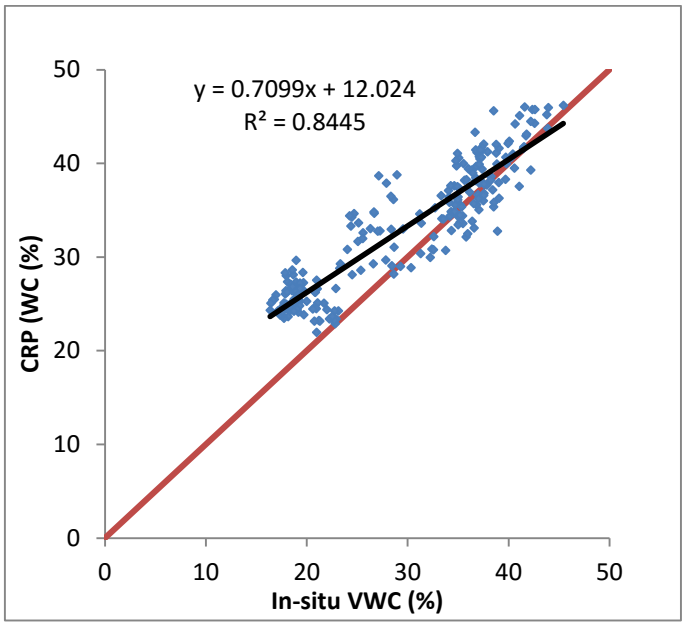

Figure 7.3 Scatterplot of *In-situ* soil moisture estimates against CRP estimates

A graph of the residuals was then plotted (Figure 7.4). The Δ VWC (%) was the difference between the in-situ (independent) and CRP (dependent) datasets. This graph is plotted to illustrate how the difference in variables change over time. From Figure 7.4, it can be seen that the majority of the residuals are negative, which indicates that the CRP soil moisture values are higher than those of the subsequent representative *in-situ* values. When the soil moisture content is high in the wet period, the residuals are lower in absolute value, which indicates less of a difference between the data sets. The residuals are negative in the dry periods and they also have the highest absolute value. In the wet periods, the residuals are lower and are mostly negative; however, there are some positive values.

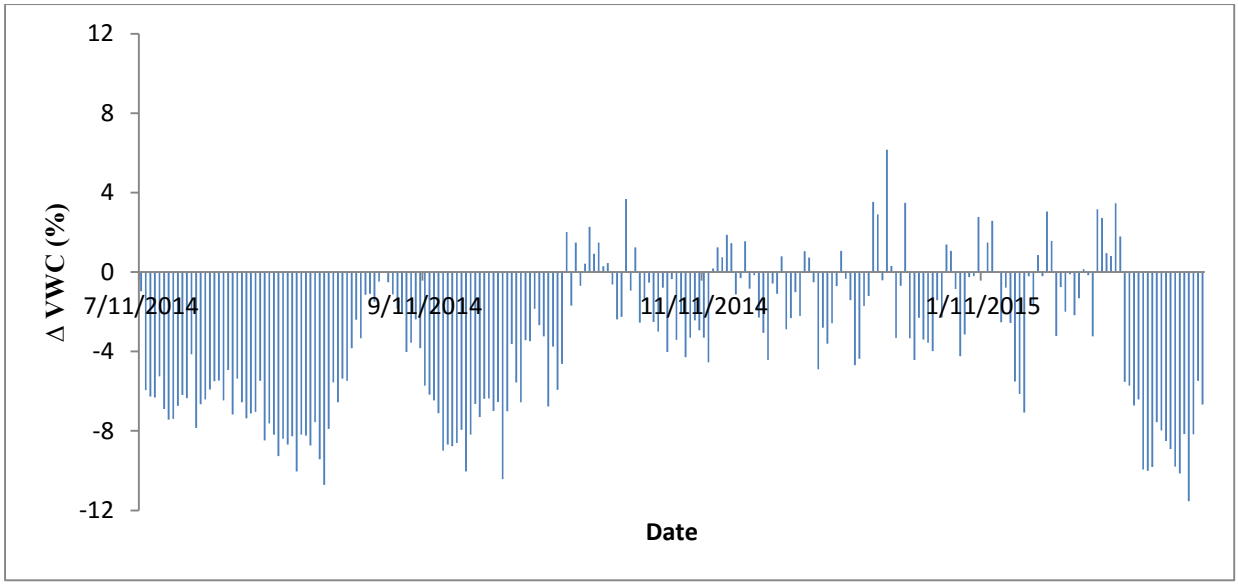

Figure 7.4 Residual graph of *In-situ* against CRP soil moisture estimates

A paired T-test was then conducted on the two data sets (Table 7.1). This analysis indicates whether the datasets were significantly different to each other. From Table 7.1, it can be seen that the mean of the CRP is greater than that of the *in-situ* dataset, which results in the t-stat value being negative. The variance, which is the average of the squared differences from the mean, is the standard deviation squared. There are 436 degrees of freedom (df). The absolute value of the t-stat (4.827) is greater than the critical two-tail value (1.965) and the P value (1.919×10^{-6}) is less than the alpha value (0.05). Therefore, there is a significant difference between the datasets.

Table 7.1 T-test of *In-situ* against CRP estimates

	In-situ	CRP
Mean	29.557	33.005
Variance	74.464	44.433
Observations	233	233
Hypothesized Mean Difference	0	
df	436	
t Stat	-4.827	
P(T<=t) two-tail	1.919×10^{-6}	
t Critical two-tail	1.965	

The inconsistencies seen in the data comparison could be due to the following. The calibration and validation of the CRP is not a straight-forward task. The calibration of the CRP could contain bias errors, due to the sampling points selected. If different sampling points were chosen, the soil moisture estimates could be different.

The *in-situ* dataset that was used to validate the CRP was not the actual average of the catchment, but the average of the sensors in the catchment. If the sensors were placed in different locations in the catchment, the *in-situ* dataset could be different. The area covered by the *in-situ* sensors was far smaller than that covered by the CRP. The *in-situ* soil moisture sensors were a maximum of 200 m away from the CRP, however, the CRP has a measurement footprint that exceeds 200 m in radius. In addition, the representative data set was biased towards the TDR pit as it was the only continous dataset, which resulted in one single point weighing more than any other point.

The CRP was not measuring soil moisture at a constant depth. The CRP measurement depth was dependent on the soil moisture content. Thus, when the soil was dry, the CRP probe was measuring at a deeper depth than when the soil was wet. The representative *in-situ* data set was meassuring constantly at an average depth of about 12 cm, whilst the CRP was measuring at around 14 cm when the soil is dry and 11 cm when the soil was wet. Therefore, the dry periods did not correlate as well as the wet periods, as the measurement depths were different. Overall, it can be seen that the CRP was suitable to provide spatial estimates of soil moisture. The CRP probe data set will then be used to validate the satellite-based estimates of soil moisture.

7.2 AMSR2 Soil Moisture Product Validation

The AMSR2 Level Three soil moisture product is on a 10 km spatial resolution grid. Although this grid is relatively small in comparison to other remote sensing soil moisture products, it is still very large in comparison to the catchment area. The catchment area is 0.68 km^2, whilst the pixel area is 100 km^2. Therefore the pixel is 147 times larger than the study area. However, validating remote sensing soil moisture products, such as the AMSR2 product, with CRP estimates is an improvement from validating remote sensing soil moisture products with *in-situ* point measurements. For this analysis, the one-year study period of the 1st of March 2014 to the 28th of February 2015 was used. A time series analysis graph was

plotted to illustrate the characteristics of the AMSR2, CRP and rainfall data over time (Figure 7.5).

From Figure 7.5, it can be seen that the AMSR2 soil moisture product underestimated soil moisture throughout the study period, when compared to the CRP. The AMSR2 soil moisture product followed the seasonal trend of the CRP estimates. The discontinuation in the AMSR2 line was due to missing data. The AMSR2 dataset fluctuated more in the wet periods, whilst it fluctuated less in the dry periods. Although the AMSR2 data set underestimated soil moisture, it followed a similar trend in daily soil moisture fluctuation and seemed to correlate well with the CRP data set.

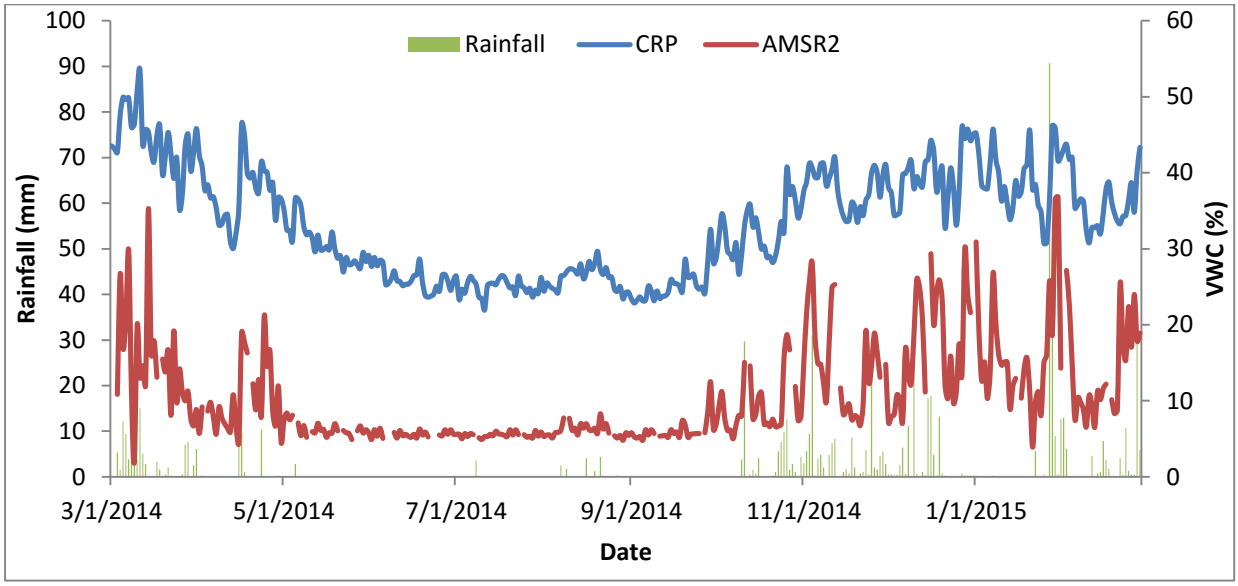

Figure 7.5 Time series analysis of CRP and AMSR2 soil moisture estimates

A day in summer and winter that had both an ascending and descending value, are shown in Figure 7.6. In summer, the spatial and temporal variation of the pixel values varied more than in winter. This was seen by the changes in the pixel values between the ascending and descending values. The differences between summer ascending and descending pixel values were greater than the differences between winter ascending and descending values. This showed the heterogenous nature of soil moisture, as well as the difference in soil moisture dynamics due to seasonality.

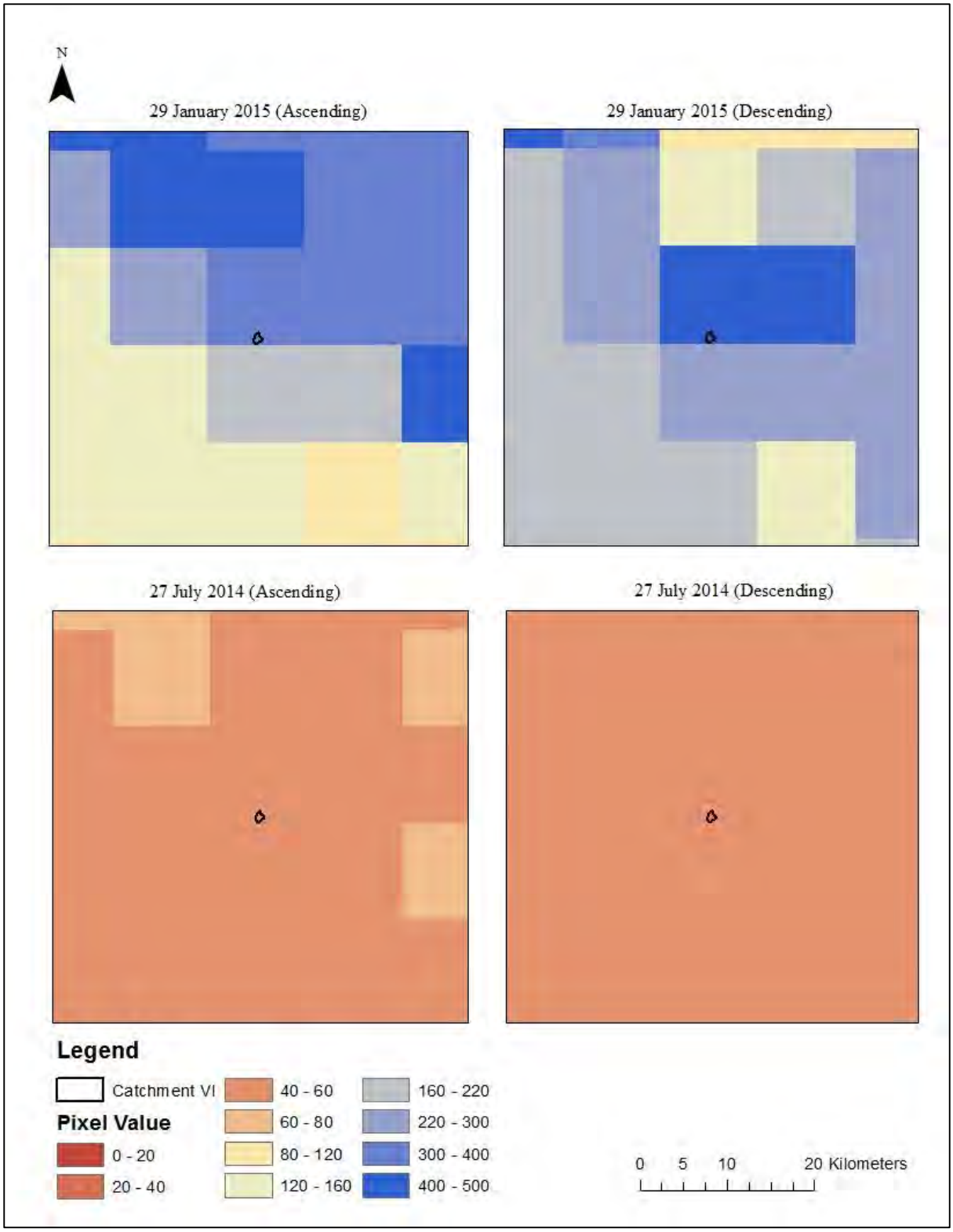

Figure 7.6 Comparison between summer and winter images of AMSR2 soil moisture estimates

A scattergraph of CRP (x-axis) against AMSR2 (y-axis) was then plotted (Figure 7.7). From Figure 7.7, all the data points are below the 1:1 line (red), which shows that the AMSR2 dataset is always under-estimating soil moisture in comparison to the CRP. The slope of the graph is 0.649, which is good. There is a positive correlation and the R^2 is 0.505, which indicates a good fit. There are some outliers above and below the line of best fit.

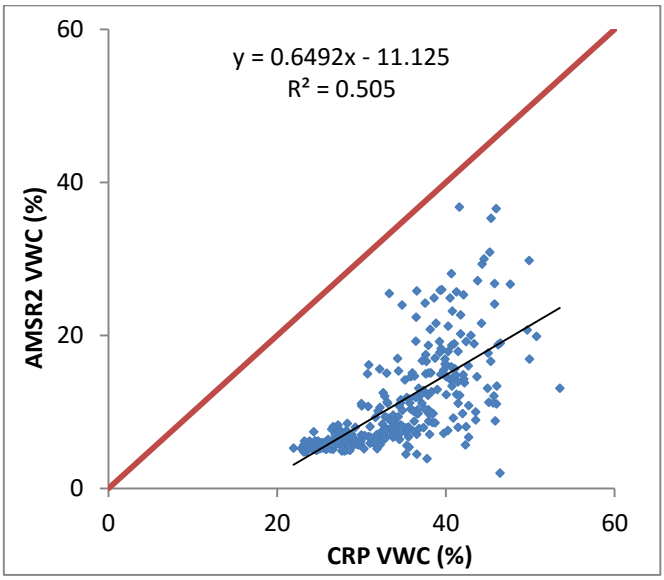

Figure 7.7 Scatterplot of CRP against AMSR2 soil moisture estimates

A residual graph of the CRP against AMSR2 soil moisture was then plotted against time (Figure 7.8). The Δ VWC (%) was the difference between the CRP and AMSR2 datasets. From the residual graph (Figure 7.8), it can be seen that the AMSR2 dataset was under-estimating soil moisture throughout the study period. In the dry period, the residuals were fairly constant, whilst in the wet periods, the residuals fluctuated more. The mean residual was 22.81. The residuals were constantly lower in the dry period, compared to the wet period, which indicates that there was less underestimation of the AMSR2 data in the dry period.

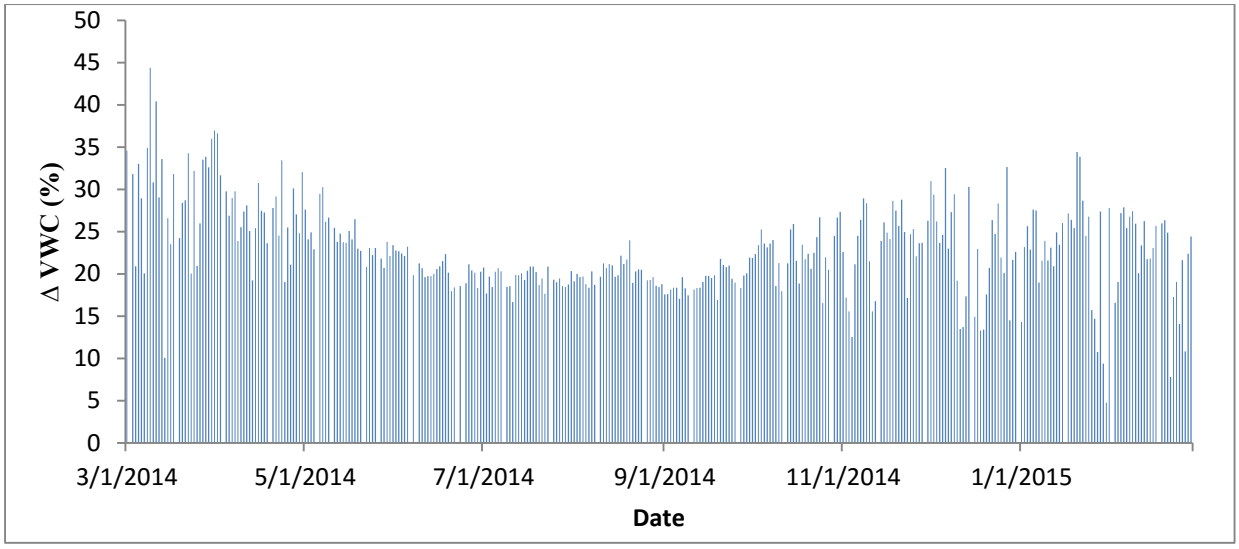

Figure 7.8 Residual graph of CRP against AMSR2 soil moisture estimates

A paired t-test was then conducted (Table 7.2). In order to properly perform a t-test, paired values were required. Therefore, the CRP values corresponding to the AMSR2 days, which had no data, were removed. From Table 7.2, it can be seen that the means are very different, as the mean of the CRP is 33.326 and AMSR2 is 10.511. The variance values are similar, as the variance of the CRP is 50.010 and the AMSR2 is 41.737. There are 669 degrees of freedom. The t-stat value (43.791) exceeds the t critical value (1.964) and the P value ($1.3x10^{-198}$) is less than alpha (0.05). Therefore, there is a significant difference between the datasets.

Table 7.2 T-test of CRP against AMSR2 estimates

	CRP	AMSR2
Mean	33.326	10.511
Variance	50.010	41.737
Observations	338	338
Hypothesized Mean Difference	0	
df	669	
t Stat	43.791	
P(T<=t) two-tail	$1.3x10^{-198}$	
t Critical two-tail	1.964	

When the AMSR2 product data was processed and the pixel values obtained, it was found that the daily data values corresponded to four different situations. There were days when only a descending pixel value was available (10th of December 2014) and there were days when only an ascending pixel value was available (11th of December 2014) (Figure 7.9).

There were days when both an ascending and descending pixel value was available (14th of December 2014) and there were days when no pixel data was available for the catchment area (15th of December 2014) (Figure 7.10).

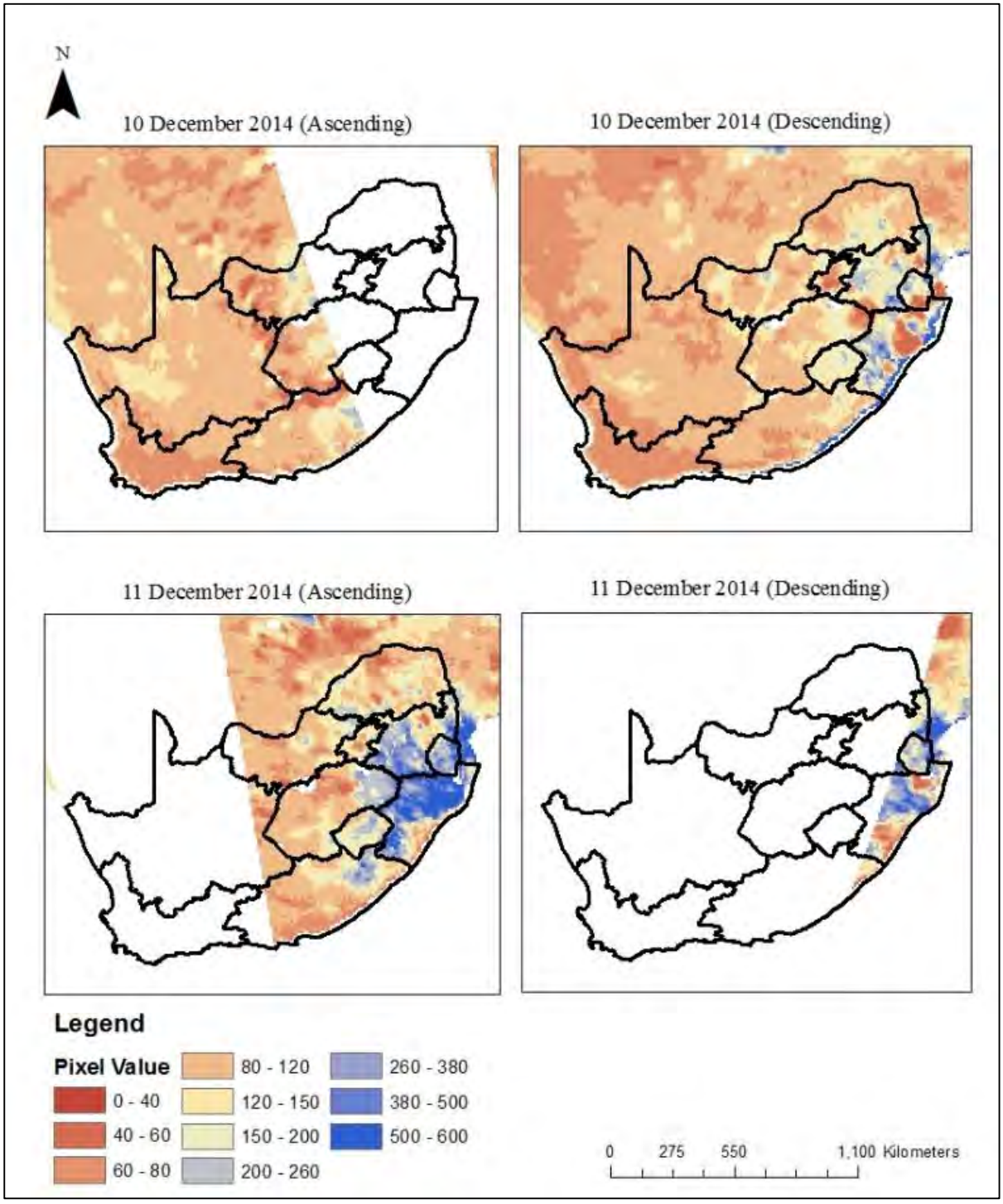

Figure 7.9 A day with a descending and a day with an ascending value for the AMSR2 soil moisture product

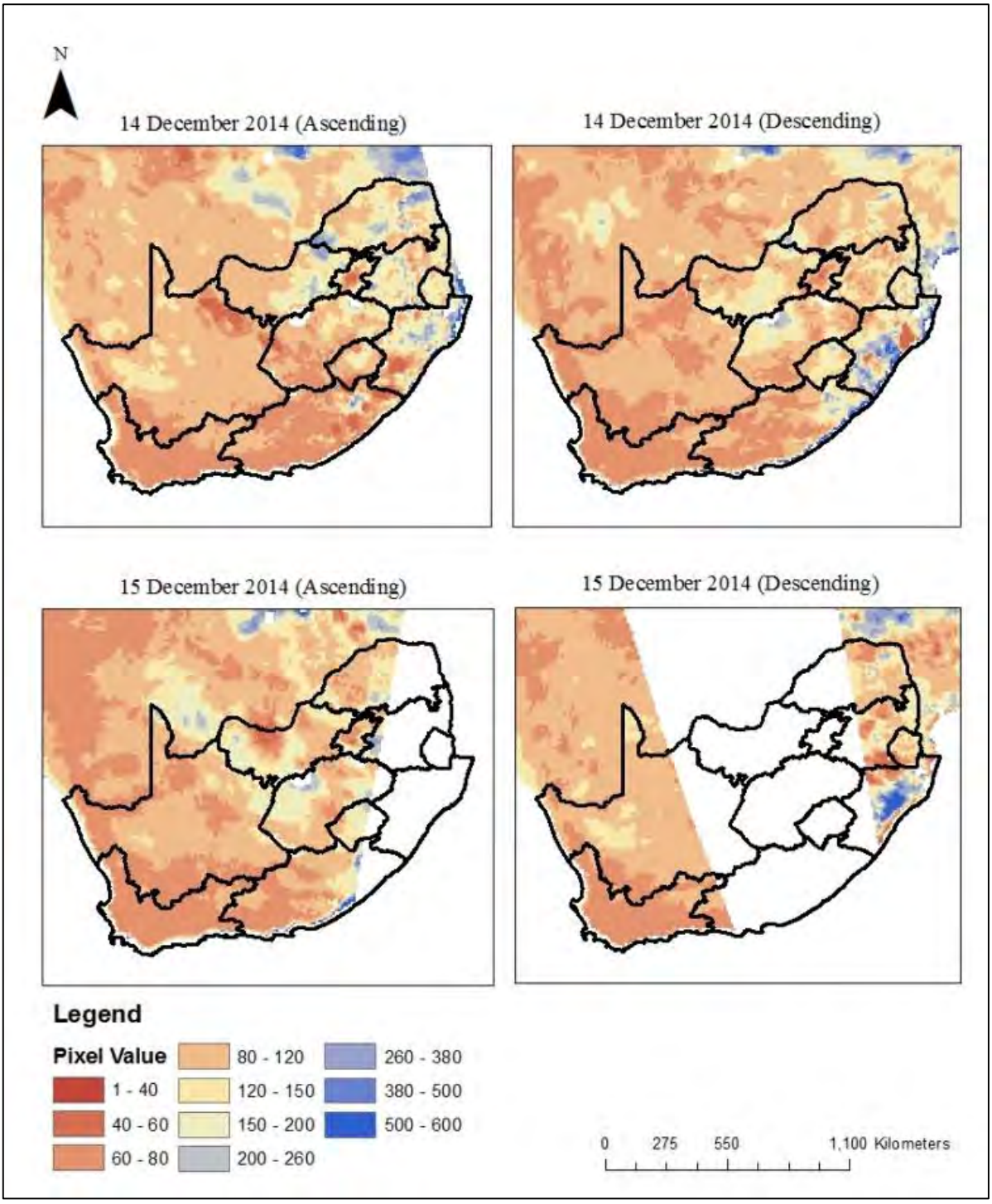

Figure 7.10 A day with both an ascending and descending value, and a day with no value for the AMSR2 soil moisture product

7.3 SMOS Soil Moisture Product Validation

The SMOS Level Three soil moisture product is on a 25 km spatial grid. Although this grid is smaller than that of the Level Two product (40 km), it is still very large in comparison to the catchment area. The catchment area is 0.68km^2, whereas the pixel area is 625km^2. Therefore, the pixel is 920 times larger than the study area.

A graph of the time series analysis of the daily CRP and SMOS datasets were plotted (Figure 7.11). The time period used, was a one year period from the 1st of March 2014 to the 28th of February 2015. The SMOS soil moisture product is a daily product; however, the satellite coverage does not scan the entire earth's surface in one-day. The data set has a lot of gaps, as only 236 images during the study period have data for the study area. Due to the numerous gaps in the SMOS dataset, the data was plotted as points to improve the representation of the data. From Figure 7.11, it can be seen that the SMOS soil moisture estimates follow the same general trend of the CRP. The SMOS dataset underestimates soil moisture the majority of the time, when compared to the CRP. There are times in the wet periods, when the SMOS product over-estimates soil moisture. In the wet periods, the fluctuation in soil moisture estimates of SMOS is great. This fluctuation is less in the dry periods, due to greater fluxes in soil moisture during summer when compared to winter.

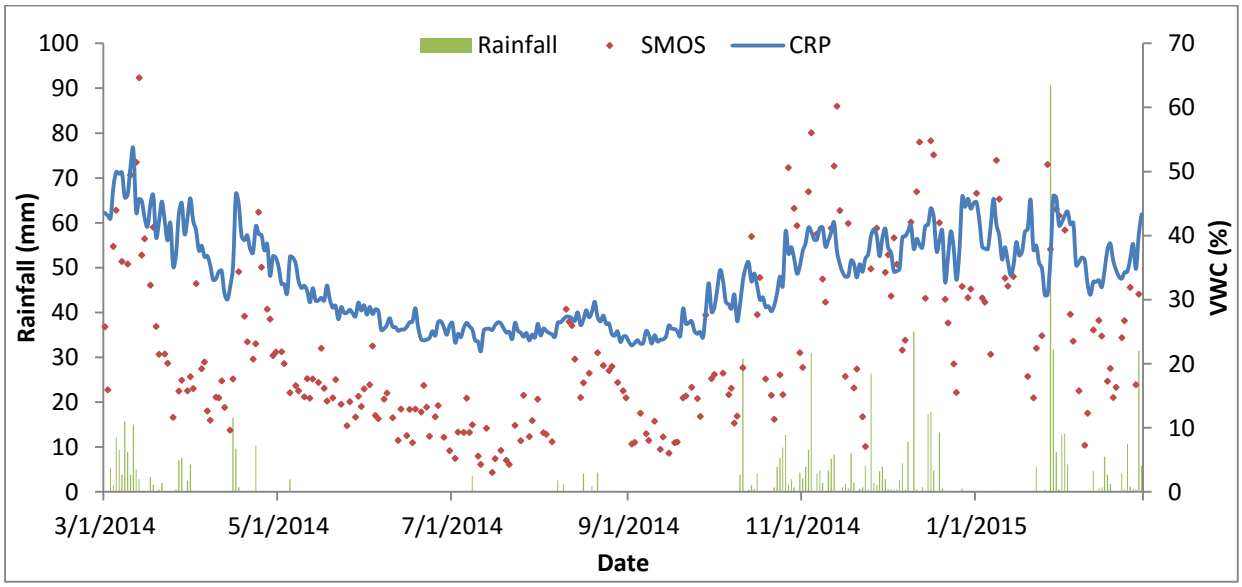

Figure 7.11 Time series analysis of CRP and SMOS soil moisture estimates for Catchment VI

A day in summer and winter with both ascending and descending SMOS data, are shown in Figures 7.12, 7.13, 7.14 and 7.15. The summer day image showed that the soil moisture was relatively higher on the east coast of South Africa and that soil moisture was high in the mountainous areas (Figures 7.12 and 7.13).

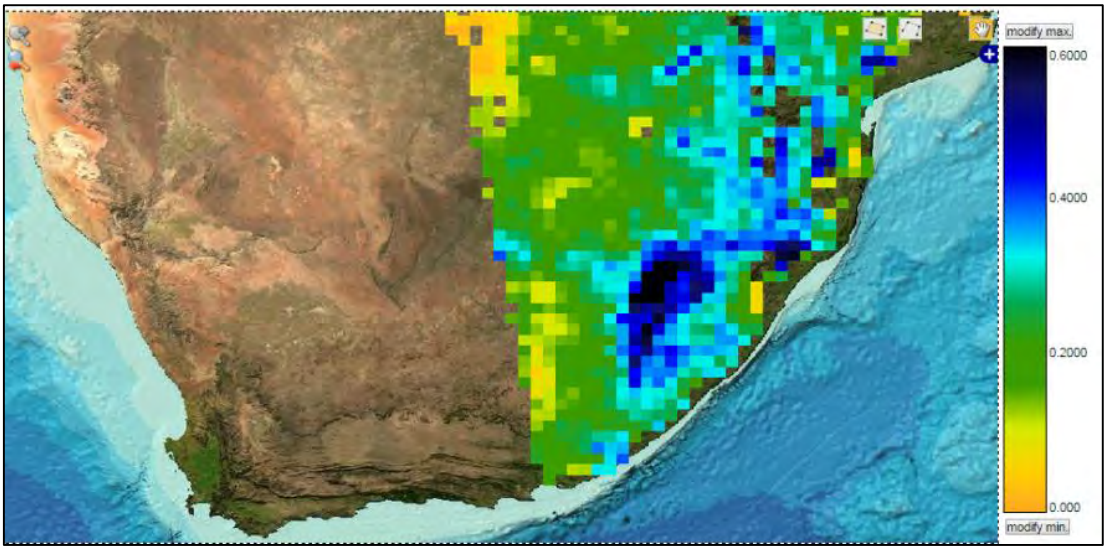

Figure 7.12 Ascending SMOS image in summer (17 December 2014)

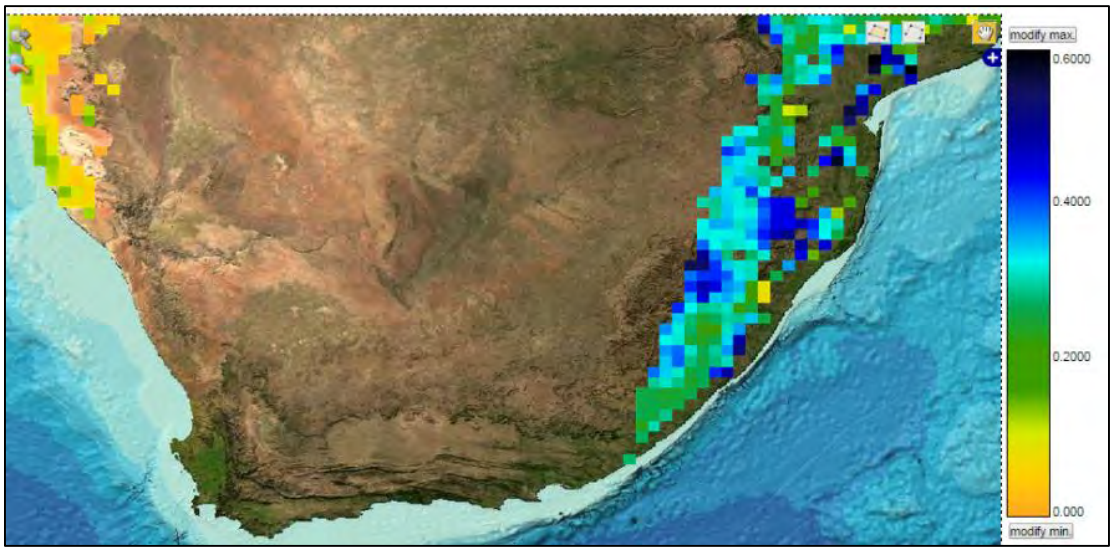

Figure 7.13 Descending SMOS image in summer (17 December 2014)

The day in winter shows that soil moisture is generally low in South Africa (Figures 7.14 and 7.15). The areas with the higher soil moisture values are also the areas that receive the most rainfall throughout the year.

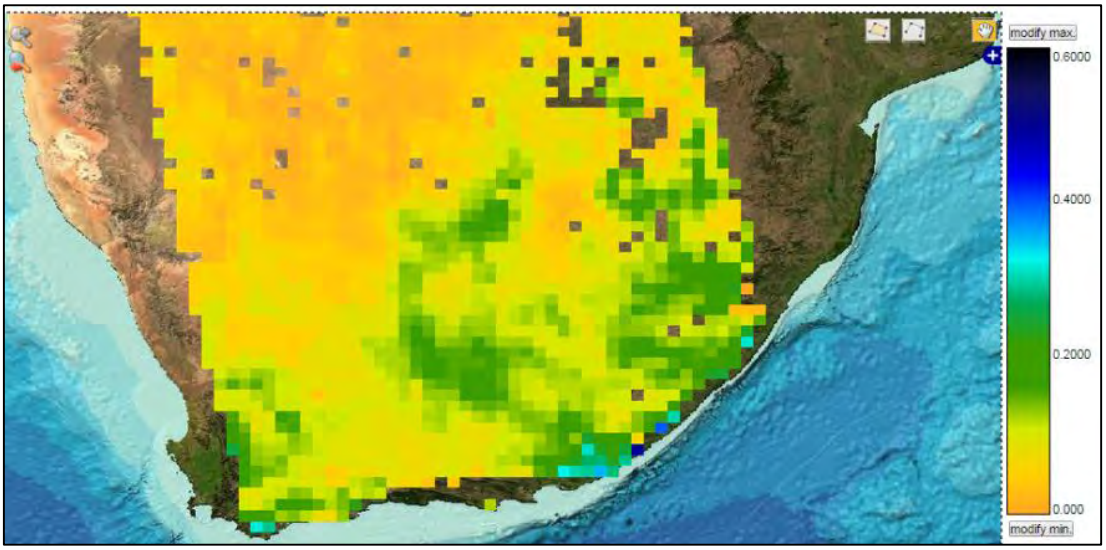

Figure 7.14 Ascending SMOS image in winter (15 August 2014)

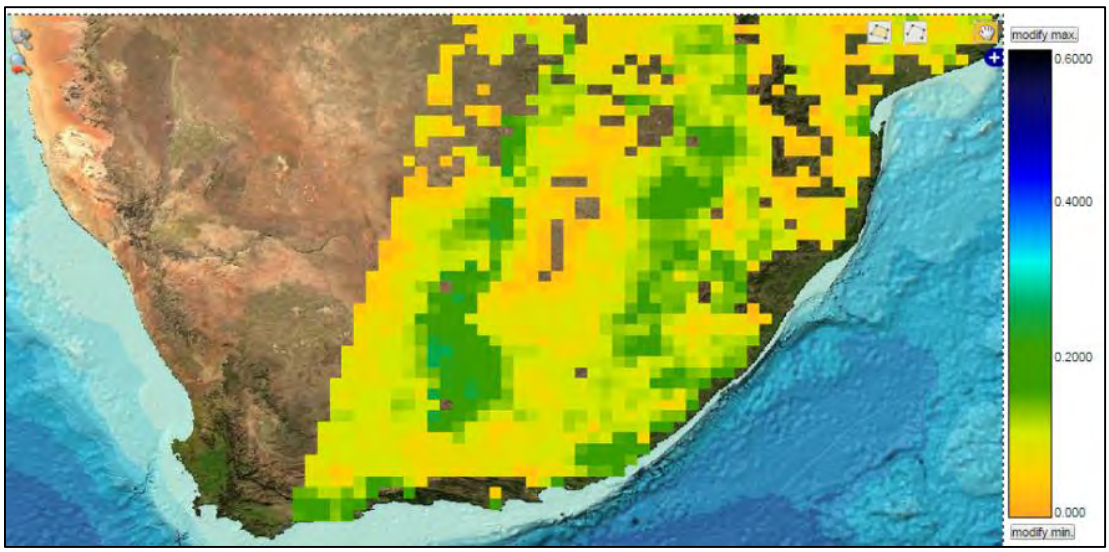

Figure 7.15 Descending SMOS image in winter (15 August 2014)

A graph of CRP (x-axis) was plotted against SMOS (y-axis) (Figure 7.16). From Figure 7.16, it can be seen that the majority of the points lie below the 1:1 line (red). This indicates that the SMOS data set generally under-estimates soil moisture. There are some points on the 1:1 line and several points above the 1:1 line. The R^2 value is 0.485, which indicates a good correlation. The slope of the graph is 1.2797.

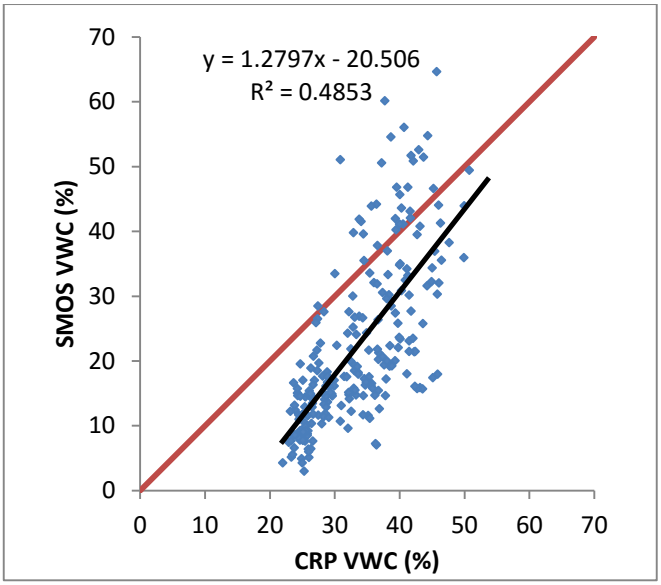

Figure 7.16 Scatterplot of CRP against SMOS soil moisture estimates

A graph of the residuals against time was plotted (Figure 7.17). The Δ VWC (%) is the difference between the CRP and SMOS datasets. The spaces between the columns are where there is missing SMOS data. From the Figure 7.17, it is seen that the residuals range from -23 to +30. The residuals are positive, except for a few instances in the wet periods, when the SMOS estimates are higher than the CRP measurements. The residuals fluctuate more than the AMSR2 soil moisture residuals.

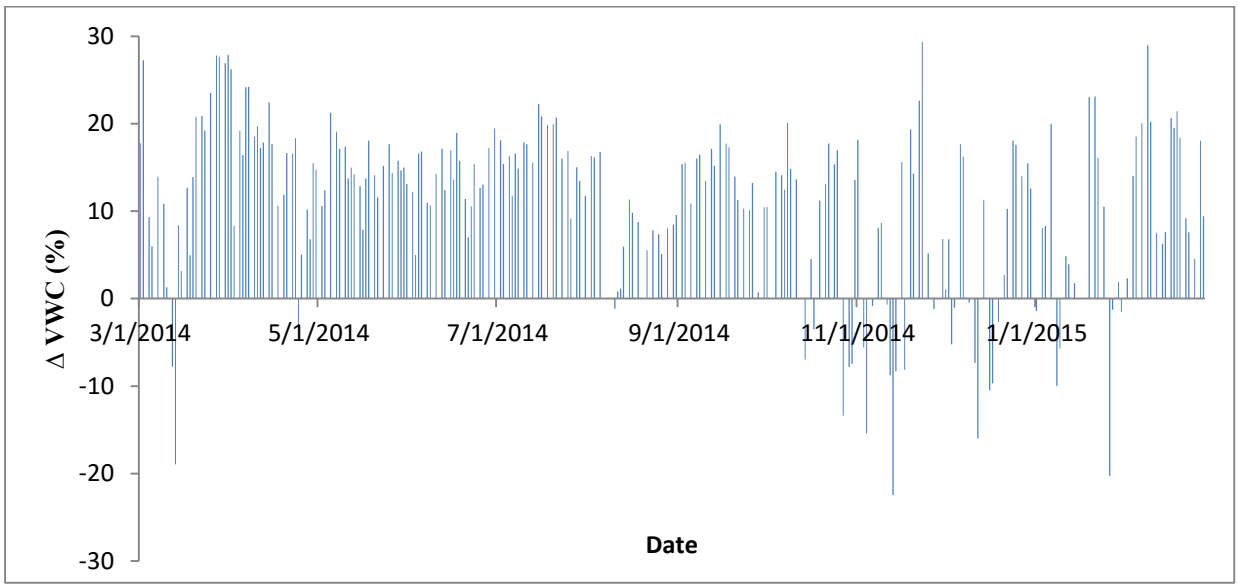

Figure 7.17 Residual graph of CRP against SMOS soil moisture estimates

A paired t-test was conducted (see Table 7.3). The t-test requires pairs of x and y values, thus the CRP data, which had no subsequent SMOS data, had to be removed. From table 7.3, it can be seen that the mean of the CRP dataset (33.396) is higher than that of the SMOS dataset (22.231). The variance of the SMOS dataset is very large (166.267), compared to that of the CRP dataset (49.276). There are 363 degrees of freedom. The t stat value is 11.683, which is larger than the critical two-tail value of 1.967 and the p value is 5.49×10^{-27}, which is smaller than the alpha value (0.05). Therefore, there is a significant difference between the datasets.

Table 7.3 T-test of CRP against SMOS estimates

	CRP	SMOS
Mean	33.396	22.231
Variance	49.276	166.267
Observations	236	236
Hypothesized Mean Difference	0	
df	363	
t Stat	11.683	
P(T<=t) two-tail	5.49×10^{-27}	
t Critical two-tail	1.967	

Like the AMSR2 dataset, there were four different situations of days processed. These included ascending only, descending only, both (ascending and descending) and neither.
The SMOS data set had cases where there was an ascending and/or descending band covering the area; however, there were pixels missing within the band itself, which resulted in the area having no pixel value (Figure 7.18).

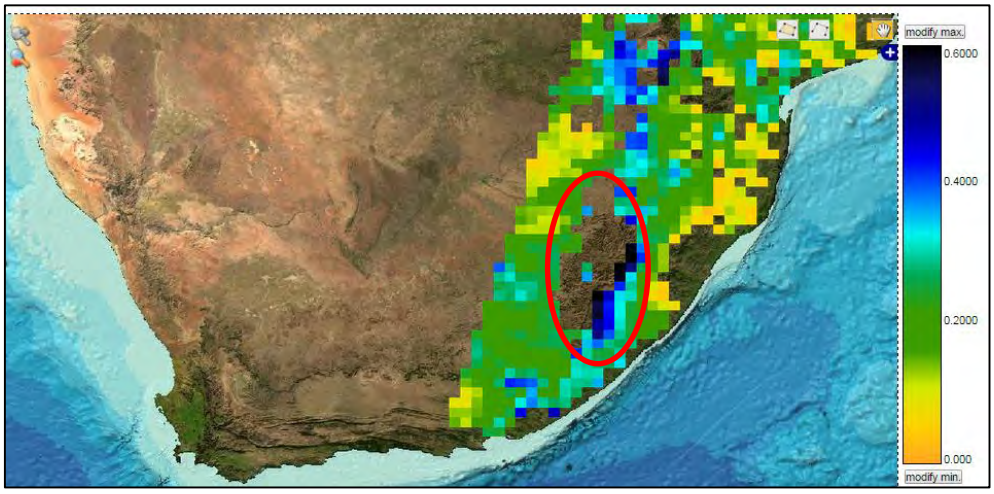

Figure 7.18 SMOS missing data within band

7.4 Comparing Remote Sensing Soil Moisture Products

In order to compare the two remote sensing soil moisture products, both were plotted on a time series graph along with CRP estimates (Figure 7.19). The AMSR2 and CRP were plotted on a line graph, whilst the SMOS data was plotted on scatter points due to the large number of missing data. It is difficult to compare the remote sensing products on a daily time-step due to the daily fluctuations.

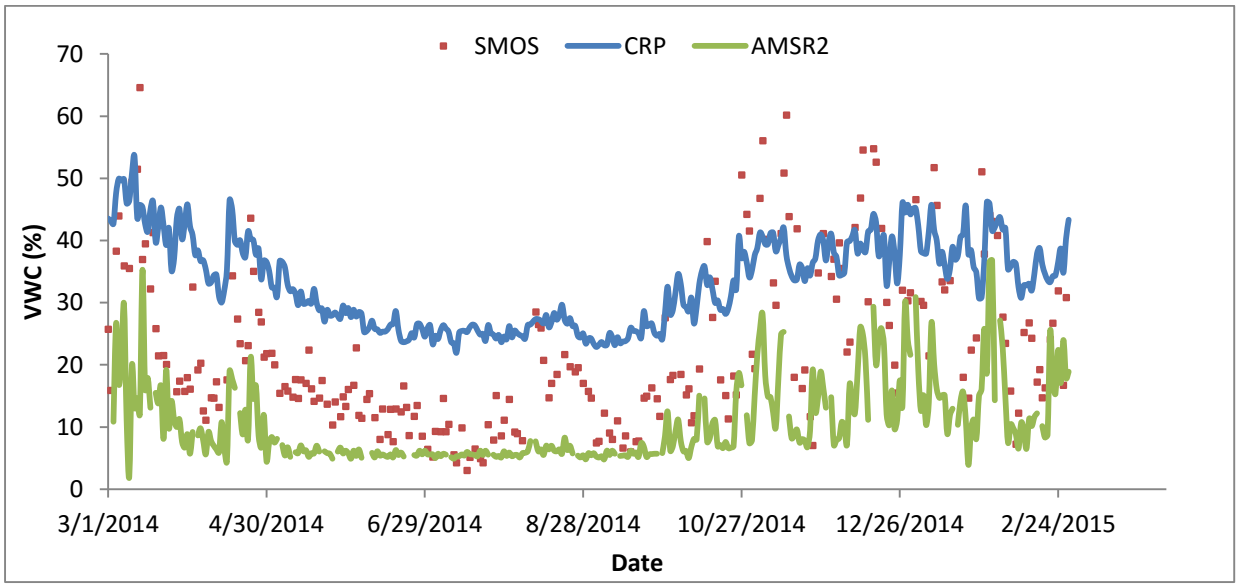

Figure 7.19 AMSR2, SMOS and CRP soil moisture estimates against time

If the daily remote sensing and CRP datasets (Figure 7.19) are converted to a three-day average (Figure 7.20) this allows the smallest averaging interval, without any gaps in the dataset. The dataset becomes smoother, as the fluctuations are averaged. This is useful when comparing the two remote sensing datasets. If the data were averaged over a longer time interval, the graphs would become smoother.

From Figure 7.20, it can be seen that the remote sensing soil moisture products followed the general trend of the CRP soil moisture estimates. However, there are still discrepancies in the validation of the remote sensing products with CRP data, which are due to the horizontal and vertical scaling.

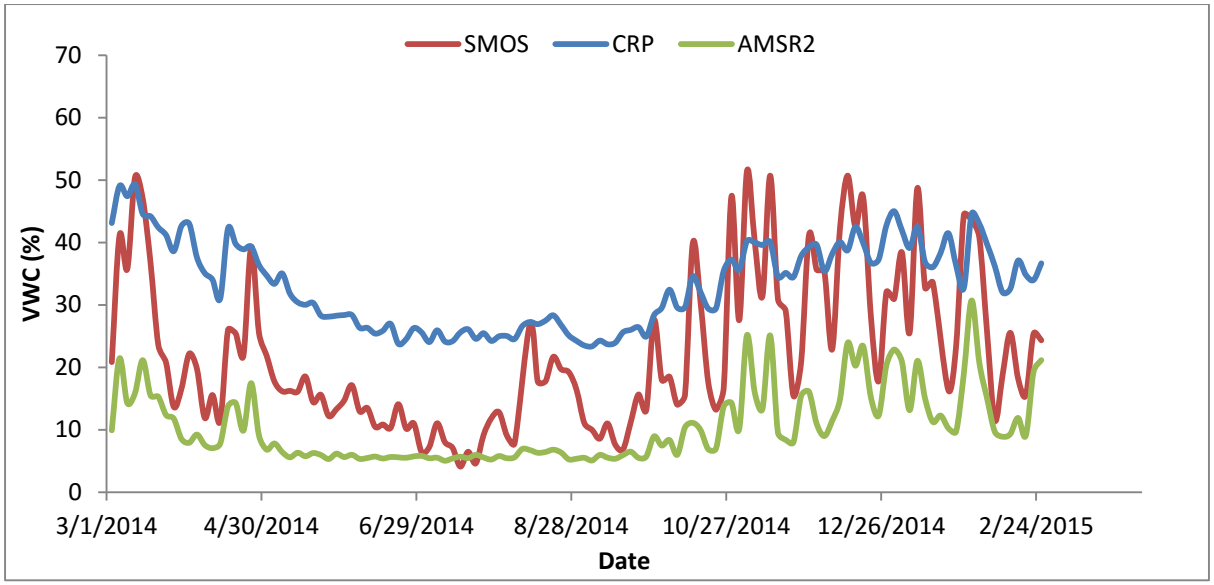

Figure 7.20 Three-day averaged soil moisture estimates

The vertical scaling errors occur, due to the CRP measuring soil moisture at a different depth, as compared to the remote sensing sensors. The CRP can theoretically measure soil moisture between depths of 0.12 to 0.72 m, depending on the soil moisture status. The remote sensing products are a measure of soil moisture at shallow depths (0.00 – 0.05 m).

The horizontal scaling issues occur, as the remote sensing products are at a very coarse resolution, which greatly exceed the measurement area of the CRP. This is a common limitation in the validation of remote sensing soil moisture products. However, using the CRP instead of traditional *in-situ* techniques, results in an area-averaged estimate instead of a series of point measurements, which is a great improvement. It is impractical and near impossible to validate current remote sensing soil moisture products with a traditional *in-situ* dataset at the same spatial resolution, due to the heterogeneity of soil moisture.

This limitation cannot currently be overcome in an applied manner, therefore remote sensing validation has been, and is currently, carried out by validating a "big" area (coarse pixel value), with a "smaller" area. This will make the coarse pixel area that is not covered by the validation dataset footprint to be neglected. Thus, true validation cannot be achieved unless both the remote sensing and validation data are on the same-scale. The term same-scale refers to an area-averaged soil moisture value and not an *in-situ* soil moisture network, which obtains an area-average value by averaging the various *in-situ* sensors in the network.

The SMOS soil moisture dataset seems to have provided better estimates of soil moisture than the AMSR2 dataset, when compared to the CRP. The SMOS Level Three product has a coarser resolution (25 km) than the AMSR2 Level Three product (10 km). However, it provided better estimates of soil moisture. This could be due to the SMOS satellite instrument using the more recent technology of the L-band wavelength to observe and measure. The SMOS satellite was launched in 2009 and although the AMSR2 sensor on-board the GCOM-W1 satellite was launched in 2012, the AMSR2 sensor implements similar instruments and methods to the previous AMSR on-board the AQUA satellite, for the purpose of data continuation. Soil moisture retrievals using lower microwave frequencies are expected to be more accurate (Kim *et al.*, 2015). Thus, although the SMOS satellite was launched before the GCOM-W1, the SMOS satellite operates at a 1.4 GHz, whilst the AMSR2 sensor operates on 10.7 GHz. The underestimation of soil moisture estimates by the AMSR2 soil moisture product was also observed in a study by Kim *et al.* (2015).

The AMSR2 dataset is a more reliable dataset in terms of providing a more complete dataset, as there are fewer missing days. The daily fluctuations in soil moisture matched the CRP more than the SMOS, and this is seen by the large variance in the SMOS dataset. In the dry periods, the AMSR2 dataset did not fluctuate nearly as much as the SMOS dataset.

7.5 SAHG Soil Moisture Product Validation

The SAHG soil moisture product is on a 12.5 x 12.5 km (roughly) spatial grid, which results in a pixel area of 156.25 km^2. In order to obtain a year-long dataset, 2920 images were downloaded and used to create 365 daily images. The SAHG dataset is continuous and possesses no gaps in the dataset. The SAHG soil moisture was obtained in SSI and converted to VWC by using a representative porosity value, which was calculated from the bulk density values. A time series analysis graph of the SAHG and CRP soil moisture estimates were plotted (Figure 7.21).

From Figure 7.21, it can be seen that the SAHG product followed the same seasonal trend as the CRP. There seems to be a close correlation between the datasets, in terms of general increases and decreases in soil moisture content. The CRP has more variation in soil moisture from day-to-day. The SAHG product has gradual changes in soil moisture and does not exhibit the same degree of temporal fluctuation, as seen by the CRP. This difference between

the datasets is easily observed. The SAHG product does fluctuate, but the occurrence of these fluctuations is less than that presented by the CRP dataset. The first nine months (march 2014 to November 2014) of the twelve month time series analysis shows a close correlation between the CRP and SAHG soil moisture estimates. The last three months (December 2014 to February 2015) shows less of a correlation, as the fluctuations of the CRP soil moisture estimates do not correspond to the fluctuations of the SAHG soil moisture estimates. This could be due to an error in the PyTOPKAPI model, such as an error in the input data.

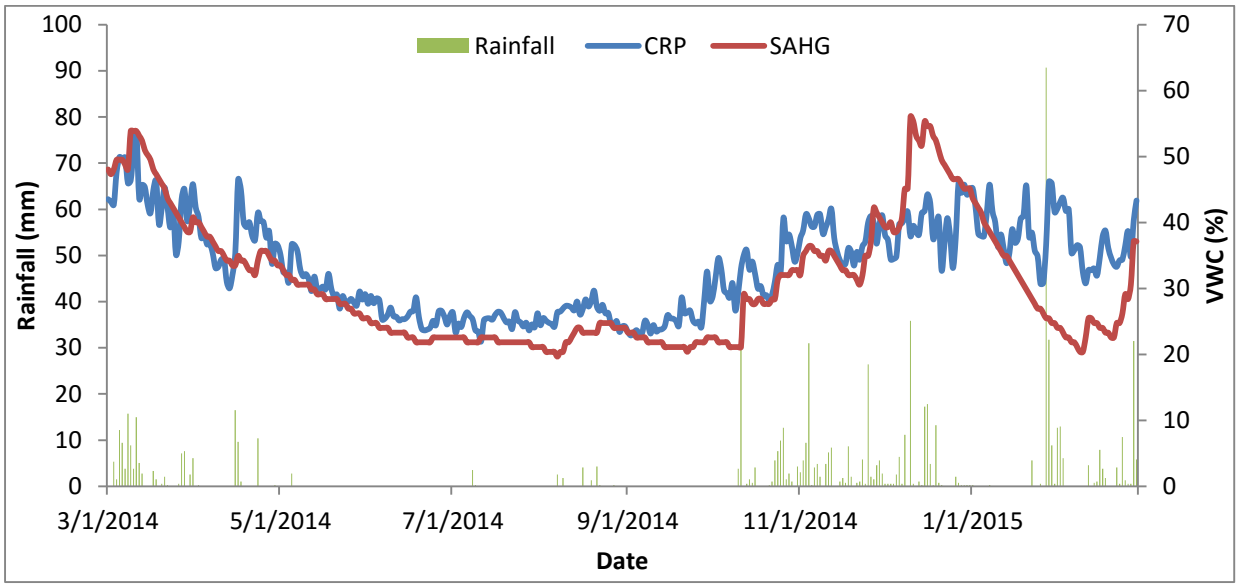

Figure 7.21 Time series analysis of SAHG and CRP soil moisture estimation

A day in summer (7 March 2014) and a day in winter (18 August 2014) are illustrated in Figures 7.22 and 7.23 respectively. The day in summer showed that the eastern side of South Africa generally had a higher soil moisture content than the western side, due to eastern side experiencing most of its rainfall in summer and having a higher mean annual precipitation. The soil moisture below is expressed as a SSI (%). The study area is adjacent to Lesotho, which is not covered by this product and therefore has no soil moisture values. In the winter period, the western side of South Africa increased in soil moisture, whilst the eastern side decreased, due to the seasonal rainfall patterns. There are still areas in the eastern side of South Africa that have a high soil moisture content.

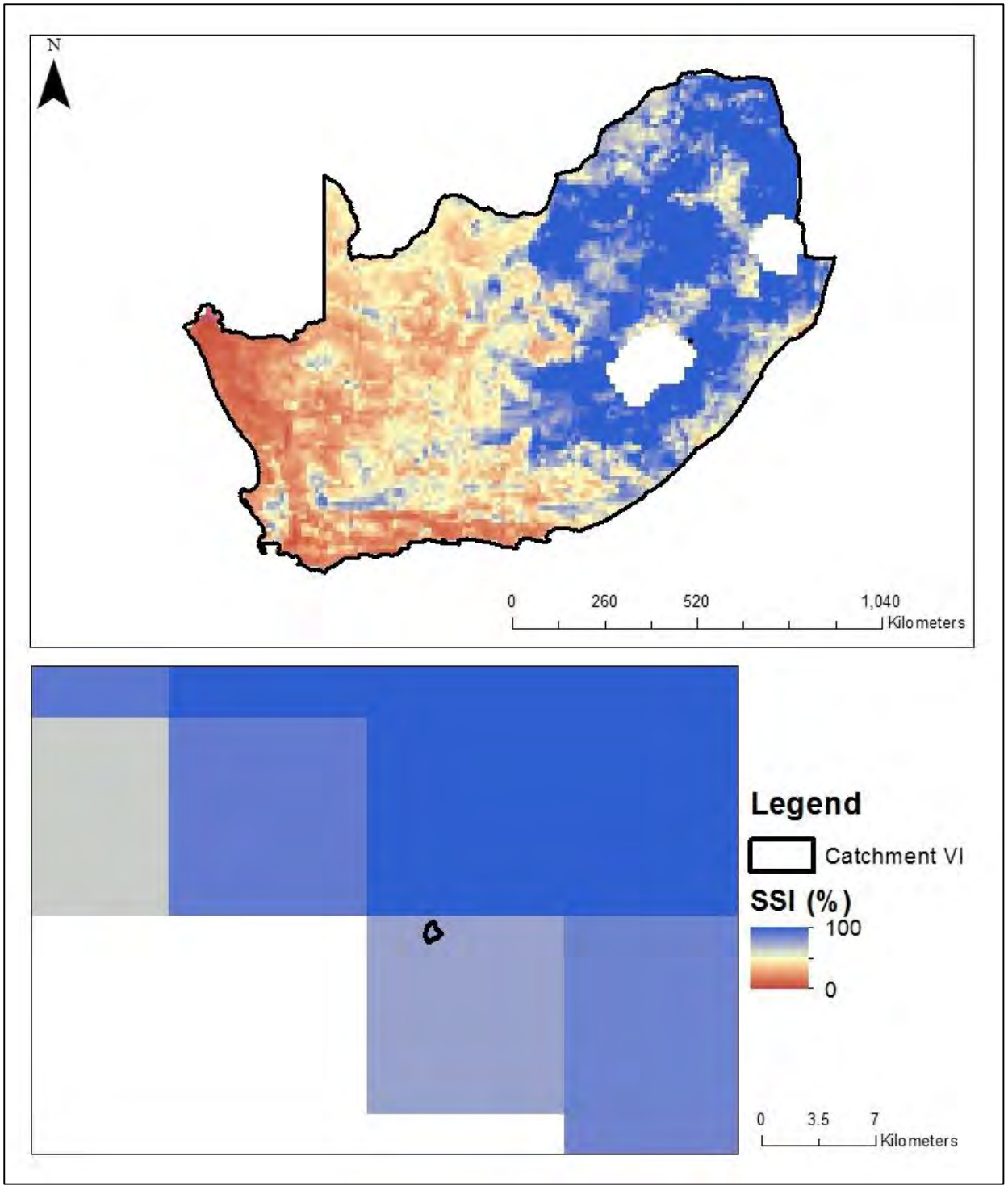

Figure 7.22 SAHG daily soil moisture (summer)

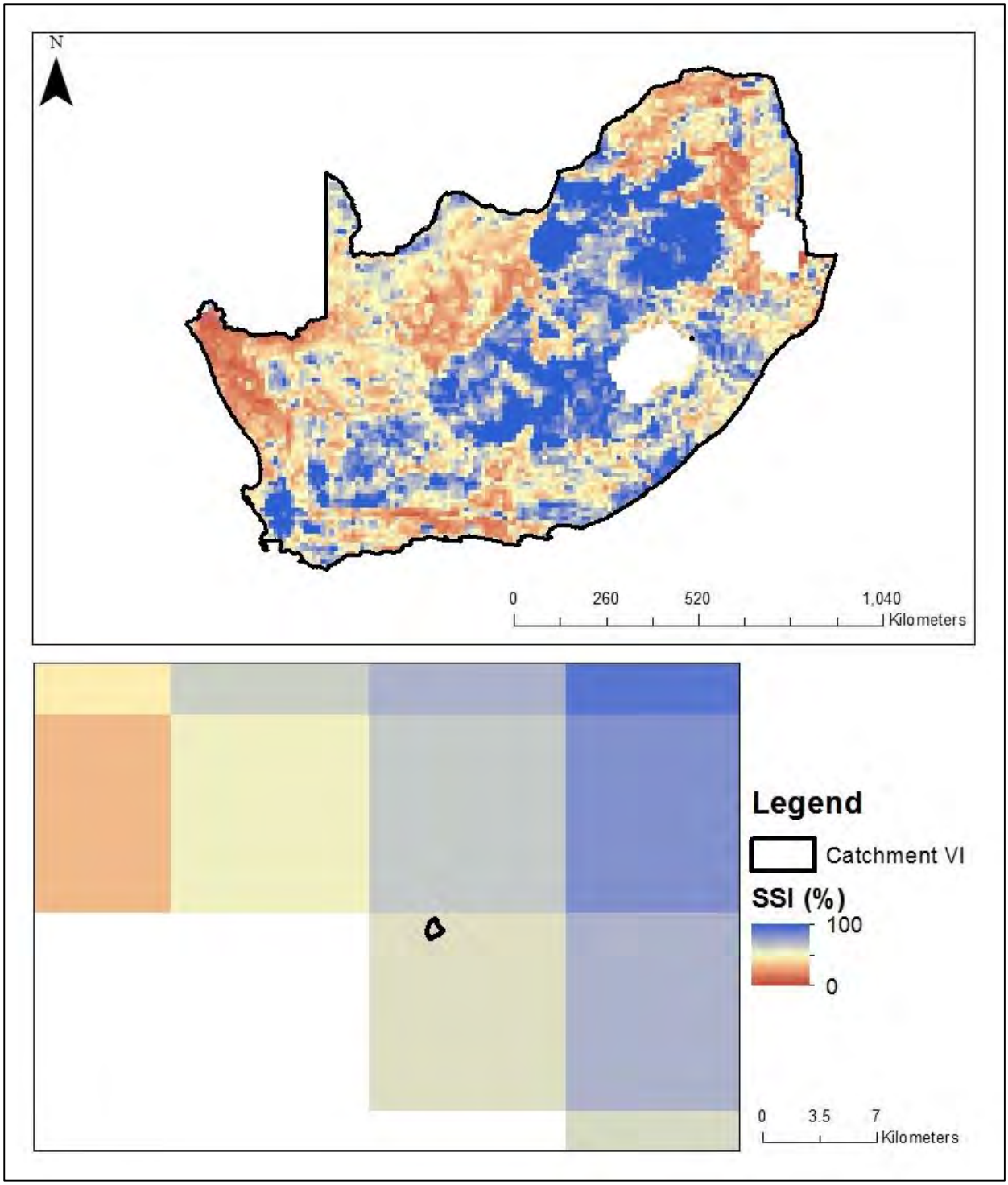

Figure 7.23 SAHG daily soil moisture (winter)

A scatter graph of the CRP (x-axis) was plotted against the SAHG product (y-axis) (Figure 7.24). From Figure 7.24, it can be seen that there is a positive and good correlation between the datasets. The points are clustered around the 1:1 line (red) and there are no extreme outliers. There are points below and above the 1:1 line, with the majority of the points being just below the 1:1 line. The R^2 is 0.624, which indicates a close linear relationship between the datasets. The slope is 1.049, which is close to 1. The points, which are noticeably above and below the 1:1 line can be attributed to the last three months of the datasets, where there was less of a correlation between the CRP and SAHG soil moisture estimates. Overall, the close correlation corresponds to the visual inspection of the data.

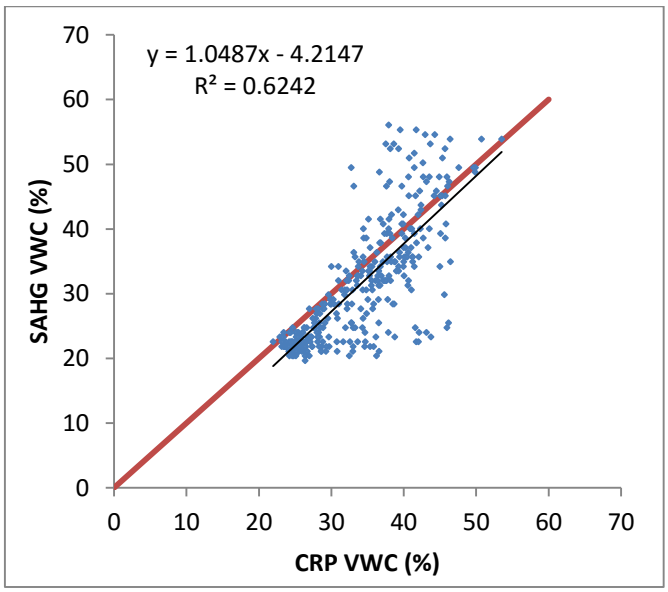

Figure 7.24 Scatter graph of CRP against SAHG soil moisture estimates

A graph of the residuals was then plotted against time (Figure 7.25). The Δ VWC (%) is the difference between the CRP and SAHG datasets. From Figure 7.25, it is evident that the majority of the residuals are positive, which indicates that the SAHG soil moisture product underestimates soil moisture for the majority of the study period. In the dry periods, the residuals are positive, whilst in the wet periods, there are both positive and negative residuals. The residuals are generally lower in absolute value in the dry periods, compared to the wet periods. Once more, the decline in the correlation between the datasets is noticeable between the first nine months of the study period and the last three months of the study period, which has the highest residuals with regards to the absolute value of the residuals.

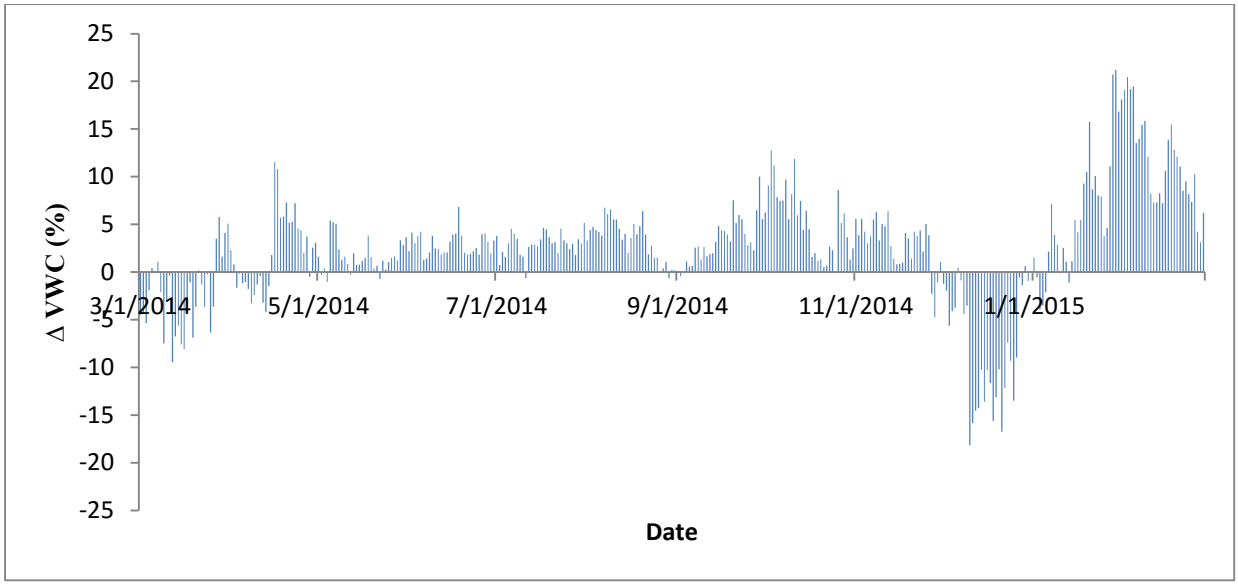

Figure 7.25 A residual graph of CRP against SAHG was plotted against time

A T-test was conducted. The CRP was variable one and the SAHG product was variable two (see Table 7.4). From Table 7.4, it can be seen that the means of both variables are similar, with the CRP mean (33.333) being slightly higher than the SAHG mean (30.742). The variance of the CRP is 50.292, which is lower than that of the SAHG product (88.607). There are 677 degrees of freedom. The t stat value is 4.201, which is larger than the t critical two-tail value of 1.964 and the p value is $3x10^{-05}$, which is larger than the alpha value (0.05). Therefore, according to the T-test, there is a significant difference between the data sets.

Table 7.4 T-test of CRP against SAHG estimates

	CRP	SAHG
Mean	33.333	30.742
Variance	50.292	88.607
Observations	365	365
Hypothesized Mean Difference	0	
df	677	
t Stat	4.201	
P(T<=t) two-tail	$3x10^{-05}$	
t Critical two-tail	1.964	

The SAHG soil moisture product provided good estimates of soil moisture, which correlated well with the CRP estimates. The SAHG soil moisture product measures the SSI (%) in the A and B soil horizons. In this case, the SSI was obtained at an average depth of one meter. Therefore, there is a vertical scaling issue, due to the CRP measuring at a depth of around

0.12 m, which falls in the range of the SAHG estimate. However, the SAHG product measures above (0.0 to 0.12 m) and below (0.12 to 1.00 m) and provides an average estimate of soil moisture. There is a horizontal scaling issue, as the SAHG product is on a 12.5 x 12.5 km spatial grid, which greatly exceeds the measurement footprint of the CRP. For this research project, all the soil moisture products were converted to volumetric water content (%), if they were not in volumetric water content (%) already. The SAHG product was in a SSI and the conversion required an accurate representative porosity value of the study area. The value determined may not have been the most representative of the study area, but rather an average of the points selected. This value would result in a constant error throughout the SAHG volumetric water content dataset.

7.6 SEBS Soil Moisture Validation

In total, 16 relative evaporation and 16 evaporative fraction maps were generated, using the SEBS Model in ILWIS 3.8.3. These maps were exported, opened and analyzed in ArcGIS 9.3, where the relative evaporation and evaporative fraction of the area within Catchment VI was determined. The relative evaporation and evaporative fraction values, which were obtained from the SEBS Model are shown in Table 7.5.

From Table 7.5, it can be seen that the relative evaporation and evaporative fraction results follow a seasonal trend, as the values are high in summer (wet period) and very low in winter (dry period), with the intermediate values between the wet and dry periods. Of the 16 estimated relative evaporation and evaporative fraction values, six have high relative evaporation values (above 0.7), two have intermediate relative evaporation values and eight have very low relative evaporation values (close to 0).

Catchment VI was burnt on the 5th of September 2014, which could be the reason for the zero values of the relative evaporation and evaporative fraction being estimated by the SEBS Model on the 6th of September 2014, 22nd of September 2014 and the 8th of October 2014. The fire would have resulted in an increase in albedo and a decrease in NDVI, which could have resulted in these low values. NDVI and albedo are amongst the parameters that the SEBS Model is most sensitive to (Gibson *et al.*, 2013). A range (high, intermediate and low) of relative evaporation and evaporative fraction are illustrated in Figure 7.26 and Figure 2.27 respectively.

Table 7.5 Relative evaporation and evaporative fraction calculated using the SEBS model for Catchment VI

Date	Relative Evaporation	Evaporative Fraction
14-Mar-14	0.73396	0.91684
30-Mar-14	0.94717	0.76871
15-Apr-14	0.87145	0.78335
1-May-14	0.29912	0.50633
17-May-14	Cloud	Cloud
2-Jun-14	0.00000	0.00000
18-Jun-14	0.00143	0.00367
4-Jul-14	0.02200	0.04683
20-Jul-14	0.00902	0.01190
5-Aug-14	0.00067	0.00016
21-Aug-14	Cloud	Cloud
6-Sep-14	0.00000	0.00000
22-Sep-14	0.00000	0.00000
8-Oct-14	0.00000	0.00000
24-Oct-14	0.11804	0.17727
9-Nov-14	0.93836	0.83581
25-Nov-14	Cloud	Cloud
11-Dec-14	0.85773	0.87569
27-Dec-14	Cloud	Cloud
12-Jan-15	0.930481	0.94974
28-Jan-15	Cloud	Cloud
13-Feb-15	Cloud	Cloud

From Figure 7.26, it can be seen that the estimated relative evaporation varies over time. The 30th of March 2014 represents a day when the relative evaporation was very high (0.9471), the 01st of May represents a day when the relative evaporation was intermediate 0.2991 and the 05th of August represents a day when the relative evaporation was very low 0.0067.

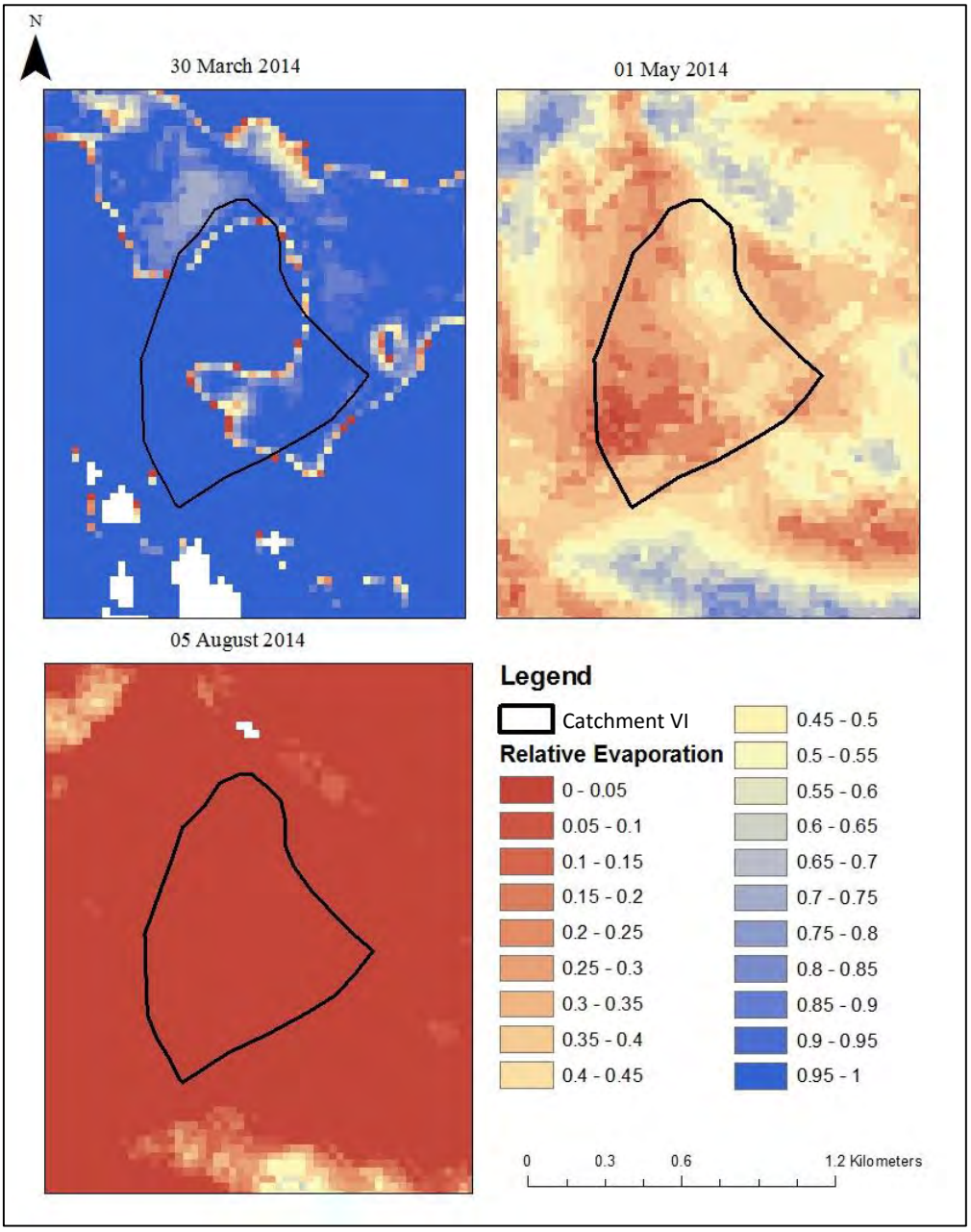

Figure 7.26 A range of different relative evaporation images for Catchment VI

From Figure 7.27, it can be seen that the estimated evaporative fraction varies over time. The 30th of March 2014 represents a day when the evaporative fraction was high (0.7687), the 01st of May represents a day when the evaporative fraction was intermediate 0.5063 and the 05th of August represents a day when the evaporative fraction was very low 0.0002.

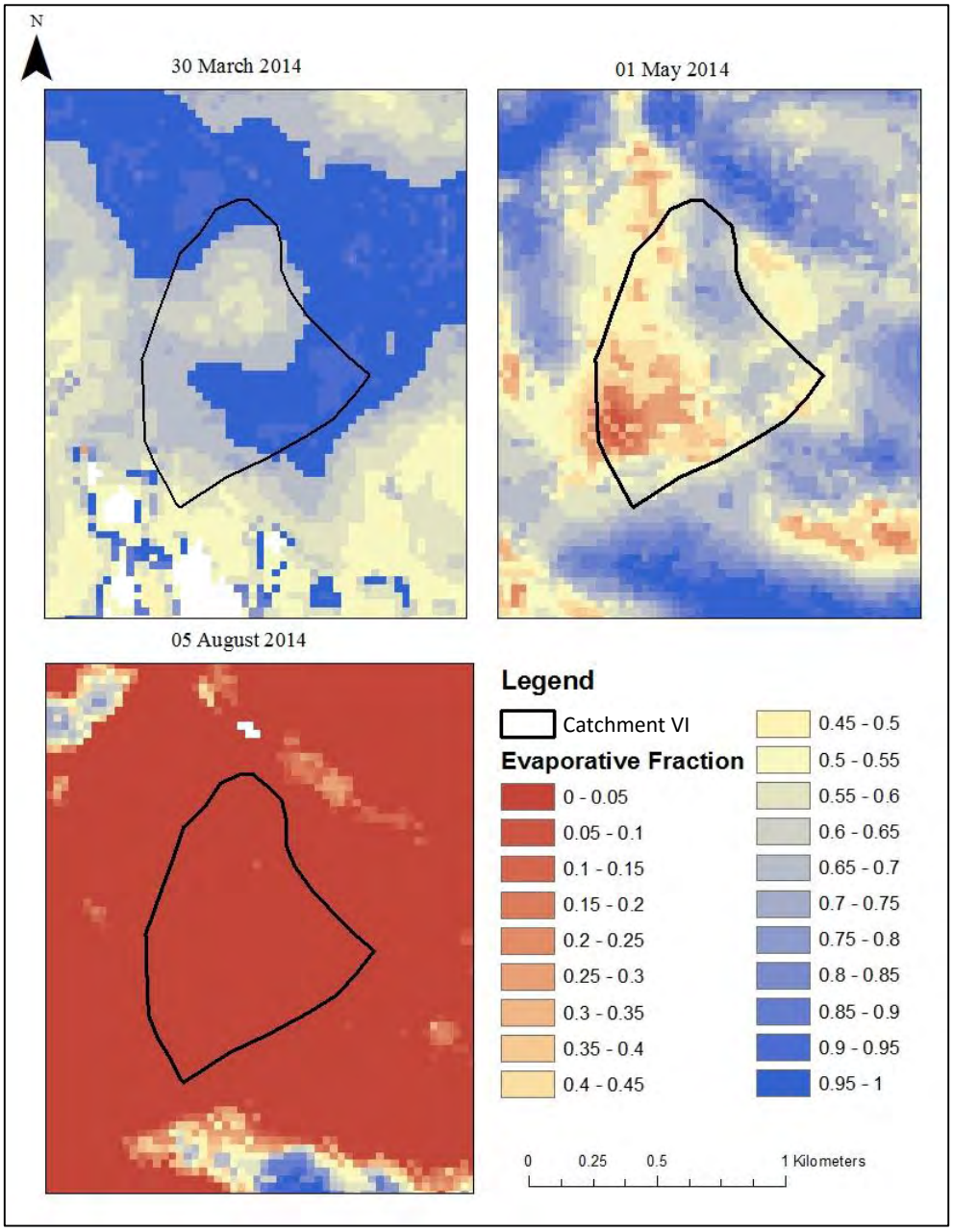

Figure 7.27 A range of different evaporative fraction images

Total evaporation consists of water that is evaporated from the land surface and water that is transpired from the vegetation. In order to estimate the actual soil moisture, the saturated soil moisture content is required, which can be inferred from the porosity. The porosity can be estimated from the bulk density.

The calculation of soil moisture from relative evaporation and evaporative fraction, estimates the soil moisture in the root zone, from which the evaporated water (soil evaporation, transpiration and interception) is sourced. The rooting zone of the grassland vegetation is 0.5

m. Therefore, the average bulk density of the soil from 0.0 to 0.5 m is required to obtain the porosity of the rooting zone. The bulk density was estimated to be 0.688 g/cm3, therefore the porosity was calculated to be 0.74. This porosity would be used as the saturated soil moisture content in the rooting zone.

Two methods for soil moisture estimation were investigated in this component of the research study. The first was developed by Su *et al.* (2003) and requires the relative evaporation (Equation 4.12). The second equation was developed by Scott *et al.* (2003) and requires the evaporative fraction (Equation 4.13). The estimated soil moisture was plotted against the corresponding CRP estimates, which were changed to match the 16-day time-step (Figure 7.28).

From Figure 7.28, it can be seen that both methods follow the same trend, as both methods generally over-estimate soil moisture in the wet period and generally under-estimate soil moisture in the dry period. Both methods follow a seasonal trend. The Scott *et al.* (2003) method seems to perform better, as it over-estimates less in the wet periods, when compared to the CRP and under-estimates less in the dry period, compared to the CRP, in comparison to the Su *et al.* (2003) method.

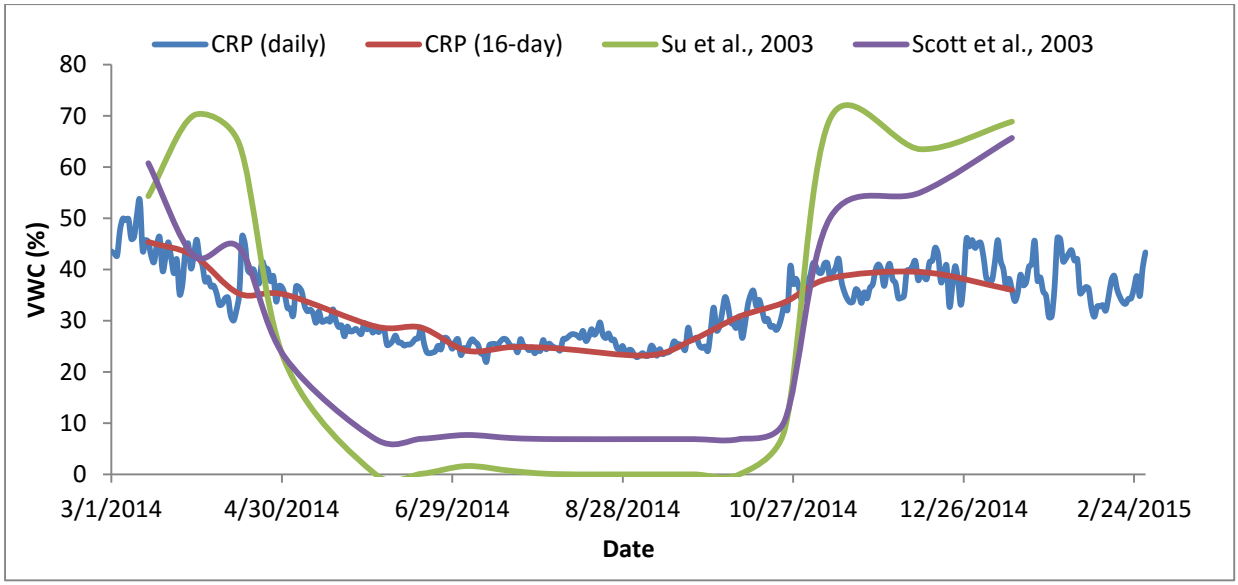

Figure 7.28 Time series of CRP estimates and soil moisture back-calculated from the SEBS model

Scatter graphs of the CRP against Su *et al.* (2003) and CRP against Scott *et al.* (2003) were then plotted (Figure 7.29). From the scatter graphs in Figure 7.29, it can be seen that both have positive correlations with points above and below the 1:1 line. The points do not cluster around the 1:1 line. The points above and below the 1:1 indicate over-estimation and under-estimation of the methods, when compared with the CRP. Both methods have a similar R^2 value but different slopes. The (Scott *et al.*, 2003) method has a R^2 value of 0.724 and a slope of 2.819. The (Su *et al.*, 2003) method has a R^2 of 0.722 and a slope of 3.862.

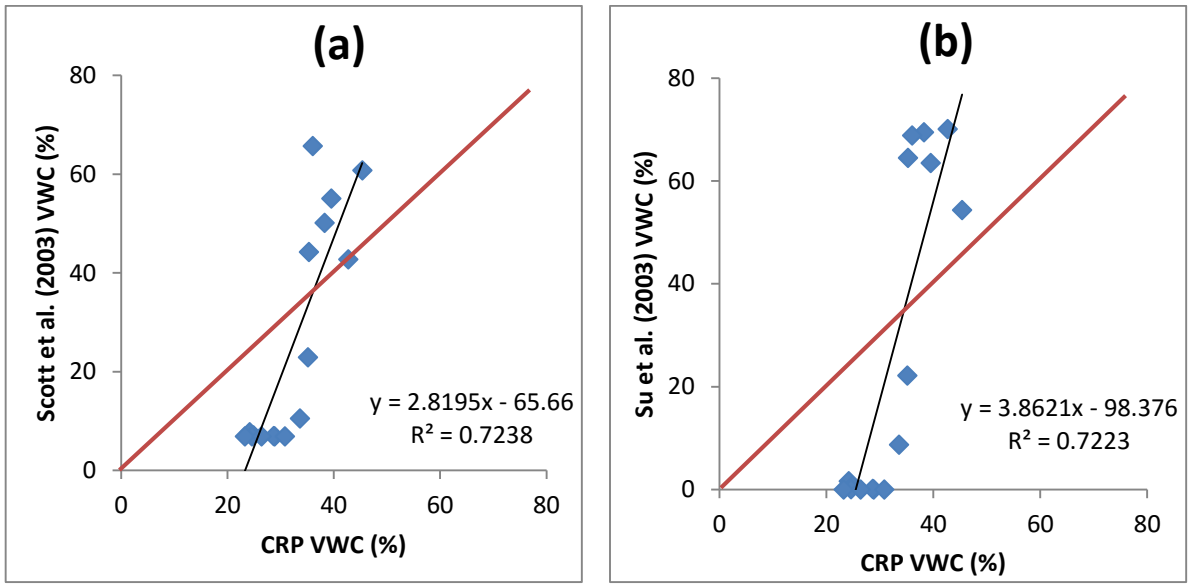

Figure 7.29 Scatter graphs of CRP against the SEBS Model estimates a) CRP against Su *et al.* (2003) and b) CRP against Scott *et al.* (2003).

A graph of the residuals for both the CRP against the Scott *et al.* (2003) method and the CRP against the Su *et al.* (2003) method are illustrated in Figure 7.30. From Figure 7.30, both residuals follow the same trend. The Su *et al.* (2003) method has greater residuals as it over-estimates and under-estimates the most in the respective periods, when compared to the CRP measurements. The Scott *et al.* (2003) method, resulted in lower absolute valued residuals than that of Su *et al.* (2003).

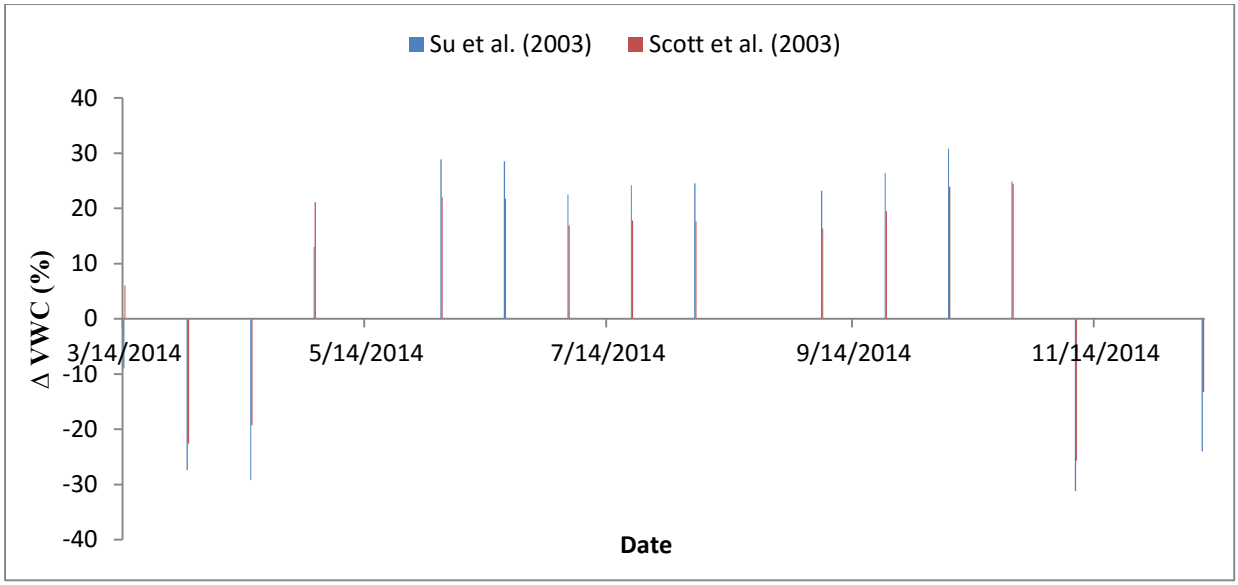

Figure 7.30 Residual graph of CRP against Su *et al*. (2003) and Scott *et al*. (2003).

The results show that the method of back-calculating soil moisture, using both equations, resulted in an over-estimation of soil moisture in the wet periods and an under-estimation of soil moisture in the dry period. This could be due to either the estimation of the relative evaporative and the evaporative fraction in the SEBS Model, or the equations used to calculate soil moisture from the relative evaporative and the evaporative fraction.

The evaporative fraction estimated using the SEBS Model can be validated with an evaporative fraction calculated from the eddy covariance system, which is situated in Catchment VI. The relative evaporation cannot be calculated using the eddy covariance system, as the relative evaporation requires the determination of H_{wet} (refer to Equations 4.4 and 4.6), which can only be reliably determined through field experiments to determine wet and dry bulb temperatures. Thus, the following will only look at determining soil moisture using the Scott *et al.* (2003) method, as only the evaporative fraction can be determined from the eddy covariance system.

The eddy covariance with infrared gas analyser measures latent and sensible heat directly. The eddy covariance system was operational from the 12th of July 2014 to present. The evaporative fraction was calculated for the same days as the SEBS estimates, using Equation 8.4 (Bastiaanssen *et al.*, 1997):

$$\Lambda = \frac{LE}{LE+H} \tag{8.4}$$

where LE is the latent-heat flux and H is the sensible-heat flux. The eddy covariance system is on a half-hourly time-step. Therefore, a daily relative evaporation value had to be determined. The evaporative fraction values determined from the SEBS Model and the eddy covariance system are seen in Table 7.6 below.

Table 7.6 Evaporative fraction estimates from the SEBS Model and eddy covariance technique

Date	SEBS ∧	EC ∧
14-Mar-14	0.91684	-
30-Mar-14	0.76871	-
15-Apr-14	0.78335	-
1-May-14	0.50633	-
2-Jun-14	0.00000	-
18-Jun-14	0.00367	-
4-Jul-14	0.04683	-
20-Jul-14	0.01190	0.17041
5-Aug-14	0.00016	0.21135
6-Sep-14	0.00000	0.14494
22-Sep-14	0.00000	0.26370
8-Oct-14	0.00000	0.46655
24-Oct-14	0.17727	0.62393
9-Nov-14	0.83581	0.73935
11-Dec-14	0.87569	0.70615
12-Jan-15	0.94974	0.75000

The SEBS Model is under-estimating the evaporative fraction in the dry periods and over-estimating evaporative fraction in the wet periods, as shown in Table 7.6. It is likely that the SEBS model was the cause of the poor soil moisture results, rather than the two equations used. The soil moisture was then estimated by using the calculated eddy covariance derived evaporative fraction in the (Scott *et al.*, 2003) method and plotted with the CRP measurements against time (see Figure 7.31).

From Figure 7.31, it can be seen that using the evaporative fraction data from the eddy covariance system, yielded better results of soil moisture, when compared to the CRP measurements. Using the eddy covariance data in the Scott *et al.* (2003) method resulted in an under-estimation of soil moisture in the dry period, but in the wet period, promising soil moisture estimates were obtained.

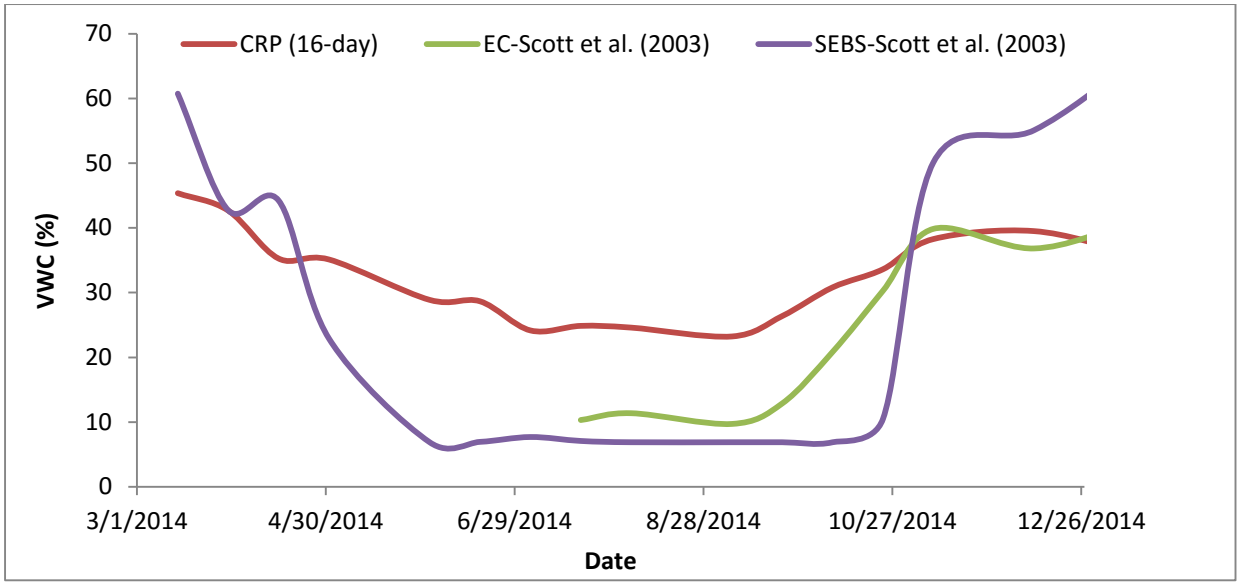

Figure 7.31 Time series of the CRP soil moisture estimates and soil moisture from the Scott *et al.* (2003) method using the evaporative fraction from SEBS and the eddy covariance method.

When the evaporative fraction of the SEBS Model is compared to the eddy covariance estimates of evaporative fraction, it is seen that the SEBS model overestimates evaporative fraction in the wet period, but under-estimates in the dry period. This indicates the limitations of the SEBS model. The SEBS model was originally created for agriculture, therefore some model parameterization is not appropriate for non-agricultural land-covers (Gibson *et al.*, 2013).

The method proposed by Scott *et al.* (2003) provided better soil moisture results than the method proposed by Su *et al.* (2003). This is mainly due to the Su *et al.* (2003) equation linking relative soil moisture to relative evaporation by a linear relationship. The use of the eddy covariance evaporative fraction estimates in the Scott *et al.* (2003) method, yielded good results in the wet period. This technique seems promising due to its spatial resolution. The technique is not limited temporally, but the choice of satellite (Landsat 8) data, introduces a temporal limitation. This temporal resolution made this method impractical as a means to monitor soil moisture, as soil moisture is highly variable over time.

7.7 Evaluating the Satellite-Based Soil Moisture Products

The satellite-based soil moisture products used in this study all have different spatial resolutions, as seen in Table 7.7. The SEBS back-calculated estimate, obtains soil moisture on a 0.09 km^2 spatial resolution. This resolution is exceptionally small, compared to the other products and is the only product that has a spatial resolution smaller than the catchment area. The AMSR2 soil moisture product has the next best spatial resolution, followed by the SAHG product. The SMOS product has the largest spatial resolution.

Table 7.7 Spatial resolution of soil moisture products

Product	Grid (km)	Spatial Resolution (km2)
AMSR2	10 x 10	100
SMOS	25 x 25	625
SAHG	12.5 x 12.5	156
SEBS	0.3 x 0.3	0.09

The spatial resolution is a key factor in remote sensing, as there is a need to obtain parameter data on the finest resolution possible. The temporal resolution is just as important, as the need to continuously monitor parameters is essential. Thus, smaller temporal resolutions are required. If the observational days of the satellite-based soil moisture products used in this study are considered, all the products, except for the SAHG product, have days with no data. The various soil moisture datasets were then compared on their temporal characteristics, over the one year study period (Figure 7.32).

From Figure 8.32, it can be seen that the SAHG product has a continuous dataset. The AMSR2 product is a "daily" product, but consists of a few missing days each month, as the product does not cover the entire surface of the earth each day. The SMOS data, which had the largest spatial resolution, also had a lot of missing days each month. This was due to the product not covering the entire earth's surface each day, as well as missing pixel values within the covering bands. The SEBS back-calculated product had the fewest observational days, as it uses Landsat 8 data, which works on a 16-day interval. This results in a maximum of two images per month. There was a problem with the sensor, which resulted in no observations in the months of January and February.

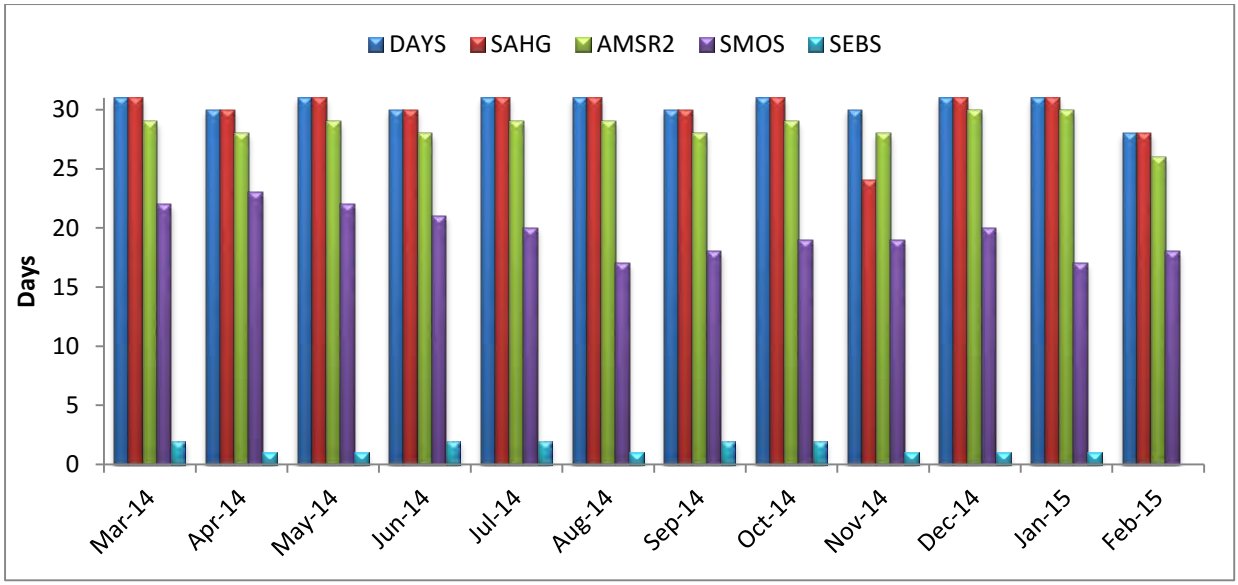

Figure 7.32 Number of observation days per month that data was available for each product

* * * * *

This section detailed the results of the various validations undertaken in the study. The calibrated CRP soil moisture data set was validated with the representative *in-situ* soil moisture data set. The results indicated a close correlation between the data sets and thus indicated that the CRP is suitable in providing spatial estimates of soil moisture in Cathedral Peak Catchment VI. The validated CRP soil moisture data set was then used to validate remote sensing and modelled soil moisture products. The validation of the AMSR2 and SMOS soil moisture products with the CRP estimates indicated that the AMSR2 and SMOS products generally underestimated soil moisture but followed the seasonal trend in soil moisture fluctuation. The SAHG soil moisture product showed the closest correlation when validated against the CRP estimates. The back-calculation of soil moisture using the relative evaporation and evaporative fraction, from the SEBS model did not correlate well with the CRP estimates. There was a general underestimation in winter and overestimation in summer when the back-calculated soil moisture estimates were compared to the CRP estimates. The use of the evaporative fraction from the eddy covariance in the method proposed by Scott *et al.* (2003), resulted in less of an underestimation in winter and a close correlation in summer when compared to the CRP estimates. The conclusions drawn from the results and discussion are detailed in the ensuing chapter.

8. CONCLUSIONS AND RECOMMENDATIONS

The conclusions and recommendations of the research study are detailed in this chapter.

8.1 Conclusions

Understanding the spatial and temporal variability of soil moisture at different scales is of great importance in many land surface disciplines, such as hydrology. Soil moisture is a key hydrological variable, as it impacts the water and energy balance at the land surface-atmosphere interface and is the main water source for natural vegetation and agriculture. It is difficult to quantify and assess the soil moisture content at an intermediate scale, due to the heterogeneity in soil and land cover properties, climate drivers and topography.

The objective of this research study was to compare CRP and satellite-based soil moisture estimates within Catchment VI of the Cathedral Peak Research Catchments. The three current methods used to estimate soil moisture were evaluated in this study. These three methods are *in-situ*, remote sensing and modelling. Although each method has its own advantages in measuring soil moisture, they are also greatly limited, as they do not provide soil moisture at an intermediate scale, which is required for hydrological applications.

The CRP is a new and innovative *in-situ* instrument that is capable of measuring soil moisture at an intermediate scale. The CRP, once properly calibrated, is suitable for providing spatial estimates of soil moisture, as the measurements correlated well with the representative *in-situ* soil moisture dataset. The CRP calibration procedure is adequate, however potential errors can be introduced throughout the procedure, which range from selecting the sample points, to determining a representative bulk density, to determining the average neutron count (N_o) value. Therefore, proper procedure must be adhered to, in order to minimize potential errors.

The validation of the CRP with a representative catchment soil moisture dataset, from the *in-situ* soil moisture network, showed that the CRP is suitable in providing continuous spatial soil moisture estimates. The *in-situ* soil moisture dataset could have been more representative

of the area, if the echo probes were not destroyed in the fire, however, the remaining *in-situ* sensors did create a valuable dataset for the CRP validation.
The calibrated CRP measurements were then used to validate the AMSR2 and SMOS Level Three soil moisture products. The AMSR2 dataset followed the trend of the CRP and correlated fairly well, but underestimated soil moisture throughout the study period. The dataset did have a few missing days. The AMSR2 product was analysed and it was found that the ascending and descending values correlated well in the dry periods, whilst greater differences were observed between ascending and descending values in the wet periods.

The SMOS dataset generally under-estimated soil moisture. The dataset did correlate well and follow the same trend of the CRP. The SMOS dataset had a larger variance and therefore its values fluctuated more. The dataset had many missing days of data. The SMOS product was analysed and it was seen that the ascending and descending values were different throughout. The key issue in the validation of the AMSR2 and SMOS soil moisture products with the CRP measurements, is the vertical and horizontal scaling issue. Although the CRP is an improvement from validating remote sensing products with *in-situ* point measurements, the difference in measurement depths and the footprint of the CRP and current remote soil moisture products still remain a limitation.

The AMSR2 and SMOS products consist of ascending and descending values. It has been shown that there were differences in these values, which could be attributed to changes in soil moisture in the 12-hour interval between ascending and descending acquisition. It was noted that there were also differences in day and night geo-physical conditions, with nocturnal conditions being more favourable for soil moisture retrieval from AMSR2 and SMOS products.

The CRP was then used to validate modeled soil moisture estimates. These included the SAHG soil moisture product and the back-calculation of soil moisture from relative evaporation estimated from the SEBS Model.

The SAHG soil moisture product was validated with the CRP. There was a close correlation between the SAHG and CRP datasets. The SAHG soil moisture followed the same seasonal trend as the CRP and had a continuous dataset (no missing values). The SAHG product generally had a slight underestimation of soil moisture. Although the SAHG product

performed well, there was still the presence of vertical and horizontal scaling issues, due to differences in the measurement depth and footprint of the two datasets. There is also the issue of the conversion of the SSI to VWC, which required a representative porosity of the study area to be determined.

The back-calculation of soil moisture from relative evaporation and evaporative fraction, estimated using the SEBS model, looked like a promising technique. The spatial resolution was less than the catchment area and the measurement depth was representative of the root zone of the vegetation (0.50 m). Therefore, this product would have the least horizontal and vertical scaling issues, when validated against the CRP. The SEBS model did not provide accurate estimates of relative evaporation and evaporative fraction compared to the evaporative fraction estimates from the eddy covariance system. The SEBS Model over-estimated the evaporative fraction in the wet period, whilst under-estimating the evaporative fraction in the dry periods, which resulted in soil moisture over-estimation in the wet periods and under-estimation in the dry periods. When the evaporative fraction derived from the eddy covariance system was used in the (Scott *et al.*, 2003) method, the resultant soil moisture estimates, under-estimated in the dry period, however promising estimates were obtained in the wet period, which correlated well with the CRP estimates. Although the back-calculation method results in soil moisture estimates on a 30 m spatial grid, the temporal resolution of the imagery used is 16 days, which is very impractical for continuous soil moisture monitoring.

8.2 Recommendations

The following recommendations can be used to address the main limitations that were experienced in this research study. This will provide assistance for future research studies.

i. The calibration of the CRP is both time and labour intensive, as calibrations over different periods are required. There are a variety of errors that could emerge throughout the calibration procedure. Therefore, the proper techniques and equipment must be used to minimize the occurrence of errors, in order to obtain reliable soil moisture measurements. The use of a TDR HydroSense probe, which obtains instantaneous measurements of soil moisture, when inserted into the soil, can potentially be used to obtain the necessary soil moisture measurements for the calibration. Thus, it would greatly reduce the time and labour required.

ii. The validation of the CRP needs to be done with *in-situ* soil moisture sensors at a variety of depths. Ideally several TDR pits, in the CRP measurement volume could be used. This would improve the validation, as the CRP doesn't measure at a constant depth and therefore, shouldn't be validated with *in-situ* measurements at a constant depth. However, this would be very capital, time and labour intensive.

iii. The potential for using temporal stability analysis to find a more representative sensor location would be useful to upscale the *in-situ* observations to the entire catchment.

iv. Current remote sensing soil moisture products are still too coarse to be validated with CRP measurements. Although the use of the CRP for the validation of remote sensing soil moisture products is an improvement, the vertical and horizontal scaling issues still remain as major limitations. This limitation could potentially be addressed through the downscaling of remote sensing soil moisture products, in order to obtain finer spatial scale soil moisture estimates.

v. The back-calculation of soil moisture using relative evaporation and evaporated fraction, from the SEBS Model, indicated that the use of the SEBS Model is not suitable in the study area for the estimation of these parameters. Future research should limit the use the SEBS model to agricultural landscapes.

9. REFERENCES

Albergel, C, de Rosnay, P, Gruhier, C, Mu˜noz-Sabater, J, Hasenauer, S, Isaksen, L, Kerr, Y and Wagner, W. 2012. Evaluation of remotely sensed and modelled soil moisture products using global ground-based in situ observations. *Remote Sens. Environ* 118: 215-226.

Allen, R, Bastiaanssen, W and Waters, R. 2002. Personal communication, the University of Idaho and the Idaho Department of Water Resources, The University of Idaho,

Bastiaanssen, W, Pelgrum, H, Droogers, P, de Bruin, H and Menenti, M. 1997. Area-average estimates of evaporation, wetness indicators and top soil moisture during two golden days in EFEDA. *Agric Forest Meteorol* 87: 119-137.

Bezerra, B, dos Santos, C, da Silva, B, Bezerra, M, Bezerra, J and Rao, T. 2013. Estimation of soil moisture in the root-zone from remote sensing data. . *Ci. Solo* 37: 596-603.

Brocca, L, Hasenauer, S, Lacava, T, Melone, F, Moramarco, T, Wagner, W, Dorigo, W and Bittelli, M. 2011. Soil moisture estimation through ASCAT and AMSR-E sensors: An intercomparison and validation study across Europe. *Remote Sensing of Environment* 115: 3390-3408.

Brocca, L, Tarpanelli, A, Moramarco, T, Melone, F, Ratto, S, Cauduro, M, Ferraris, S, Berni, N, Ponziani, F, Wagner, W and Melzer, T. 2013. Soil moisture estimation in Alpine Catchments through modeling and satellite observations. *Soil Science Society of America*

Desilets, D and Zreda, M. 2013. Footprint diameter for a cosmic-ray soil moisture probe: theory and Monte Carlo simulations. *Water Resources Research* 49: 3566-3575.

Desilets, D, Zreda, M and Ferre, T. 2010. Nature's neutron probe: land surface hydrology at an elusive scale with cosmic rays. *Water Resources Research* 46: 1-7.

Dorigo, W, Wagner, W, Hohensinn, H, Paulik, C, Xaver, A and Jackson, T. 2011. The International Soil Moisture Network: A data hosting facility for global in situ soil moisture measurements. *Hydrology and Earth System Sciences. Hydrol. Earth Syst. Sci* 15: 1675-1698.

Draper, CS, Walker, JP, Steinhle, P and Holmes, TRH. 2009. An evaluation of AMSR–E derived soil moisture over Australia. *Remote Sensing of Environment* 113 (4): 703-710.

Dutta, R and D'este, C. 2013. Virtual Calibration of Cosmic Ray Sensor: using supervised ensemble machine Learning. *IJACSA) International Journal of Advanced Computer Science and Applications* 4: (8): 104-110.

Engman, ET. 1991. Application of microwave remote sensing of soil moisture for water resources and agriculture. *Remote Sensing of Environment* 35: 213-226.

Everson, CS, Molefe, GL and Everson, TM. 1998. *Monitoring and modelling components of the water balance in a grassland catchment in the summer rainfall area of South Africa*.

Fang, B and Lakshmi, V. 2014. Soil moisture at watershed scale : Remote sensing techniques *Journal of Hydrology* 516: 258-272.

Franz, T. 2014. Personal communication, Franz Hydrogeophysics Lab Group, 1-4.,

Franz, T, Wang, T, Avery, W, Finkenbiner, C and Brocca, L. 2015. Spatiotemporal characterization of soil moisture fields in agricultural areas using cosmic-ray neutron probes and data fusion. *EGU General Assembly* 17

Franz, T, Zreda, M, Ferre, T and Rosolem, R. 2013. An assessment of the effect of horizontal soil moisture heterogeneity on the area-average measurement of cosmic-ray neutrons. *Water Resources Research* 49: 1-9.

Franz, T, Zreda, M, Rosolem, R and Ferre, T. 2012a. Field Validation of a cosmic-ray neutron sensor using a distributed sensor network. *Vadose Zone Journal* 11

Franz, T, Zreda, M, Rosolem, R and Ferre, T. 2012b. A universal calibration function for determination of soil moisture with cosmic-ray neutrons. *Hydrology and Earth System Sciences Discussions* 9: 10303-10322.

Gibson, L, Jarmain, C, Su, Z and Eckardt, F. 2013. Estimating evapotranspiration using remote sensing and the Surface Energy Balance System - A South African Perspective. *Water SA* 39: 477-484.

Gokman, M, Vekerdy, Z, Verhoef, A, Verhoef, W, Batelaan, O and van der Tol, C. 2012. Integration of soil moisture in SEBS for improving evapotranspiration estimation under water stress conditions. *Remote Sensing of Environment* 121: 261-274.

Gruber, A, Dorigo, WA, Zwieback, S, Xaver, A and Wagner, W. 2013. Characterizing coarse-scale representativeness of in situ soil moisture measurements from the International soil moisture network. *gsvadzone* 12 (2):

Gruhier, C, Albergel, C, de Rosnay, P and Zeiner, B. 2011. Comparison between H-SAF large scale surface soil moisture, H-SAF assimilated soil moisture and SMOS Level 2 soil moisture. *CESBIO, Toulouse, France.*

Guillem, M. 2010. Multi-scale soil moisture retrievals from microwave remote sensing observations. Unpublished thesis, Remote Sensing Lab, Dept. Teoria del Senyal I Comunicacions Universitat Polit Ecnica de Catalunya,

Gush, M, Scott, DF, Jewitt, GPW, Schulze, RE, Lumsden, T, Hallowes, L and Gorgens, A. 2002. *Estimation of streamflow reduction resulting from commercial afforestation in South Africa*.

Hawdon, A, Mcjannet, D and Wallace, J. 2014. Calibration and correction procedures for cosmic-ray neutron soil moisture probes located across Australia. *Water Resources Research* 50 (6): 5029-5043.

Hillel, D. 2008. In: ed. Hillel, D, *Soil in the Environment*. Academic Press, San Diego.

Imaoka, K, Kachi, M, Kasahara, M, Ito, N, Nakagawa, K and Oki, T. 2010. Instrument performance and calibration of AMSR-E and AMSR2. *International Archives of the Photogrammetry, Remote Sensing and Spatial Infromation Science* 38: 13-16.

Jackson, TJ, Cosh, MH, Bindlish, R, Starks, PJ, Bosch, DD, Seyfried, M, Goodrich, DC, Moran, MS and Du, J. 2010. Validation of advanced microwave scanning radiometer soil moisture products. *IEEE Transactions on Geoscience and Remote Sensing* 48 (12):

Jarmain, C, Govender, M and Everson, CS. 2004. *Improving the basis for predicting total evaporation from natural veld types in South Africa*.

JAXA, JAEA. 2013a. *AMSR Level 3 Product Format Description Document*.

JAXA, JAEA. 2013b. GCOM-W1 "SHIZUKU" Data Users Handbook. *First Edition.*

Jiao, Q, Zhu, Z and Du, F. 2014. Theory and application of measuring mesoscale soil moisture by cosmic-ray fast neutron probe. *35th International Symposium on Remote Sensing of Environment* 17

Jones, SB, Wraith, JM and Or, D. 2002. Time domain reflectometry measurement principles and applications. *Hydrological Processes* 16: 141-153.

Kerr, YH, Waldteufel, P, Richaume, P, Wigneron, JP, Ferrazzoli, P, Mahmoodi, A, Al Bitar, A, Cabot, F, Gruhier, C, Juglea, SE, Leroux, D, Mialon, A and Delwart, S. 2012. The SMOS soil moisture retrieval algorithm. *Geoscience and Remote Sensing, IEEE Transactions on* 50 (5): 1384-1403.

Kerr, YH, Waldteufel, P, Wigneron, JP, Delwart, S, Cabot, F, Boutin, J, Escorihuela, MJ, Font, J, Reul, N, Gruhier, C, Juglea, SE, Drinkwater, MR, Neira, M and Mecklenburg, S. 2010. The SMOS mission: new tool for monitoring key elements of the global water cycle. *Proceedings of the IEEE* 98 (5): 666-687.

Kim, S, Liu, YY, Johnson, FM, Parinussa, RM and Sharma, A. 2015. A global comparison of alternate AMSR2 soil moisture products: Why do they differ ? *Remote Sensing of Environment*

Kohli, M, Shron, M, Zreda, M, Schmidt, U, Dietrich, P and Zacharias, S. 2015. Footprint characteristics revised for field-scale soil moisture monitoring with cosmic-ray neutrons. *Water Resources Research* 10: 5772-5790.

Koike, T, Nakamura, YK and Fujii, I. 2004. Development of an Advanced Microwave Scanning Radiometer (AMSR-E) Algorithm of soil moisture and vegetation water content. *Annual Journal of Hydraulic Engineering* 48 (2): 217-222.

Kuenene, BT, van Huyssteen, CW and Hensley, M. 2009. Soil water saturation in the Cathedral Peak VI catchment, KwaZulu-Natal. *SAGA Biennial Technical Meeting and Exhibition* 11: 565-570.

Lakshmi, V. 2013. Remote sensing of soil moisture. *ISRN Soil Science* 2013: 33 pages.

Leroux, D, Kerr, YH, Al Bitar, A, Bindlish, R, Jackson, TJ, Berthelot, N and Portet, G. 2013. Comparison between SMOS, VUA, ASCAT and ECMWF soil moisture products over four watersheds in United States. *IEEE Transactions on Geoscience and Remote Sensing* 1-20.

Lu, H, Koike, T and Yang, K. 2014. Improvement of AMSR2 soil moisture algorithm with considering temperature profile effects in dry soil: a case study in Heihe Basin. *IEEE* 3299-3302.

Ma, W, Hafeez, M, Rabbani, U, Ishikawa, H and Ma, Y. 2012. Retrieved actual ET using SEBS model from Landsat-5 TM data for irrigation area of Australia. *Atmospheric Environment* 59: 408-414.

Markham, B, Storey, J and Morfitt, R. 2015. Landsat-8 sensor characterization and calibration. *Remote Sens* 2015 (7): 2279-2282.

Mecklenburg, S, Drusch, M, Kerr, Y, Font, J and Roger, O. 2013. ESA's soil moisture and ocean salinity mission: mission performance and operations. *European Space Agency, ESA-ESRIN, Via Galileo Galilei, Frascati, Italy.*

Mekonnen, D. 2009. Satellite remote sensing for soil moisture estimation: Gumara catchment, Ethiopia. Unpublished thesis, International institute for geo-information science and earth observation, Netherlands.

Meng, L and Quiring, SM. 2008. A Comparison of Soil Moisture Models Using Soil Climate Analysis Network Observations. *American Meteorological Society* 9: 641-659.

Mengistu, MG, Everson, CS, Moyo, NC and Savage, MJ. 2014. *The validation of the variables (evaporation and soil moisture) in hydrometeorological models.*

Merlin, O, Al Bitar, A, Walker, JP and Kerr, Y. 2009. A sequential model for disaggregating near-surface soil moisture observations using multi-resolution thermal sensors. *Remote Sensing of Environment* 113 (10): 2275-2284.

Merlin, O, Al Bitar, A, Walker, JP and Kerr, Y. 2010. An improved algorithm for disaggregating microwave-derived soil moisture based on red, near-infrared and thermal-infrared data. *Remote Sensing of Environment* 114 (10): 2305-2316.

Merlin, O, Rudiger, C, Al Bitar, A, Richaume, P, Walker, JP and Kerr, YH. 2012. Disaggregation of SMOS soil moisture in southeastern Australia. *Geoscience and Remote Sensing, IEEE Transactions on* 50 (5): 1556-1571.

Merlin, O, Walker, JP, Chehbouni, A and Kerr, Y. 2008. Towards deterministic downscaling of SMOS soil moisture using MODIS derived soil evaporative efficiency. *Remote Sensing of Environment* 112 (10): 3935-3946.

Ni-Meister, W. 2005. Soil moisture initialization for climate prediction: characterization of model and observation errors. *Journal of Geophysical Research* 110: 11-29.

Ochsner, TE, Cosh, MH, Cuenca, RH, Dorigo, WA, Draper, CS, Hagimoto, Y, Kerr, YH, Larson, KM, Njoku, EG, Small, EE and Zreda, M. 2013. State of the art in large-scale soil moisture monitoring. . *Soil Science Society of America.*

Parrens, M, Zakharova, E, Lafont, S, Calvet, JC, Kerr, YH, Wagner, W and Wigeron, JP. 2012. Comparing soil moisture retrievals from SMOS and ASCAT over France. *Hydrol. Earth Syst. Sci* 16: 423-440.

Piles, M, Camps, A, Vall-llossera, M, Corbella, I, Panciera, R, Rudiger, C, Kerr, YH and Walker, JP. 2011. Downscaling SMOS-derived soil moisture using MODIS visible/infrared Data. *IEEE Transactions on Geoscience and Remote Sensing* 49 (9):

Qin, J, Yang, K, Chen, Y, Zhao, L and Han, M. 2013. Spatial up-scaling of in-situ soil moisture measurements based on MODIS-derived apparent thermal inertia. *Remote Sensing of Environment* 138: 1-9.

Sabins, FF. 2007. *Remote Sensing Principles and Interpretation*. Waveland Press, Illinois.

Scott, C, Bastiaanssen, W and Ahmad, M. 2003. Mapping spatio-temporal distributions of soil moisture throughout irrigated watersheds using optical and high resolution imagery. *ASCE Irrigat and Drain Eng* 129

Scott, DF. 1994. The hydrological effects of fire in South African catchments. . Unpublished thesis, Department of Agricutural Engineering, University of Natal, South Africa,

Scott, DF, Prinsloo, FW, Moses, G, Mehlomakulu, M and Simmers, ADA. 2000. *A re-analysis of the South African catchment afforestation experimental data*

Shin, Y and Mohanty, BP. 2013. Development of a deterministic downscaling algorithm for remote sensing soil moisture footprint using soil and vegetation classifications. *Water Resources Research* 49: 6208-6228.

Sinclair, S and Pegram, GGS. 2010. A comparison of ASCAT and modeled soil moisture over South Africa, using TOPKAPI in land surface mode. *Hydrol. Earth Syst. Sci.* 14: 613-626.

Sinclair, S and Pegram, GGS. 2012. PyTOPKAPI – an open-source implementation of the TOPKAPI hydrological model. *Pegram and Associates.*

Sinclair, S and Pegram, GGS. 2013a. *HYLARSMET: A hydrologically consistent land surface model for soil moisture and evapotranspiration modelling over Southern Africa using remote sensing and meteorological data*.

Sinclair, S and Pegram, GGS. 2013b. A sensitivity assessment of the TOPKAPI model with an added infiltration module. *Journal of Hydrology* 479: 100-112.

Song, C, Jia, L and Menenti, M. 2013. Retrieving high-resolution surface soil moisture by downscaling AMSR-E brightness temperature using MODIS LST and NDVI data. *IEEE Journal of Selected Topics in Applied Earth Observations and Remote Sensing* (2013): 1939-1404.

Stoof, CR, Vervoort, RW, Iwema, J, van de Elsen, E, Ferreira, AJD and Ritsema, CJ. 2012. Hydrological response of a small catchment burned by experimental fire. *Hydrol. Earth Syst. Sci* 16: 267-285.

Su, Z. 2002. The Surface Energy Balance System (SEBS) for estimation of turbulent heat fluxes. *Hydrology and Earth System Sciences* 6: 85-99.

Su, Z, Yacob, A, Wen, J, Roerink, G, He, Y, Gao, B, Boogaard, H and van Diepen, C. 2003. Assessing relative soil moisture with remote sensing data: theory, experimental validation, and application to drought monitoring over the North China Plain. *Physics and Chemistry of the Earth* 28: 89-101.

USGS. 2013. Using the USGS Landsat 8 Product. [Internet]. Available from: http://landsat.usgs.gov/Landsat8_Using_Product.php. [Accessed: February].

USGS. 2015. *Landsat 8 (L8) data users handbook*

Villarreyes, CAR, Baroni, G and Oswald, SE. 2013. Calibration approaches of cosmic-ray neutron sensing for soil moisture measurement in cropped fields. *Hydrology and Earth System Sciences* 10: 4237-4274.

Vischel, T, Pegram, GGS, Sinclair, S and Parak, M. 2008. Implementation of the TOPKAPI model in South Africa: initial results from the Liebenbergsvlei catchment. *Water SA* 34 (3): 1-12.

Wagner, W. 2008. Remote sensing of soil moisture in support to hydrological and meteorological modelling. *METIER Training Course "Remote Sensing of the Hydrosphere" Finish Environment Institute, Helsinki, Finland.*

Wagner, W, Dorigo, W, de Jeu, R and Fernandez, JC. 2012. Fusion of active and passive microwave observations to create an essential climate variable data record on soil moisture. *Vienna University of Technology, Institute of Photogrammetry and Remote Sensing, Gusshausstrasse, 1040 Wien, Austria.*

Walker, JP, Willgoose, GR and Kalma, JD. 2004. In situ measurement of soil moisture: a comparison of techniques. *Journal of Hydrology* 2963: 85-99.

Wang, L and Qu, J. 2009. Satellite of remote sensing application for surface soil moisture monitoring. *Front. Earth Sci.* 3 (2): 237-247.

Zazueta, FS and Xin, J. 1994. Soil Moisture Sensors. *University of Florida.*

Zhang, A, Jia, G, Wang, S, Zhoa, TB and Feng, JM. 2011. Evaluation of AMSR-E derived soil moisture over Northern China. *China. Atmospheric and Oceanic Science.* 4 (4): 223-228.

Zhao, W and Li, A. 2013. A downscaling method for improving the spatial resolution of AMSR-E derived soil moisture product based on MSG-SEVIRI data. *Remote Sensing of Environment* 5 (2013): 6790-6811.

Zreda, M, Desilets, D, Ferre, TPA and Scott, RL. 2008. Measuring soil moisture content non-invasively at intermediate spatial scale using cosmic-ray neutrons. *Geophysical Research* 35

Zreda, M, Shuttleworth, WJ, Zeng, X, Zweck, C, Desilets, D, Franz, T and Rosolem, R. 2012. COSMOS: the COsmic-ray Soil Moisture Observing System. *Hydrol. Earth Syst. Sci.* 16: 4079-4099.